

This is a pre print version of the following article:

The 2.0–1.88 Ga Paleoproterozoic evolution of the southern Amazonian Craton (Brazil): An interpretation inferred by lithofaciological, geochemical and geochronological data / Roverato, M.; Giordano, D.; Giovanardi, T.; Juliani, C; Polo, L. - In: GONDWANA RESEARCH. - ISSN 1342-937X. - 70:(2019), pp. 1-21. [10.1016/j.gr.2018.12.005]

*Terms of use:*

The terms and conditions for the reuse of this version of the manuscript are specified in the publishing policy. For all terms of use and more information see the publisher's website.

07/01/2026 11:16

Manuscript Number: GR-D-18-00274R1

Title: The 2.0-1.88 Ga Paleoproterozoic evolution of the southern Amazonian Craton (Brazil): an interpretation inferred by lithofaciological, geochemical and geochronological data.

Article Type: Research Paper

Corresponding Author: Dr. Matteo Roverato, PhD

Corresponding Author's Institution: Yachaytech

First Author: Matteo Roverato, PhD

Order of Authors: Matteo Roverato, PhD; Daniele Giordano; Tommaso Giovanardi; Caetano Juliani; Liza Polo

**Abstract:** The study of Paleoproterozoic rocks is crucial for understanding Earth's tectonic evolution during the time when most of the modern crust and ore deposits were formed. The rocks of the Brazilian Amazonian Craton record some of the most-complete and best-preserved Paleoproterozoic magmatic and volcanic episodes on Earth. Following previous investigations, we present new lithofaciological and stratigraphic records of the felsic rocks of the Tapajós Mineral Province (TMP) (~ 2-1.88 Ga) and the São Felix do Xingú region (SFX) (~ 1.88 Ga) which, combined with new petrological and geochronological data, help providing a more complete understanding of the tectonic, magmatic and volcanological evolution of the Amazonian Craton. This magmatism/volcanism is thought to be formed in a late-/post-orogenic to extensional regime confirmed by the new geochemical data presented here. The transition from late-convergent to extensional tectonic setting could register the beginning of the taphrogenesis that marked the Amazonian Craton throughout the Mesoproterozoic. The volcanological approach of this contribution can serve as a strategy for the modelling of the evolution of Precambrian volcano-sedimentary basins around the world. The large amount of rocks analyzed are divided into primary and secondary volcanoclastic products depending on if they resulted from a direct volcanic activity (pyroclastic) or processes that reworked pyroclastic fragments. Furthermore, the deposits are subdivided into massive and stratified, depending on their primary mechanisms of transport and emplacement. By confirming the results from previous studies, our study permits to depict a more precise paleo-environmental picture of the processes that occurred in the Amazonian Craton during the Late-Paleoproterozoic. In particular, the presence of large regional-scale fissural systems and caldera collapses produced large silicic explosive volcanic eruptions, also accompanied by the emission of large volume effusive products. Although studies on the Amazonian Craton are still scarce and controversial, the present study provides new evidence that this volcanism may have formed one of the largest Silicic Large Igneous Provinces (SLIP) on earth. Our data also confirm that at least two major Paleoproterozoic periods of formation of volcanic rocks exist in the Amazonian craton. This point is of great relevance for any future interpretation of the geological evolution of this craton.

Response to Reviewers: To reviewer 1 Nils Lenhardt:

Dear reviewer,  
we respected and changed most of the corrections suggested in  
particularly we followed the suggestions to divide the lithofaciological  
description and simplify the geological framework.  
Thank you for the time you spent reading this long manuscript.

To reviewer 2 Roberto Dall'Agnol:

Dear reviewer,  
thank you for your suggestions especially those related to the geological  
framework and geochemical analyses. We considered and accepted most of  
the changes suggested.  
Now, the manuscript appears more clear.

Research Data Related to this Submission

-----  
There are no linked research data sets for this submission. The following  
reason is given:  
Data will be made available on request

Dear Editor of Gondwana Research,

Please find attached the manuscript: "*The 2.0-1.88 Ga Paleoproterozoic evolution of the southern Amazonian Craton (Brazil): an interpretation inferred by lithofaciological, geochemical and geochronological data.*" by Roverato M., Giordano D., Giovanardi T., Juliani C., and Polo L. which we would like to submit on Gondwana Research. This study documents in detail the extremely well preserved Paleoproterozoic architecture of a series of felsic volcanic and volcanoclastic rocks found in the southern part of the Amazonian Craton, Brazil. We aim to improve the current knowledge of the rare subaerial volcanism investigated in Precambrian volcanic regions by adding new textural data useful to better constrain this still poorly known volcanism. We provide also new geochemical and geochronological data that will increase the dataset of the study volcanic rocks. We use here a modern volcanological approach to describe the wide range of different lithofacies that our deposits display. We believe that this contribution will help to further our understanding of the geology of the Amazonian craton and, also, of other Precambrian volcanic areas worldwide.

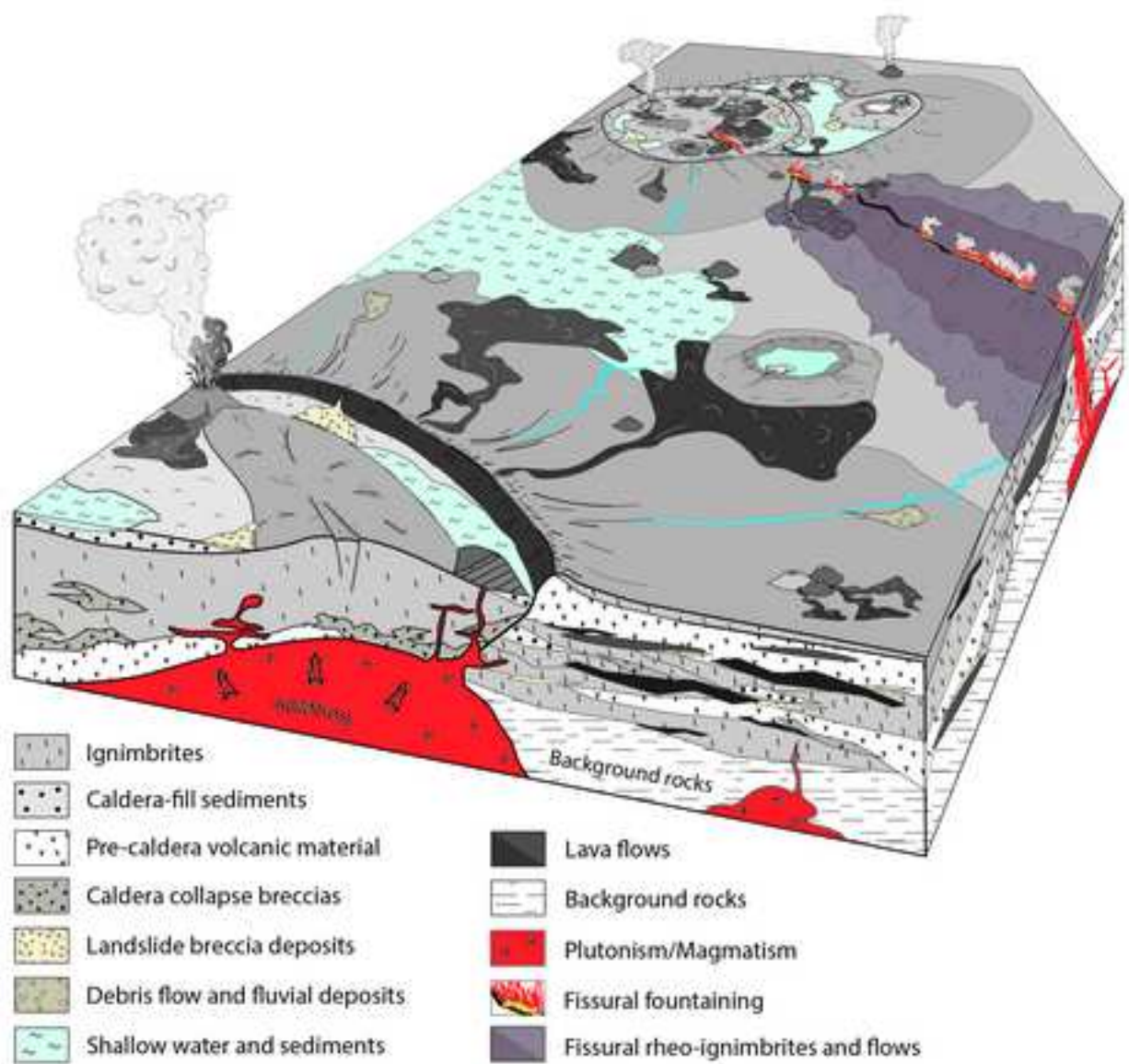
We hope that the manuscript will be of interest for a first class international journal like GR.

Yours sincerely,

Dr. Matteo Roverato

## Highlights

- The modern lithofaciological approach is used here to described the volcanic and volcanoclastic rocks of the Precambrian Amazonian Craton.
- The U-Pb geochronological data presented in the manuscript yielded three new ages of ca. 2.0 Ga and one new age of ca. 1.88 Ga that, linked with 31 geochemical analyses, increase the dataset available for the Amazonian craton and ancient terrains in general.
- The Paleoproterozoic volcanic activity that formed the large felsic rocks cropping out in the southern Amazonian craton is characterized by a fissure-fed and caldera volcanism with production of extensive lava flows and/or high-grade to rheomorphic ignimbrites, linked with other fragmental products of different type.



Reviewers' comments:

Reviewer #1: One of the main concerns of this manuscript is the lithofacies description and interpretation that oversimplifies the different lithofacies by only distinguishing them by their massive or stratified appearance. The observations and related interpretations seem to be of good value. However, I would suggest to make more subdivisions and adopt the terminology of McPhie et al. (1993) for non-genetic descriptive terms for each single lithofacies.

The manuscript contains too many different abbreviations for geological provinces, lithofacies types, etc. After a while, this appears rather confusing. Therefore, I would suggest to keep the abbreviations at a minimum, for instance for the lithofacies types and few other long terms that are constantly repeated throughout the text.

In the following paragraphs, some major suggestions are provided in detail. Further comments and suggestions (or questions) can be found in the attached commented manuscript.?

**Author response:**

Line 139:

**Reviewer:** What are the errors for the 2100 and 2875 Ma ages?

Line 148: What is the error for the 1880 Ma age?

**Author:** The reviewer further on suggests to simplify this chapter. We deleted the paragraph as suggested.

Lines 127-206:

**Reviewer:** A lot of information is presented here including many information on geochronology. Some of this information that is not particular of help for the understanding of the rest of the manuscript can probably be deleted or shortened. Furthermore, I suggest to show all mentioned locations on a map.

**Author:** Done! As suggested by Reviewer 1 we reduced this part by keeping some of the literature information useful to put our study in a wider context.

**Rev:** it would be good to see the detailed stratigraphy of the area: well we should wait for to more fieldwork.

**Author:** That's the problem, very few data are available nowadays, and actually this is one of the first work that try to present more detailed stratigraphy. We should organize a fieldwork there together!

line 226-229:

**Rev:** The way you describe the volcanoclastic rocks here, they are all fragmental rocks that are primary and syn-eruptive. However, effusive eruptions do not form fragments

**Aut:** yes they do! One example is a basal breccia of a thick lava flow. You can find a very well developed clastic deposit underneath the flow. In any case we deleted the point to avoid confusion.

Line 237:

**Rev:** Surely, no all volcanic products exhibit the same features. Otherwise, there would only be one lithofacies type. Please better describe what you mean.

**Aut:** Changed

Lines 239-243:

**Rev:** Not so many words are needed for this. Simply state that Table 1 shows all documented lithofacies including their descriptions and interpretations.

**Aut:** Done!

Lines 281-288

**Rev:** should be rephrased as they are difficult to read and understand. In particular, the paper of White and Houghton (2006) should be used here in order to define the terms pyroclastic and volcanoclastic. As it is, this part is not particularly clear. For once, effusive eruptions do not form volcanoclastic sediments. Furthermore, ignimbrites may also form due to PDCs.

**Aut:** Ok. We changed the sentence

Lines 297-486:

**Rev.:** There are some good observations and interpretations in here. However, the simplification into massive and stratified volcanoclastic rocks (containing everything from PDC deposits to autobreccias of a lava flow) and epiclastis rocks (containing everything from fluvial to mass-flow deposits) makes the chapter quite confusing. I suggest to make more subdivisions and describe the single lithofacies types one by one, probably adopting the non-genetic descriptive terms of McPhie et al. (1993). This way, the text may become slightly longer. However, the scientific value of the observations will significantly increase.

**Aut.:** Done! As the reviewer suggested, we divided the lithofacies descriptions and interpretations. Thank you for the suggestion!

Lines 785-789:

**Rev:** "Here we also image that an ideal late-convergent to extensional geotectonic environment was likely similar to that proposed in our discussion paragraph, where a post-orogenic to extensional regime for the period ~ 1.88 Ga was characterized by the emission of large volcanic felsic products." This sentence sounds very confusing and should be rephrased. For instance:

"The described volcano-sedimentary sequences that were characterized by the emission of large volcanic felsic products were formed in a post-orogenic to extensional regime during ~ 1.88 Ga."

**Aut:** Done! We changed the sentence!

Lines 789-791:

**Rev:** "With this contribution we want also stress the importance of the results obtained by investigating the lithofaciological character of the deposits instead of only carrying out geochemical studies." This should rather be obvious and can be omitted.

**Aut:** Done! We deleted the sentence



Reviewer #2: I appreciated your manuscript, in particular, the careful and detailed field and petrographic descriptions of lava flows and volcanoclastic sequences. Your data confirm the existence of, at least, two major Paleoproterozoic periods of formation of volcanic rocks in the Amazonian craton and this point is of great relevance for understanding the craton evolution. Your model to explain the origin of volcanic sequences is also a significant contribution. I made a series of comments and suggestions that I hope will help you to improve your manuscript. Most of them are not mandatory and should be evaluated for you. I have attached a pdf version indicating the main criticisms and indicating possible formal corrections.

Best regards,

Roberto Dall'Agnol

**Author response:**

1 - Abstract, p. 5, l. 41-45 - Please, rewrite. It is not clear.

**Done**

2 - Introduction, p. 5, l. 54-55 - I suggest to delete.

**Done**

3 - p. 5, l. 58-59 - References?

**Done**

4 - p. 5, l. 62 - the crust is...or the rocks are...???

**Done**

5 - p. 5, l. 63-67 - You are talking about the entire Amazonian craton but your references refer only to the regions of your direct interest. It is not reasonable to talk about mineral resources in the craton without any mention to the world-class mines of Carajás (iron, IOCG). I suggest to include also references of that province or to make clear that you are talking essentially about the Tapajós and Xingu regions.

**Done**

6 - p. 6, l. 71-74 - All this is the normal view of the Amazonian craton and it is correct in some degree. But I wonder if your contribution should not be directed to show that, in spite of the dominant conditions in the region, there are many areas where field information can be obtained and fresh rocks are available. This makes possible the petrological, geochemical and metallogenetic research on the craton that preserves better than one could imagine the signature of Precambrian events. You could illustrate this comment with the comprovado occurrence in the Tapajós province of Paleoproterozoic alluvium (Juliani et al., 2005). In other words, better than reinforce the general view, you should show that many things are possible in the geological studies of the craton.

**We deleted the sentence**

7 - p. 6, l. 84-89 - This remark is very important but it looks contradictory with you have said before (cf. my remark 6) about the geological research in Amazonia. Please, make consistent changing the previous generic and not representative description of Amazonian conditions.

**Done!**

8. p. 66, l. 89-90 - This statement was entirely true in the pioneer works of the research group but now it looks not very appropriate to say that they 'are novel in this area'. You have said before that the present work is a continuity of previous research developed by the group in the last 15 years.

## Changed it!

9 - p. 6, l. 99-101 - This description of the Amazonian craton evolution is oversimplified and do not give a clear idea of the more recent tectonic models proposed to explain it. You should present it more critically. E.g., the existence of a large Archean platform is not entirely demonstrated. You are mentioning the models of tectonic-geochronologic provinces and the existence of domains formed after the Trans-Amazonian event in the following. These topics should be better integrated and more consistent.

10 - p. 7, l. 104-107 - The relevance of the Uatumã Group in the Paleoproterozoic evolution of the craton is clearly demonstrated but it cannot be said that "All volcano/plutonic rocks forming the craton are attributed to the Uatumã Supergroup". There are many magmatic units, including Paleoproterozoic ones, that have nothing to do with the Uatumã Supergroup. You should clarify these points, showing the relevance of the Uatumã event but with a more rigorous description of it.

11 - p. 7, l. 108-110 - Your statement is not helping to show the real stage of knowledge of the Amazonian craton. I would say that we have now a general picture of the craton evolution and there are some portions of it relatively well studied, side by side with poorly known areas.

**These last 3 points (9,10,11) are related to the geological framework chapter. We changed the chapter in accordance with the correct suggestions of reviewer 2 and, also the points commented by reviewer 1 who suggests to simplify the information. As suggested by Reviewer 2 we also changed figure 1 so to provide the wider context of application of our research**

12 - p. 7, l. 116-119 - Is this context of ocean-continent subduction and flat subduction consistent with the hypothesis of "The transition from late-convergent to extensional tectonic setting could register the beginning of the taphrogenesis that marked the Amazonian Craton throughout the Mesoproterozoic (your abstract)"?

**Yes, because the volcanic rocks studied (specially the andesitic rocks well described in Fernandes et al., 2011 and Roverato et al., 2017, but also the felsic older rocks in TMP) are related to a continental arc tectonic environment. The idea is that the system passes from an ocean-continent flat-subduction setting to a post-orogenic /extensional tectonism (as proved by the presence of younger felsic A-type rocks in SFX)**

13 - p. 8, l. 148 - Some authors employ the term 'aluminous' for some A-type granites that vary generally from metaluminous to mildly peraluminous (e.g., King et al., 1997; Larmarão et al., 2002). However, this is a not rigorous term because these A-type granites are typically low Al<sub>2</sub>O<sub>3</sub> granites (Dall'Agnol and Oliveira, 2007, Lithos). King et al. (Australian Journal of Earth Sciences, 2001, 48, p.501) have abandoned and advised against the use of this term because 'aluminous' can be related to S-type peraluminous granites that are entirely distinct of the A-type granites. For this reason, I suggest to the authors to avoid the use of the term 'aluminous' for A-type granites.

**This is the only point where we used this term. In any case due to changes, we deleted the entire paragraph**

14 - p. 8, l. 151 - Please, verify the error of 1870  $\pm$  0.008 Ma.  
**It is correct in Juliani et al., 2005**

15 - p. 8, l. 158 and 160 - alkaline is ambiguous in this context because it can be confused with peralkaline. I suggest to delete alkaline.

**Done**

16 - p. 9, l. 172, Fig. 1 and 2 - The presentation of the figures is very poor and should be improved. In figure 1, only the Brazilian part of the Amazonian craton is represented and the reference of the model of geochronologic provinces adopted is not informed in the caption of the figure. The Rio Negro province is not correctly represented.

The schematic geologic maps of Figure 2 do not follow the classical conventions. The colors adopted for different geologic units are inappropriate. I suggest to revise entirely figures 1 and 2.

**Improved fig 1 and 2. In figure 2 we added the location of the outcrops and rocks presented in the paper. I don't agree that about the geological unit, I'm using my symbols well expressed in the legend.**

17 - p. 9, l. 178-181 - It would be more appropriate to say that the basement of the volcano-plutonic complex is not exposed. It could be similar to the Mesoarchean units of the Carajás province, as suggested by Nd TDM ages obtained by Teixeira et al. (2002) in andesites and rhyolites of Xingu area. It was published recently a synthesis of new geochronological data about the 1.88 Ga granites of the Carajás province (Teixeira et al., 2018, J South American Earth Sci). The authors have also presented a discussion about the relevance of the 1.88 Ga event in the craton and elsewhere.

**We deleted the paragraph.**

19 - p. 10, l. 217-220 - Independent of the degree of alteration and lithification, pyroclastic and volcanoclastic sequences need to be defined in the field, because they mix igneous and sedimentary features. Hence, I suggest you to emphasize the relevance of field observations in your work better than to put in relief the restrictions you had. Another point is that 'alteration' should be possibly mean hydrothermal alteration and it should be distinguished of weathering alteration because readers can suppose that your rocks were intensely weathered and you are clearly showing that you were able to collect fresh samples for petrographic, geochemical and geochronologic studies.

**We deleted the paragraph as also suggested by the other reviewer.**

20 - p. 10, l. 230 - Coastal? Is it accurate?

**YES**

22 - p. 11, l. 250, Fig. 3 and its caption - It should be given a general idea of the location and informed the point of sampling where the photographs were taken and the units presented in each case. This should be done also in the captions of figures 4 and 5.

**Done and thank you for the suggestion**

24 - p. 11, l. 264 - 265 - pervasive does not give an idea of abundance. 10 vol % to how much in vol %?

**Done!**

25 - p. 13, l. 312, Fig. 5B - There is an euhedral crystal in the central lower part of Figure 5B that is named plg (plagioclase). I suspect that it can be a crystal of alkali-feldspar. Please, verify.

**Sure! Changed it!**

26 - p. 13, l. 326 -330, Fig. 6 - It is important to indicate the location of that sequence in the geological map of Figure 2.

**Done**

27 - Fig. 8, 9, 10, 11 - You present an extremely valious register of field and macroscopic aspects of the studied volcanic sequences. It looks very important to me that the location of the documented points should be given. These points will be a relevant reference for future studies.

**Done**

28 - p. 18, l. 491, Fig. 12 and its caption - In the caption of the figure are mentioned the TAS, AFM and SiO<sub>2</sub>-K<sub>2</sub>O digrams. However, in the available version of your manuscript the Figure 12 is identical to Figure 13 and the diagrams mentioned in Figure 12 are not presented. Without the figures it is difficult to evaluate the consistence of your text.

**Done**

29 - p. 18, l. 489 Geochemistry, Table 2 - You should give information about the methods employed and the laboratory where the chemical analyses were done.

**we have added a small 'Analytical Methods' chapter to the text.**

30 - Chemical Analyzes, Table 2 - It should be included on Table 2 the classification and the volcanic facies of the analyzed rock. It is important to distinguish, if possible, the rocks with I-type and A-type affinity. The meaning of V, I and R should be explained in the foot of the table.

**the meaning of VC, I and R is already in the figure caption. We have reformulated the text to make it more clear. We have also added the classification of I- and A-type affinity**

31 - p. 19. l. 524 - 529, Fig. 14 - The distribution of the studied rocks in the Pearce's diagram of 1984 suggest in fact that they can be related to a post-collisional setting (cf. Pearce, 1996, Episodes).

**we have added the diagram to Fig. 14 and add it to the chapter.**

32 - p. 20-23, l. 571-659; 7. Discussion

7.1 Subduction-related to extensional setting - In general, this topic of discussion section is well organized and looks consistent to me. I have some remarks that hope can help you in the review.

- p. 20, l. 573-576, Fig. 14 - As mentioned before, if you consider Pearce (1996), the distribution of the whole of your samples suggest a post-collisional setting for the studied rocks.

**we have taken it into account and added some paragraphs at the discussion.**

p. 20, l. 576-577, Fig 14, diagram FeO<sub>t</sub>/MgO vs. Zr+Nb+Ce+Y - The analyzed rocks plot mostly to the right of the fields of typical I and S granites because they are enriched in HFSE compared to these granites. It is not correct to say that your rocks have low HFSE. On the contrary, the relatively high HFSE contents distinguish your rocks of typical I and S granites and approach them of A-type rocks.

**We agree. The sentence was not clear; we want to point out that TMP volcanics have enrichment in incompatible elements with respect HSFE which suggest the occurrence of crustal component in the melt. We have rephrased the sentence to make it more clear and pointing that our samples have also high HSFE content which shift the volcanics composition from the I- and S-type granites to the A-type field.**

It is also relevant to mention that your ~2.0 Ga volcanic rocks are a little distinct in this respect of the Vila Riozinho formation rocks (Lamarão et al., 2002) that show a little lower HFSE contents when compared to your TMP samples. Besides, the hypothesis of a more evolved character for your rocks compared to VR of Lamarão et al. (2002), you should consider the possibility that the 2.0 Ga volcanism is not uniform in composition and advocate for TMP rocks an intermediate geochemical character between the VR and MA. The rocks of TMP analyzed (Fig. 2) are dispersed in a large area and not restricted to the VR type area. So, is it reasonable that some geochemical variations could occur.

**notwithstanding we think that the TMP derived from more evolved melts with respect to the VR, as observed by higher Si, K, trace elements and evidences of fractional crystallization in the TMP melts, we agree that these features could be possibly related to 'heterogeneities' in the magmatism. We have added a paragraph to point out this possibility,**

- p. 22, l. 631-639 - The 2.0-1.88 Ga event in the craton and also in the scale of the planet, as indicated by Antonio et al. (2018), has effectively great relevance. A similar discussion about the 1.88 Ga anorogenic granites of the Carajás province was recently presented (Teixeira et al., 2018; SAMES) and it can allow you to go deep in this point of the discussion.

**we appreciate the indication and we have provided to discuss a little further the geodynamic setting of the TMP and SFX magmatism.**

**The 2.0-1.88 Ga Paleoproterozoic evolution of the southern Amazonian Craton (Brazil): an interpretation inferred by lithofaciological, geochemical and geochronological data.**

Roverato<sup>\*1,2</sup> M., Giordano<sup>3,4</sup> D., Giovanardi<sup>5</sup> T., Juliani<sup>2</sup> C., Polo<sup>2</sup> L.

1. YachayTech University, School of Geological Sciences and Engineering, Hacienda San José, Urcuquí, Ecuador.
2. ~~Departamento de Geologia Sedimentar e Ambiental (GSA)~~, Instituto de Geociências (IGC), Universidade de São Paulo, INCT – Geociam, SP, 05508080, Brazil.
3. Università degli studi di Torino, Dipartimento di Scienze della Terra, via Valperga Caluso 35, 10125, Torino, Italy.
4. Centro Nazionale delle Ricerche (CNR), Istituto di Geoscienze e Georisorse (IGG), via G. Moruzzi 1, 56124, Pisa, Italy.
5. Università di Modena e Reggio Emilia, Dipartimento di Scienze Chimiche e Geologiche, 41125, Modena, via Campi 103, Italy.

\*Corresponding Author: ~~matteomroverato1809@yachaytech.edu.ec@gmail.com~~

Keywords: Paleoproterozoic volcanism; Amazonian craton; Fissure eruption; Felsic volcanism; Lithofacies analyses

**Abstract**

~~The study of Paleoproterozoic rocks is crucial for understanding Earth's tectonic evolution during the time when most of the modern crust and ore deposits were formed. Paleoproterozoic rocks represent some of the most interesting rocks to comprehend Earth's tectonic evolution during the Precambrian Supereon when most of modern crust and ore deposits formation occurred. The rocks of the Brazilian Amazonian Craton record one of the most-complete and best-preserved Paleoproterozoic magmatic episodes on Earth. Amazonian rocks record one amongst the most complete and best-preserved Paleoproterozoic magmatic episodes on Earth.~~ Following previous investigations, we present new lithofaciological and stratigraphic records of the felsic rocks of the Tapajos Mineral Province (TMP) (~ 2-1.88 Ga) and the São Felix do

Formatted: Default Paragraph Font, Font: 12 pt

Formatted: Font: Times New Roman, No underline, Not Highlighted

Formatted: Font: Times New Roman, No underline, Not Highlighted

Formatted: Font: Times New Roman, No underline

Xingu region (SFX) (~ 1.88 Ga) which, combined with new petrological and geochronological data, help providing a more complete understanding of the tectonic, magmatic and volcanological evolution of the Amazonian Craton. This magmatism/volcanism is thought to be formed in a ~~late-/post--~~orogenic to extensional regime confirmed by the new geochemical data presented here. The transition from late-convergent to extensional tectonic setting could register the beginning of the taphrogenesis that marked the Amazonian Craton throughout the Mesoproterozoic. The modern volcanological approach of this contribution can serve as a model for the evolution of Precambrian volcano-sedimentary basins around the world. The large amount of rocks analyzed are divided into primary and secondary volcanoclastic volcanoclastic and sedimentary products depending on if they resulted from a direct volcanic activity (pyroclastic) or reworked processes that reworked pyroclastic fragments. In this second group are also included the epiclastic rocks constituted by all sediments that had been reworked before, independent of their source and composition. Furthermore, the deposits are divided in ~~and~~ massive ~~and~~ stratified, depending on their different transport and emplacement mechanisms. By confirming the results from previous studies, our study permits to depict a more precise paleo-environmental picture of the processes that occurred in the Amazonian Craton during the Late-Paleoproterozoic. In particular, the presence of large regional-scale fissural systems with caldera collapses produced large silicic explosive volcanic eruptions, which were also accompanied by the emission of large volume effusive products. Although studies on the Amazonian Craton are still scarce and controversial, the present study provides new evidence that this volcanism may have formed one of the largest Silicic Large Igneous Provinces (SLIP) on earth.

## 1. Introduction

The Proterozoic Eon (2500 – 541 Ma) is the longest and youngest part of the Precambrian Supereon. This ~~E~~eon represents the time just before the proliferation of oxygen accumulation and complex life on Earth. This period was likely the most tectonically active in Earth's history. In fact, it is also the period during which the largest portion of the modern crust (43%) and mineral ores were produced (Condie, 2000). Studies by Condie (2000) and Rino et al. (2004) suggest that crust production took place episodically, forming predominantly granitoid crust and secondary volcanic and metamorphic rocks, some of which are extraordinarily well preserved.

Formatted: Font: Times New Roman, 12 pt, No underline

Formatted: Font: Times New Roman, 12 pt, No underline

Formatted: Indent: First line: 0 cm

The Amazonian Craton (AC) is one of the largest Precambrian terrains in the world ( $4.6 \times 10^6 \text{ km}^2$ ) (Almeida et al., 1981). It occupies approximately half of the Brazilian territory and it is the location of important mineral resources such as gold, iron, copper, and tin, among others (Faraco et al., 1997; Bahia and Quadros, 2000; Juliani, 2002; Klein et al., 2002, ~~;~~ Klein et al., 2004; Reis et al., 2006; Klien and Carvalho, 2008; Monteiro et al., 2008; Juliani et al., 2014, Dall'Agnol et al., 2017). Although the geological investigation of the AC has recently seen a renewed interest of the national and international scientific community, mainly because of the massive presence of ore deposits, a general consensus related to the interpretation of its complex Paleoproterozoic evolution is still missing. Ancient volcanic regions represent a challenge for the understanding of emplacement dynamics especially when the stratigraphic relationships are difficult to decipher or blurred by erosion or vegetation cover.

~~In fact, the difficult access to the outcrops, due to dense forest cover and to the presence of extensive water basins together with, in most cases, the bad preservation of the ancient outcrops with frequently obliterated structures and textures, significantly complicate this task.~~

The present work constitutes the natural prosecution of previous investigations, carried out by our research group (Juliani et al., 2005, ~~;~~ Juliani et al., 2010, 2014; Fernandes et al., 2011; Juliani et al., 2014; da Cruz et al., 2015; Roverato, 2016; ~~;~~ 2015; Roverato et al., 2016; Roverato, 2016; Roverato et al., 2016, 2017), which are devoted to characterize the dynamics of emplacement of Precambrian volcanic rocks and their relationships to sedimentary facies. The study area comprises of the Tapajós Mineral Province (TMP) and the São Felix do Xingú (SFX) region, Pará state, northern Brazil. This contribution provides a means to interpret the volcanic processes active in this region during the Precambrian, mainly based on field observation and detailed lithofacies analyses. In addition, ~~new~~ geochemical and geochronological data are provided. The superb preservation of the rock textures investigated here is such that they help us to better constrain the genetic mechanisms that brought to the formation of the investigated felsic deposits. Our study demonstrates how powerful is the approach of rock structure and texture characterization to the interpretation of the eruptive processes that governed the emplacement of volcanic and volcanoclastic sequences. The detailed lithofacies characterization and the stratigraphic reconstruction are ~~novel~~ important in this area and constitute a powerful ~~new~~ key-tool to appropriately interpret

Formatted: No underline, Superscript

Formatted: No underline, Superscript

Formatted: Indent: First line: 0 cm

Formatted: No underline, Font color: Auto, Highlight



the evolution of Precambrian volcano-sedimentary basins. Such an approach would turn to be useful when employed to investigate ancient terrains associated both to the ancient Amazonian felsic volcanism and Precambrian terrains in general.

## 2. Geological evolution of the southern portion of the Amazonian craton

The AC (Almeida et al., 1981) is located in the northern part of South America and is divided into two Precambrian shields, the Central-Brazil (or Guaporé, southern portion) and Guiana Shields (northern portion), which are separated by the Phanerozoic Amazonian Sedimentary Basin (Fig. 1) (Almeida et al., 1981). The entire craton has become stable before the end of the Precambrian (Dall'Agnol et al., 1994).

The AC (Almeida et al., 1981) has been considered (Amaral, 1974; Hasui et al., 1993; Costa and Hasui, 1997) as a large Archean platform that had been reworked and reactivated during the ca. 2100 Ma Trans-Amazonian event (Amaral, 1974; Hasui et al., 1993; Costa and Hasui, 1997). The AC is located in the northern part of South America and is divided into two Precambrian shields, the Central-Brazil (or Guaporé) and Guiana Shields, which are separated by the Phanerozoic Amazonian Sedimentary Basin (Fig. 1) (Tassinari and Macambira, 1999; Santos et al., 2000). All igneous rocks forming the craton are attributed to the Uatumã Supergroup, which extends to an area of at least 1,500,000 km<sup>2</sup> (Dall'Agnol et al., 1999; Lamarão et al., 1999).

Alternative ideas Although several approaches have been used to unravel the complex tectonic evolution of these huge and frequently inaccessible territories, a clear understanding of the geological past of this area is still largely unknown. Based on geochronological and isotopic data, Teixeira et al. (1989), (Teixeira et al., 1989; Tassinari and Macambira, 1999), and Santos et al. (2000) divided the craton into several, predominantly NW-oriented geochronological provinces, which have been interpreted as successive continental accretionary events, followed by granitic magmatism and tectonic reworking (Tassinari and Macambira (1999), Santos, (2003), and Vasquez et al. (2008) identified six and eight geochronological provinces, respectively (Fig. 1).

In a recent review Teixeira et al. (2019) report that the AC is the host of four LIP-scale (or SLIP) magmatic events discriminated by the Orocaina, Uatumã, Avanavero and Rincón del Tigre events, among other intra-plate activity through time and space. The igneous rocks described in the present manuscript are widely attributed to the Uatumã event (Dall'Agnol et al., 1999; Lamarão et al., 1999). More recently,

Formatted: Indent: First line: 0 cm

Formatted: Adjust space between Latin and Asian text, Adjust space between Asian text and numbers

Formatted: No underline, Not Highlight

The studied ~~Juliani and Fernandes (2010), Fernandes et al. (2011) and Roverato et al. (2017)~~ suggested that the entire region is located between TMP and SFX, which may be considered to be related to a continental arc, with a NE-SW arc migration as suggested by Giuliani and Fernandes (2010), Fernandes et al. (2011) and Roverato et al. (2017). According to these authors a migration from the Serra do Cachimbo graben (in TMP where the subduction trench is located) towards the SFX could be explained by a change in the subducting angle of the oceanic plate beneath the continental plate. This is in agreement with the flat-subduction plate settings proposed by previous authors in other parts of the world (Ferrari et al., 2012; Gutscher et al., 2000; Kay et al., 2005; Mori et al., 2007; Manea et al., 2012; ~~Fernandes et al., 2011; Giuliani et al., 2014~~).

## 2.1. The TMP (Tapajós Mineral Province)

The TMP (~~Fig. 2a~~) is primarily situated in the Tapajós–Parima geochronological/tectonic province (Santos et al., 2000) with the eastern part belonging to the Amazonia Central geochronological/tectonic province (Fig. 1). Based on Sm–Nd data and U–Pb ages (2100–1870 Ma), Santos et al. (2001, 2004) and Vasquez et al. (2008), identified several different domains for the Tapajós–Parima geochronological province and consider the TMP as a sequence of continental magmatic arcs (~~Ferreira et al., 2000; Santos et al., 2000, 2004; Vasquez et al., 2000; Klein et al., 2001; Lamarão et al., 1999, 2002).~~ The oldest granitoids and gneisses in this region belong to the Cuiú–Cuiú magmatic arc complex; the Conceição tonalite (Cuiú–Cuiú magmatism) yielded a U–Pb zircon age of  $2019 \pm 23$  Ma (Santos et al., 2000). The supracrustal sequences of the Jacareacanga Group are considered broadly coeval with the Cuiú–Cuiú complex. Both units are related to early stages of magmatic arc development (Ferreira et al., 2000; Klein et al., 2001). Detrital zircon ages of ca. 2100 and ca. 2875 Ma have been obtained for the Jacareacanga Group (Santos et al., 2000). Stratigraphically above the Jacareacanga Group is the Vila Riozinho Formation, formed by ca. 2000–1990 Ma intermediate to felsic volcanic rocks (Lamarão et al., 2002). These units are intruded by the ca. 2000–1970 Ma syn- to late-orogenic calc-alkaline granitoids of the Creporizão suite (Lamarão et al., 1999; Vasquez et al., 2000). Following this first intrusive event, a second intrusive event was characterized by the ~~1907  $\pm$  9 and 1892  $\pm$  6 Ma granitoid rocks of the Tropas Suite (Santos et al. 2001, 2004). The ca. 1880 Ma Parauari suite corresponds to a younger generation of post-orogenic, calc-alkaline granitoids and is mainly exposed in the northeastern part of the~~

Formatted: Indent: First line: 0 cm

Formatted: Indent: First line: 1.27 cm

~~region. The Maloquinha ca. 1880 Ma aluminous A-type granite plutons are also found in the province and closes the sequence.~~ Late Paleoproterozoic volcanism of the Tapajós domain is represented ~~by the Vila Riozinho Formation, formed by ca. 2000-1990 Ma intermediate to acid volcanic rocks (Lamarão et al., 2002), and~~ by the Iriri Group that can be divided into the Bom Jardim (Almeida et al., 2000), Salustiano (1870 ± 0.008 Ma; Juliani et al., 2005) and Aruri (Pessoa et al., 1977) formations.

~~The Bom Jardim Formation (1898 ± 5 Ma, Santos et al., 2001) consists of mafic to intermediate high-K to shoshonitic calc-alkaline rocks while the latter formations are characterized by rhyolites, dacites and their pyroclastic and epiclastic derivatives. Juliani et al. (2005) considered the Bom Jardim volcanism as a preliminary step of the Iriri event representing pre-caldera volcanism followed by the Salustiano and Aruri caldera-related felsic activity. Post-caldera volcanism is characterized by ring-felsic volcanic structures that produced alkaline A-type (Vasquez and Dreher, 2011) rhyolitic lavas and volcanoclastic deposits. Lamarão et al. (2002, 2005) described the alkaline-felsic A-type Moraes Almeida volcanic sequence (1890 ± 6 Ma rhyolite, 1875 ± 4 Ma ignimbrite) represented by lavas and ignimbrites as part of the Iriri Group. Juliani et al. (2014) consider these last A-type alkaline rocks as similar in composition and age to the Santa Rosa Formation that crops out in the São Felix do Xingú region (SFX), which is considered to have formed by the same fissural-type volcanism (Juliani and Fernandes, 2010; Fernandes et al., 2011; Roverato et al., 2016). Preliminary data indicate that these rocks, for both TMP and SFX, display a very low grade of metamorphism, falling into the prehnite-pumpellyite field (Echeverri-Misas, 2010; Lagler et al., 2011; Fernandes et al., 2011).~~

## 2.2. The SFX (São Felix do Xingú region)

According to the work of Santos (2003) and Vasques et al. (2008) the SFX region belongs to the Amazonia Central province (Fig. 1). The study area (Fig. 2b) is located near to São Felix do Xingú city, which corresponds to the southern portion of the Carajás Province. ~~The geographical limits of SFX are still uncertain, mainly due to the difficult access to the area. The eastern limit is marked by the Archean TTG rocks several km east to Xingu River while the dense vegetation cover does not permit access to the south. The northern limit is roughly marked by the Archean Xingu complex and younger intrusive formations (Macambira and Vale, 1997). The basement of the SFX region is represented by the Archean Rio Maria Granite-Greenstone~~

~~Terrain and the metavolcano-sedimentary units of the Itacaiúnas Supergroup (Araújo et al., 1988).~~ The Paleoproterozoic volcanic sequences in the SFX comprise the basal Sobreiro and upper Santa Rosa formations (Macambira and Vale, 1997; Juliani and Fernades, 2010), which are crosscut by the Sn-bearing A-type granitoids of the Velho Guilherme Suite (Teixeira et al., 2002). Antonio et al. (2017) published the first U-Pb ages on zircons for the Santa Rosa Formation with  $1877.4 \pm 4.3$  Ma for a rhyolite and  $1895 \pm 11$  Ma for a dike. Recent geochronological data on a felsic porphyritic dike belonging to the Velho Guilherme suite yielded an age of  $1857 \pm 8.4$  Ma (Shrimp U/Pb zircon analyses; Roverato, 2016). Other available geochronological data yielded ca.  $1880 \pm 6$  Ma (TIMS Pb–Pb in zircon) for the Sobreiro Formation and ca.  $1879 \pm 2$  Ma (TIMS Pb–Pb in zircon) for the Santa Rosa Formation (Fernandes et al., 2011; Pinho et al., 2006; Teixeira et al., 2002). Despite their similar ages, their geochemical compositions, geological features and eruption styles point to their non-cogeneticity (Fernandes et al., 2011). ~~The Sobreiro Formation was defined for the first time by Macambira (1997) and Macambira and Vale (1997) as constituted by andesitic, trachy-andesitic and trachytic magmatism.~~ The Sobreiro Formation (SF) comprises basaltic andesite, andesite and less dacite massive lava flows and volcanoclastic rocks with high-K calc-alkaline signature (Fernandes et al., 2011; Roverato et al., 2017). According to da Cruz et al. (2015) late- to post-magmatic hydrothermal alteration in these rocks is responsible for a secondary paragenesis characterized by epidote, chlorite, carbonate, clinozoisite, sericite, quartz, albite, hematite and pyrite. The Santa Rosa Formation (SRF) is described by Fernandes et al. (2011) as characterized by four lithological facies with A-type signature: (i) rhyolitic lava flow and thick dikes of banded rhyolite and ignimbrite; (ii) highly rheomorphic felsic ignimbrite associated with un-welded ash tuff; (iii) felsic crystal tuff, lapilli-tuff and co-ignimbritic breccias; (iv) granitic porphyry stocks and dikes and subordinate equigranular granitic intrusions.

### 3. Results

~~Lithofaciological, petrological, geochemical and geochronological analyses were carried out in the course of this study in order to understand the geodynamic evolution of the study area. 31 new geochemical data for the TMP rock samples are presented here and compared with published data of Lamarão et al. (2002) and SFX previous results (Fernandes et al. (2011). The geochemical signature of SFX rock samples have~~

Formatted: Indent: First line: 0 cm

already recently been reported by Fernandes et al. (2011) who made unnecessary new analysis for our study. Four new geochronological data of rock samples from the TMP (3 samples) and SFX (1 sample) are also provided to compare with dating available for the AC. Finally, so far it concerns with the lithofaciological analysis we remind that a characterization of the granulometry of the deposits and of the shape of the fragments was qualitatively defined in the field, since the degree of alteration and lithification would have been impossible in the laboratory.

#### 34. Lithofacies analyses ~~and stratigraphy~~

Lithofaciological analyses were carried out in the course of this study in order to understand the geodynamic evolution of the study area. Here we report ~~onf~~ the lithofacies analysis of rocks recognized during our field campaigns (and after in petrological thin section) at the TMP and SFX provinces. Within the study area (TMP and SFX), massive to banded lava flows and rheomorphic ignimbrites (Fig. 3) as well as felsic volcanoclastic rocks of various origin (Figs. 4-8, 11) are frequently found. ~~Massive and banded lava flows and rheomorphic ignimbrites deposits (fig. 3) as well as volcanoclastic felsic rocks of various origin (e.g. pumiceous, effusive, ignimbritic) (fig. 4,5,6,7,8,11) are frequently found in both the studied areas (TMP and SFX).~~ Reworked (secondary) volcanoclastic rocks (Ffig. 9,10) and sedimentary alluvial/coastal clastic deposits (epiclastic) are also widely distributed in both TMP and SFX areas. Primary v~~V~~olcanoclastic rocks are here defined as those fragmental products formed during a syn-eruptive explosi~~onve or effusive events~~, which were deposited regardless of whether their transport occurs through air, water, granular debris or a combination of them (McPhie et al., 1993; White and Houghton, 2006, Manville et al., 2009; Roverato et al., 2017). On the other hand, all the units deposited as a consequence of a reworking process of pre-existing volcanic units are defined here as ~~sedimentary/reworked~~secondary volcanoclastic rocks. We also introduce into this group all those epiclastic products that constitute sediments that had been reworked before, independent of their source and composition.~~All TMP and SFX volcanic products share the same features both at outcrop scale and at hand specimen scale and for such a reason they will be presented together in the lithofaciological description. In~~ Table 1 we proposeshows a description and interpretation of the volcanoclastic

Formatted: Indent: First line: 0 cm

Formatted: Font: Times New Roman, 12 pt, No underline

lithofacies, both primary (~~volcaniclastic~~) and ~~reworked (secondary sedimentary)~~, for the deposits identified in the study areas. ~~In the following we will also provide an interpretation of the processes involved in their transport and emplacement.~~

#### ~~4.14.~~ Lava flows and rheo-ignimbrites

As already discussed by Roverato et al. (2016), the absence of unequivocal vitroclastic textures complicates the distinction between volcaniclastic and layered lava flows in general and, more in particular, for the ancient volcanic rocks investigated here. Lava flows found in the TMP and SFX provinces have both massive and banded structures (Fig. 3) while still maintaining, in some cases, glassy (obsidian) and aphanitic to porphyritic texture. Their composition varies from trachytic to rhyolitic with various content of alkalis (see section 5.8). The phenocryst assemblage consists mainly of plagioclase, quartz, Fe–Ti oxides and accessory-amount of zircon and apatite. Plagioclase and bipiramidal quartz crystals (Fig. 3a), with a maximum size of 3–4 mm, range from euhedral to anhedral, showing moderate to intense resorption. Plagioclase shows sieve texture indicating non-equilibrium conditions likely determined by magmatic transport. ~~Potassic~~ K-feldspar is also present as anhedral crystals in the groundmass often associated with sericite as alteration phase. Samples are generally affected by variable intensity of hydrothermal alteration. Plagioclase phenocrysts, in particular, present diffuse potassic and minor propylitic alterations. Abundant spherulites and lithophysae of variable size, from millimetric to decimetric, were recognized in almost every sample and are thus common in these rocks (Fig. 3b, c). The spherulites (radiating fibers of K-feldspar and cristobalite), ranging from few millimeters to 2 cm, are typically associated with perlitic fractures. Their content can vary from 10 vol% to ~~pervasive 70%~~ in the investigated rocks. A large amount of the spherulites developed into lithophysae commonly reaching 10–12 cm as a consequence of cooling and degassing processes. In the obsidian-type lavas (Fig. 3c), the groundmass is characterized by a micro-granophiric-like devitrification texture characterized by crystallization of amorphous quartz and alkali feldspar, a process that occurred after the emplacement of lava bodies. Several rocks show textures that are not easy to be associated to either lava flows or flows of fragmented material which underwent rheomorphism (Fig. 3d–g). Both banded lavas and rheo-ignimbrites display folds (Fig. 3d–g, see also Fig. 11e) and sub-parallel bands on mm- to dm-scale, planar to wavy (Fig. 3e, see also Fig. 6 and 7) (parataxitic fabric), that deform and

Formatted: Indent: First line: 0 cm

flattened around lithic fragments and crystals which alignment suggests the flow direction. In thin sections, the bands are characterized by extremely flattened vitroclastic textures with the former glass completely replaced by a mixture of quartz and feldspar (Roverato et al., 2016).

#### 5.4.2. Primary volcaniclastic rocks

We consider primary volcaniclastic rocks those dense, scoriaceous and pumiceous products of fragmental character emplaced by primary-low intensity explosive processes, ~~frequently associated to effusive manifestations or highly explosive events associated to fall out, small pyroclastic density currents (PDC) or ignimbrites~~. With pyroclastic we refer to fragmental material generated by any kind of explosive volcanic activity and transported as ash-fall and pyroclastic density currents ~~by an explosive volcanism~~ (Manville et al., 2009), which deposition occurs by suspension settling, from traction, by en masse freezing, or any combination of these (White and Houghton, 2006). Depending on the mechanism of transport and the eruptive style these clastic rocks were distinguished into two different categories, i.e. massive and stratified; and they can vary from well sorted, poorly sorted or unsorted. The rocks are predominantly rhyolitic in composition (Fernandes et al., 2011, Roverato et al., 2016) and there is no significant geochemical difference from the lava flows. Nine main lithofacies (Lf) have been recognized for the volcaniclastic rocks: six of them are massive and three are stratified.

#### 5.1. 4.2.1. Massive

Six massive lithofacies (mAL, mLA, mLB, l-gwLA, m-gwLA and h-gwLA) were recognized during our field campaign, three of them belong to the welded ignimbrites sub-group (Table 1). By using the granulometric classification proposed by Fisher (1961), ash is defined as any fragment with size <2 mm, lapilli are fragments with size between 2 to 64 mm and blocks (or bombs) have sizes > 64 mm. Massive lithofacies includes all those deposits that display a massive coherent structure. Outcrops of such kind of lithofacies are constituted by a high percentage of ash up to block-rich textures. Most of the observed samples appear to have been affected by devitrification processes of the juvenile pyroclastic fragments and matrix. The presence of juvenile material linked with other observed textures such as broken crystals (Best and Christiansen, 1997) and eutaxitic fabric allows us to confirm that the rocks

Formatted: Indent: First line: 0 cm

Formatted: Indent: First line: 0 cm

Formatted: Font: Not Italic, No underline

Formatted: Font: Not Italic



belonging to lithofacies mAL, mLA, *l*-gwLA, *m*-gwLA and *h*-gwLA are fragmental and pyroclastic in origin. We discuss the meaning of Lf mLB below in section 5.1.2.

#### 5.1.1. Lf mAL; mLA (massive Ash to Lapilli; massive Lapilli and Ash)

Description: the ash to lapilli (mAL) and lapilli and ash (mLA) deposits (Fig. 4a-e, Fig.6) are heterolithologic, matrix supported, containing angular to sub-rounded medium to coarse devitrified lapilli (displaying axiolitic fabric), banded fragments, occasional (or absent) lithics and angular-shaped broken crystals of plagioclase, bipiramidal quartz and rare oxides (Fig. 5). In mLA, clasts <25 cm in size are randomly immersed in the groundmass (Fig 4d and 4e, 11d). Some of them are altered by carbonate minerals. Groundmass of mAL and mLA is formed by K-feldspar and quartz crystals, devitrified ash fragments and sericite crystals as phase of alteration (Fig. 5).

Interpretation: the general massive aspect and the poor sorting of mAL and mLA point to a laminar granular flow transport regime and the fine content suggests the deposition from a dilute fluid escape-dominated flow-boundary zone in which turbulent shear-induced tractional segregation is suppressed (Branney and Kokelaar, 2002; Sulpizio et al., 2007, Roverato et al., 2017). These lithofacies are interpreted as ash flow deposits suggesting the deposition from a pyroclastic density current (PDC) (Lenhardt et al., 2011; Sulpizio et al., 2014; Roverato et al., 2017). The coarser lithofacies mLA (fig. 4e) could be related to proximal co-ignimbritic breccias as result of deposition by denser pyroclastic granular flows (Branney and Kokelaar, 2002). The angular aspect of the clasts indicates short-period transport.

#### 5.1.2. Lf mLB (massive Lapilli and Block)

Description: this lithofacies (fig. 4f, fig.7) represents monolithologic coarse-grained rocks having high-clast content (clast:matrix ratios up to 3:1). Angular/sub-angular coarse lapilli and blocks up to 50-60 cm of devitrified banded or massive lava fragments are immersed in a devitrified fine lapilli and coarse ash matrix.

Interpretation: the blocky and monolithologic coarse-grained aspect of the lithofacies mLB and its position underneath thick flow-deposits is attributed to the basal auto-brecciation of lava flows and/or rheo-ignimbrite flows. Despite the lithofacies is likely a consequence of an effusive volcanic activity (in the lava-flow



case) it is considered anyway as part of the volcaniclastic group due to its fragmental character.

### 5.1.3. Lf *l*-gwLA; *m*-gwLA; *h*-gwLA (welded Ignimbrites)

Description: all massive deposits displaying welding characteristics have been grouped in the “welded ignimbrites” group (table 1), following the idea of “grade of welding” (Walker, 1983) (i.e. the amount of welding and compaction exhibited by deposits). The rocks are matrix-supported with sub-rounded to angular lapilli and ash lithic clasts, euhedral, subhedral and broken crystals (plagioclase and less quartz) and deformed devitrified juvenile fragments (*fiamme*). Slightly- (low-grade, *l*-gwLA), medium- (medium-grade, *m*-gwLA), well-stretched (high-grade, *h*-gwLA) *fiamme* (Fig. 6), as well as, devitrified shards define the eutaxitic fabric (Roverato et al., 2016). These fragments varying from millimetric to 3–4 cm in size are immersed in a homogeneous micro-granophiric-like devitrified groundmass (see Roverato et al., 2016 for details). Figure 6 shows a stratigraphic column representing a 35 m thick sequence of ignimbrite deposits found in the TMP, displaying very low-grade to high-grade welded fabric where the grade of welding increases toward the top of the succession. The very top of the sequence is characterized by columnar jointing.

Interpretation: the massive aspect and the poor sorting of the lithofacies *l*-gwLA, *m*-gwLA and *h*-gwLA point to a laminar granular flow transport regime, interpreted to be deposited from a pyroclastic density current (PDC). The welded character of these lithofacies is indicative of hot PDC emplacement and compaction that result into the low- up to high-grade eutaxitic fabric. This process is favored by loading-compaction, low-viscosity fragments, high temperature (i.e. > 900°C), cooling of gas-permeable fragments (pumices) and dissolved water (Branney and Kokelaar, 2002; Roverato et al., 2016 and references therein).

~~Six massive lithofacies were recognized during our field campaign, three of them belong to the ignimbrites sub-group (Table 1). By using the granulometric classification proposed by Fisher (1961), ash is defined as any fragment with size < 2 mm, lapilli are fragments with size between 2 to 64 mm and blocks (or bombs) have sizes > 64 mm. Massive lithofacies includes all those deposits that display a massive coherent structure. Outcrops of such kind of lithofacies are constituted by a high percentage of ash up to block rich textures. The ash to lapilli (mAL) and lapilli and ash~~

Formatted: Indent: First line: 0 cm

Formatted: Font: Not Italic, No underline

Formatted: Font: Not Italic, No underline

Formatted: Font: Not Italic, Font color: Black

Formatted: Font color: Auto

Formatted: Font: Not Italic, Font color: Auto

Formatted: Indent: First line: 0 cm

(mLA) deposits (fig. 4a/b/c/d/e, fig. 6) are heterolithologic, matrix-supported, containing angular to sub-rounded medium to coarse devitrified lapilli (displaying axiolitic fabric), banded fragments, occasional (or absent) lithics and angular-shaped broken crystals of plagioclase, bipiramidal quartz and rare oxides (fig. 5). In mLA, elasts <25 cm in size are randomly immersed in the groundmass (Fig. 4d/e, 11d). Some of them are altered by carbonate minerals. Groundmass of mAL and mLA is formed by K-feldspar and quartz crystals, devitrified ash fragments and sericite crystals as phase of alteration (Fig. 5). mLB (massive Lapilli and Block) facies (fig. 4f, fig. 7) represent monolithologic coarse-grained rocks having high-elast content (elast:matrix ratios up to 3:1). Angular/sub-angular coarse lapilli and blocks up to 50–60 cm of devitrified banded or massive lava fragments are immersed in a devitrified fine lapilli and coarse ash matrix.

All massive deposits displaying welding characteristics have been grouped in the “ignimbrites” group (table 1), following the idea of “grade of welding” (Walker, 1983) (i.e. the amount of welding and compaction exhibited by deposits). The rocks are matrix-supported with sub-rounded to angular lithic elasts, euhedral, subhedral and broken crystals (plagioclase and less quartz) and deformed devitrified juvenile fragments (fiamme). Slightly (low grade, l-gwLA), medium (medium grade, m-gwLA), well-stretched (high grade, h-gwLA) fiamme (Fig. 6), as well as, devitrified shards define the eutaxitic fabric (Roverato et al., 2016). These fragments varying from millimetric to 3–4 cm in size are immersed in a homogeneous micro-granophiric-like devitrified groundmass (see Roverato et al., 2016 for details). Figure 6 shows a stratigraphic column representing a 35 m thick sequence of ignimbrite deposits found in the TMP, displaying very low grade to high grade welded fabric where the grade of welding increases toward the top of the succession. The very top of the sequence is characterized by columnar jointing.

#### 4.2.2. Interpretation—

Most of the observed samples appear to have been affected by devitrification processes of the juvenile pyroclastic fragments and matrix. The presence of juvenile material linked with other observed textures such as broken crystals (Best and Christiansen, 1997) and eutaxitic fabric allows us to confirm that the rocks belonging to lithofacies mAL, mLA, l-gwLA, m-gwLA and h-gwLA are fragmental and

pyroclastic in origin. The general massive aspect and the poor sorting of mAL and mL A point to a laminar granular flow transport regime and the fine content suggests the deposition from a dilute fluid escape dominated flow boundary zone in which turbulent shear induced tractional segregation is suppressed (Branney and Kokelaar, 2002; Sulpizio et al., 2007; Roverato et al., 2017). These lithofacies are interpreted as ash flow deposits suggesting the deposition from a pyroclastic density current (PDC) (Lenhardt et al., 2011; Sulpizio et al., 2014; Roverato et al., 2017). The coarser lithofacies mL A (fig. 4e) could be related to proximal co-ignimbritic breccias as result of deposition by denser pyroclastic granular flows (Branney and Kokelaar, 2002). The angular aspect of the clasts indicates short period transport. The blocky aspect of the lithofacies mL B is attributed to the basal auto-brecciation of lava flows and/or rheo-ignimbrite flows. The welded character of the lithofacies l-gwLA, m-gwLA and h-gwLA is indicative of hot PDC emplacement and compaction that result into the low-up to high-grade eutaxitic fabric. This process is favored by loading compaction, low-viscosity fragments, high temperature (i.e. > 900°C), cooling of gas permeable fragments (pumices) and dissolved water (Branney and Kokelaar, 2002; Roverato et al., 2016 and references therein).

#### 5.4.2.23. Stratified

These lithofacies, although commonly associated with ignimbrites, are not very spread in the studied areas. We also didn't find any alternation between massive and stratified deposits even if this association is a common occurrence in PDC deposits (Sulpizio et al., 2014; Roverato et al., 2017), alternating dilute (stratified deposits resulting) and concentrated (massive deposits resulting) regimes during transport (Sulpizio et al., 2014). Just one example has been found in TMP and is reported in the stratigraphic reconstruction of fig. 11.

#### 5.2.1 Lf sA; xsA; dsAL (stratified Ash; cross-stratified Ash; diffusely stratified Ash to lapilli)

**Description:** The stratified samples and outcrops analyzed comprise well sorted very fine to fine ash organized in millimetric to sub-millimetric parallel (sA) or cross-stratified (xsA) layers, with sharp or gradational changes in grain size (Fig. 8). The fragments are represented by devitrified shards, crystals (plagioclase), and rare (or absent) lithics (fig. 8d) immersed in a devitrified groundmass. Diffuse-stratified

Formatted: Font color: Black

Formatted: Indent: First line: 0 cm

Formatted: Indent: First line: 0 cm

lithofacies dsAL display a coarser character with coarse lithic and devitrified ash and lapilli fragments forming well developed parallel continuous meter-long stratification (or very-low angle cross-stratification) at centimeter scale (fig. 11b), with gradational changes in grain-size. The sorting varies from well to moderate.

#### 4.2.4. Interpretation:

The fine parallel layering of shards material displayed by lithofacies sA is interpreted here as being deposited under the product of sedimentation by the upper and highly dilute ash-cloud that accompany a pyroclastic-density current. We don't exclude the direct sedimentation from tephra fall-out activity. Cross-stratified (Lf xsA) and diffuse-stratified (Lf dsAL) deposits indicate tractive processes usually attribute to pyroclastic surge-type depositional condition from dilute currents (Cas and Wright 1987; Lenhardt et al., 2011; Roverato et al., 2017). We interpreted these as pyroclastic surge deposits although Lf dsAL could also be the product of coarse ash fall-out processes. Pyroclastic surge deposits usually display small volume and rarely reach more than 10 km from their source (Lenhardt et al., 2011). Conversely, fall-out deposits could emplace tens of kilometers from their source.

#### 6.——4.3. Secondary volcanoclastic/epiclasticSedimentary rocks

The nomenclature of Fisher et al. (1961) is applied also for the sedimentary secondary volcanoclastic rocks as follow: silt ( $2 < \phi < 64 \mu\text{m}$ ), sand ( $64 \mu\text{m} < \phi < 2 \text{ mm}$ ), gravel ( $2 < \phi < 64 \text{ mm}$ ), cobble ( $64 < \phi < 256 \text{ mm}$ ). These rocks are considered as the product of reworking and erosive processes. The clasts belonging to this group show a wide range of composition, size and shape variations. Based on their component, texture and fabric, we recognized five massive, both matrix- and clast-supported, and four stratified lithofacies (fig. 9).

##### 6.3.1.1. Massive

##### 6.1.1. Lf mS (massive Sand)

Description: this lithofacies consists of reddish moderately to well-sorted, massive, fine- to medium grained sand forming parallel strata intercalated to clast-supported conglomerate deposits (Lf csG) (fig. 9a). The sandstone strata extend tens of meters and present thinness between 0.4-0.8 m. Lf mS is predominantly composed of

Formatted: Font: Not Italic, No underline, Font color: Auto

Formatted: Font: Not Italic, No underline, Font color: Auto

Formatted: Indent: First line: 0 cm

Formatted: Font: Not Italic, No underline, Font color: Auto

Formatted: Font: Not Italic

quartz, feldspar and minor rock fragments. Contacts between mS and csG are sharp with rare slightly erosional surfaces. The tops of the sandstone are characterized by the presence of centimeters ripples (fig. 9b).

Interpretation: the massive sand (mS) and the small ripples found at the top of the strata indicate low energy under tractional currents in shallow water conditions (Collison and Thompson, 1982; Lenhardt et al., 2011). The alternation of Lf csG and mS indicates changes in energy conditions of sedimentation. We interpret these oscillations as belonging to a subaqueous-subaerial fan-delta interface setting where continental supply of material alternates to under-water sand accumulation (Lf mS).

#### 6.1.2. Lf csG (clast supported Gravel)

Description: this lithofacies~~The Lf csG~~ (Fig. 9a, c, d) is massive, clast to matrix supported, with heterolithic felsic rounded high-spherical coarse gravel with a sandy inter-clast matrix. Clasts are mainly characterized by massive and banded medium- to coarse-size felsic lava fragments (and rare quartz; size does ~~not~~ exceed 5 cm) and present rounded with low- to high-sphericity. We found lithofacies csG also associated to xsSG (see below section 6.2.2.) (Fig. 9c, 10b).

Interpretation: lithofacies csG is dominated by water flow processes where matrix plays a secondary role. The clast-supported character and less matrix content indicates that water removed the finer particles during transport and deposition. Lf csG display rounded clasts and well-sorting indicative of good selection during transport and emplacement. The rounded character of csG and the presence of matrix in the deposits suggest a laminar debris-flow regime in medial reaches of stream-dominated fluvial/alluvial fans (Mueller and Corcoran, 1998).

#### 6.1.3. Lf csGS (clast supported Gravel to Sand)

Description: Lf csGS (Fig. 9e, 11c) is massive, moderately well-sorted and clast-supported. Clasts (gravel to sand) present sub-rounded to sub-angular with low/medium sphericity with maximum size of 2-3 cm. The rocks belonging to this lithofacies are mainly formed by massive felsic lava fragments with different color and crystallinity.

Interpretation: Lf csGS is dominated by water flow processes where matrix plays a secondary role. The clast-supported character and less matrix content indicates that water removed the finer particles during transport and deposition. This lithofacies

Formatted: Level 1, Adjust space between Latin and Asian text, Adjust space between Asian text and numbers

Formatted: Indent: First line: 0 cm

represents deposition within a debris-flow dominated fluvial/alluvial environment.  
Poor sorting, clast-supported and sub-angular clasts point to deposition by localized  
laminar hyperconcentrated-flows in volcanic fans fringing flanks of volcanic edifices.  
Single cross-beds are usually ca. 1 cm thick

#### 6.1.4. Lf csGC (clast supported Gravel and Cobble)

**Description:** Lithofacies csGC (Fig. 9f) is massive, low-sorted and clast-supported. The clast population is characterized by sub-rounded, low/medium sphericity, massive felsic porphyritic fragments with maximum size up to 20 cm. This lithofacies has an interstitial matrix characterized by medium to coarse sand.

#### 4.3.2. Interpretation:

Lf esG, esGS and csGC (fig. 9a/d/f) isare dominated by water flow processes where matrix plays a secondary role. The clast-supported character and less matrix content indicates that water removed the finer particles during transport and deposition. This Lf esG display rounded clasts and well sorting indicative of good selection during transport and emplacement. The rounded character of esG and the presence of matrix in the deposits suggest a laminar debris flow regime in a medial reaches of stream-dominated fluvial/alluvial fans (Mueller and Corcoran, 1998). The alternation of Lf esG and mS (fig. 9a) indicates changes in energy conditions of sedimentation. We interpret these oscillations as belonging to a subaqueous subaerial fan-delta interface setting where continental supply of material alternates to under water sand accumulation (Lf mS). The massive sand grain size (mS) and the small ripples found at the top of the strata indicate low energy under tractional currents in shallow water conditions (Collison and Thompson, 1982; Lenhardt et al., 2011). Lithofacies esGS and esGC represents deposition within a debris-flow dominated fluvial/alluvial environment. Poor sorting, clast-supported and sub-angular clasts likely points to deposition by localized laminar hyperconcentrated-flows (esGS) and non-cohesive debris-flows (esGC) in volcanic fans fringing flanks of volcanic edifices. Single cross-beds are usually ca. 1 cm thick.

#### 6.4.3.23. Stratified

#### 6.2.1 Lf xsS (cross-stratified Sand)

Formatted: Indent: First line: 0 cm

Formatted: None, Don't adjust space between Latin and Asian text, Don't adjust space between Asian text and numbers

Formatted: Font: Not Italic, No underline, Font color: Auto

Formatted: None, Don't adjust space between Latin and Asian text, Don't adjust space between Asian text and numbers

Formatted: Font: Not Italic, No underline, Font color: Auto

Formatted: Font: Not Italic

Formatted: Indent: First line: 0 cm

Formatted: Font: Not Italic, No underline, Font color: Auto

Formatted: Font: Not Italic, No underline, Font color: Auto

Formatted: Font: Not Italic

**Description:** Lithofacies cross-stratified ~~Ssandstone (xsS)~~ (Fig. 10a) consist of white to brownish low-angle cross-stratified coarse quartzitic sandstone. The sandstones are characterized by lobe to sheet-shaped bodies. Major bedsets are recognized ranging in thickness from 0.5 to 1.5 m, composed of fine-grained sandstone dominated by medium-angle cross strata (18-20°). Single cross-beds are usually 0.7-1 cm thick. The outcrops displaying this lithofacies extend tens of meters with sharp upper and lower contact.

**Interpretation:** the cross-stratification of xsS is interpreted as formed in fluvial channels attesting the deposition from crested dune bed-forms that formed under condition of lower flow regime (Collinson, 1996; Miall, 1996; Capuzzo and Wetzel, 2004; Went, 2016). The deposition of medium-angle cross-bedding within large-scale examples of beds indicates that these larger beds are likely a product of bar migration. The beds are interpreted as channel-fill deposits (Lenhardt et al., 2017) related to a fluvial environment likely associated to meandering or braided rivers. Shoreline deposition developed around margins of immature marine basins is also considered.

#### 6.2.2. Lf xsSG (cross-stratified Sand and Gravel)

**Description:** Lf xsSG ~~Lf xsSG~~ (Fig. 10b) is characterized by crystal-lithic fine to coarse sand and fine gravel (max 5-6 mm in size) organized in cross-bedded stratification. Clasts display medium roundness and sphericity and are mostly composed by felsic fragments. Stratification is defined by alternating of well to poorly sorted, fine to coarse millimeters-thick strata. The finer black layers are formed by sub-millimetric hematite sand.

**Interpretation:** Lf xsSG correspond to cross-stratified water reworked deposits. The cross-stratified thicker fine gravelly strata, alternated with sandy layers laterally discontinuous, were interpreted as different pulses as the result of rapid deposition from hyperconcentrated flows (Zanchetta et al., 2004) in a stream-dominated fluvial/alluvial setting. Alternation with csG (Fig. 9c) represents difference of energy condition.

#### 6.2.3. Lf dsSt (diffusely layered Silt)

**Description:** ~~Lf dsSt~~ this lithofacies consists of parallel, lenticular, truncated, and locally low-angle cross-stratified multicolor millimetric well-sorted fine- to very fine-grained sand and silt strata (Fig. 10c). Within the sandy bedset, a thinning- and

Formatted: Font color: Custom Color(RGB(35,31,32))

Formatted: Indent: First line: 0 cm

Formatted: Font color: Text 1

Formatted: Indent: First line: 0 cm



fining-upward trend may be distinguished. Small and straight groove marks have been detected and reduced tiny slump folding is also presence in some parts.

Interpretation: lithofacies dsSt displays diffuse fine stratification with tiny ripples, suggesting transport and sedimentation in shallow water. The thin sheet-shaped is interpreted as flood sediments (Lenhardt et al., 2011). These deposits are interpreted to have been formed in low energy lacustrine environment or ponds (Collinson, 1996; Roverato et al., 2017) characterized by small turbidities successions affected by scouring and tiny deformations (slumps) of the sediments.

#### 6.2.4. Lf bChS (bedded Chert and Sand)

Description: tThe bedded chert lithofacies (with sand) (bChS) (Ffig. 10d) crops out in both regions and it is characterized by outcrops that can be traced on strike for hundreds of meters. The facies consist of thin laminated pinkish chert (layers < 1mm in thickness) with darker laminae intercalated, formed predominantly by hematite (Lenhardt et al., 2017). The layers are composed by microcrystalline quartz. In some portions, these lithofacies are associated with fine to medium sand composed mainly by quartz and less volcanic fragments.

4.3.4. Interpretation: this lithofacies is interpreted as inorganic precipitation of silica in a closed lake basin mainly due to its association with volcanic rocks and fine sandstone (Blatt et al., 1980; Eriksson et al., 1994). The picture in figure 10d shows elongated ripped-up millimetric fragments of chert immersed in the sandstone eroded by low-energy stream flow or local lacustrine turbidites. As suggests by Lenhardt et al. (2017) the chert may have formed during repeated pulses of hydrothermal fluids that circulated into the lake water during hiatuses in the volcanism (Van Kranendonk, 2006).

### 7. Analytical methods for geochemistry and geochronology

A total of 19 new samples (9 volcaniclastics and 10 lava flows) from the Tapajos region (associated with the data published in Roverato et al., 2016; Table 2) were analysed for bulk rock major and trace elements. Major element bulk rock analyses were performed by X-ray fluorescence, using a wavelength dispersive Philips PW 2400 spectrometry, using fused glass disks according to procedures described by

Formatted: Indent: First line: 0 cm

Formatted: Font: Not Italic, No underline, Font color: Auto

Formatted: No underline, Font color: Text 1

Formatted: No underline, Font color: Text 1

Formatted: Font color: Text 1

Formatted: Left, Indent: First line: 1.27 cm, Line spacing: 1.5 lines



Mori et al. (1999). Accuracy was greater than 2%. Trace element analyses in selected samples were performed by Inductively Coupled Plasma-Mass Spectrometry (ICP-MS) using the procedure described by Navarro et al. (2008). Accuracy, determined with respect to the reference standards BHVO-2 and BR, was 0.5–2%.

Zircon grains were examined with a FEI-QUANTA 250 scanning electron microscope equipped with secondary-electron and cathodoluminescence (CL) detectors at the Instituto de Geociências - Centro de Pesquisas Geocronológicas - Universidade de São Paulo (IGc-CPGeo-USP); the most common conditions used in CL analysis were 60  $\mu$ A of emission current, 15.0 kV of accelerating voltage, 7  $\mu$ m of beam diameter, 200  $\mu$ s of acquisition time, and a resolution of 2048x1887 pixels and 345 dpi. Selected samples were analyzed for U-Pb isotopes using a SHRIMP-IIe also at IGc-CPGeo-USP, following the analytical procedures of Williams (1998) as reported by Giovanardi et al. (2015). Correction for common Pb is based on the measured  $^{204}\text{Pb}$ , and the typical error for the  $^{206}\text{Pb}/^{238}\text{U}$  ratio is less than 2%; U abundance and U-Pb ratios were calibrated against the TEMORA-II standard. The dataset consists of 56 new U-Pb SHRIMP-II analyses and is reported in Table 3. Thirty-five analyses were performed on zircon grains from the Tapajos region as follow: 11 analyses on sample NP380-C, 11 analyses on sample NP183 and 13 analyses on sample NP396-B. Eleven analyses were performed on zircon grains from Xingu sample XU08. For all samples,  $^{207}\text{Pb}/^{235}\text{U}$  and  $^{206}\text{Pb}/^{238}\text{U}$  concordia ages (with 95% of confidence level and  $2\sigma$  error) are calculated using Isoplot 4.1 software (Ludwig, 2009).

~~The cross-stratification of lithofacies xsS is interpreted as formed in fluvial channels attesting the deposition from crested dune bedforms that formed under condition of lower flow regime (Collinson, 1996; Miall, 1996; Capuzzo and Wetzel, 2004; Went, 2016). The deposition of medium angle cross-bedding within large scale examples of beds indicates that these larger beds are likely a product of bar migration. The beds are interpreted as channel-fill deposits (Lenhardt et al., 2017) related to a fluvial environment likely associated to meandering or braided rivers. Shoreline deposition developed around margins of immature marine basins is also considered. Lf xsSG correspond to cross-stratified water-reworked deposits. The cross-stratified thicker fine-gravelly strata, alternated with sandy layers laterally discontinuous, were interpreted as different pulses as the result of rapid deposition from hypereconcentrated~~

Formatted: Font: Not Italic, No underline, Font color: Auto

flows (Zanchetta et al., 2004) in a stream-dominated fluvial/alluvial setting. Alternation with csG (fig. 9c) represents difference of energy condition. Lithofacies dsSt display diffuse fine stratification with tiny ripples, suggesting transport and sedimentation in shallow water. The thin sheet-shaped is interpreted as flood sediments (Lenhardt et al., 2011). These deposits are interpreted to have been formed in low energy lacustrine environment or ponds (Collinson, 1996; Roverato et al., 2017) characterized by small turbidities successions affected by scouring and tiny deformations (slumps) of the sediments. The Lf bChS is interpreted as inorganic precipitation of silica in a closed lake basin mainly due to its association with volcanic rocks and fine sandstone (Blatt et al., 1980; Eriksson et al., 1994). The picture in figure 10d shows elongated ripped-up millimetric fragments of chert immersed in the sandstone eroded by low-energy stream flow or local lacustrine turbidites. As suggests by Lenhardt et al. (2017) the chert may have formed during repeated pulses of hydrothermal fluids that circulated into the lake water during hiatuses in the volcanism (Van Kranendonk, 2006).

## 8.5. Geochemistry of the TMP samples

Independently of their nature (lavas or volcaniclastic), the rocks of the TMP follow a typical calc-alkaline trend (Fig. 12). They are mostly rhyolitic in composition (Table 2), with four exceptions which fall in the trachytic field. In addition, their low LOI values (0.32-3.51%) and the low FeO content (0.78 – 3.26%) together with the negative correlation FeO vs SiO<sub>2</sub> appears to indicate that the investigated volcanic rocks neither underwent significant alteration processes nor they belong to sedimentary suites which commonly contain water rich clay minerals. TMP volcaniclastic and lava flows show similar negative correlation between TiO<sub>2</sub>, Al<sub>2</sub>O<sub>3</sub>, MgO, FeO, CaO, Na<sub>2</sub>O and P<sub>2</sub>O<sub>5</sub> with SiO<sub>2</sub>. A negative correlation between K<sub>2</sub>O and SiO<sub>2</sub> also exists for the volcaniclastic, but not for the lava flows. The similar trends observed suggest that both these kind of rocks are originated by similar the same magmatic sources. Such a conclusion is supported by similar variation paths, although with different values, of minor and trace elements (Fig. 13). In particular, TMP lava flows show LREE enrichment ((La/Yb)<sub>N</sub>=10.68-21.45; normalized to Chondrite I from Anders & Ebihara, 1982) and a negative Eu anomaly which increases from trachytes ((Eu/Eu\*)<sub>N</sub>=0.89-0.78) to rhyolites ((Eu/Eu\*)<sub>N</sub>=0.69-0.31) (Fig. 13). The Eu negative

Formatted: Indent: First line: 0 cm

anomaly, shown from all the samples, is expression of feldspar fractionation. On the other hand, volcanoclastic rocks show similar LREE enrichment ( $(La/Yb)_N=11.12-28.10$ ) and negative Eu anomaly ( $(Eu/Eu^*)_N=0.97-0.37$ ) (Fig. 13). In addition, volcanoclastics have higher LREE abundances with respect to lavas (La between 35.5-91.3 ppm and between 40.5-71.9 ppm, respectively) while they have similar MREE and HREE contents (Yb between 1.56-3.43 ppm and between 1.83-4.11 ppm, respectively). Volcanoclastics commonly show higher Rb (121-272.9 ppm) and Pb (4.5-137.1 ppm) with respect to lavas (Rb=96.1-232 ppm and Pb=2.7-45.8 ppm). Volcanoclastics are enriched in LILE, Th and U with respect to MORB (Fig. REE13; normalization to MORB from Hoffman, 1988), with the exception of Sr, which commonly show a pronounced negative anomaly ( $(Sr/Sr^*)_N=0.55-0.05$ ). The Sr negative anomaly is consistent with feldspar fractionation. Negative anomalies are also present for Nb and Ta, while Ba and Pb are commonly enriched (Fig. 13). Lavas show a similar trace pattern, but higher values dispersion (Fig. REE13). The Ba enrichment is less pronounced with respect to volcanoclastics (Ba between 75-1965 ppm and 310-2245 ppm, respectively) and the Nb/Ta ratio show higher dispersion (3.29-14.63 and 6.73-13.9, respectively), indicating more limited fractionation of feldspar. According to the fractionation of feldspar, the trachytes have less pronounced negative Sr anomalies with respect to rhyolites ( $(Sr/Sr^*)_N=0.61-0.35$  and  $0.34-0.04$ , respectively). Geochemical affinity of Tapajos volcanoclastics and lava flows suggests that the magmatism occurred in active continental margin setting (Fig. 14). Using the tectonic discriminant diagrams of  $Zr+Nb+Ce+Y$  (ppm) vs  $FeO_{tot}/MgO$  (wt.%), Yb vs Ta and Th-Ta-Hf/3 (Wahlen et al., 1987; Pearce et al., 1984; Wood, 1980), the magmatism in the Tapajos region appears related to a syn- to post-collisional setting with few samples falling into the intraplate field (Fig. 14). According to the refined diagram Nb+Y vs Rb of Pearce (1996), all the Tapajos volcanics, together with the majority of volcanic rocks from the Sobreiro formation (Fernandes et al., 2011) are consistent with a late- to post-collisional setting (Fig. 14).

## 96. U-Pb zircon Geochronology

Zircons from Tapajos samples are colorless, sometimes fractured and euhedral to sub-euhedral. They can contain inclusions of apatite or spinel and are display commonly low emission in Cathodoluminescence (CL). All crystals show magmatic

Formatted: Indent: First line: 0 cm

oscillatory zoning and commonly a dark core which, in most cases, appears to be homogenous. Nonetheless, in few cases an inner core with discordant and partially reabsorbed domains is recognized. Some of the zircons also show a bright CL rim with transgressive or sub-concordant contacts with the inner oscillatory zoning. Zircons from sample XU08 from the Xingu region are colourless, rarely fractured and sub-euhedral. Inclusions of apatite or spinel are also observed sometimes. Crystals are medium in CL emissions and commonly show a homogeneous core and a concordant magmatic oscillatory zoning. Few zircons show a core with discordant zoning. No transgressive bright CL rims were recognized. Analyses were carried out on zircons that do not show transgressive or resorption features and discordant inner cores.

Zircons from sample NP183 (Ignimbrite) provide 4 discordant ~~ages~~ and 7 concordant analyses that provide ~~for~~ an upper intercept at  $1984 \pm 8.5$  Ma (95% confident decay-const. errs included, MSWD 1.09) and a concordia age at  $1986 \pm 8.2$  Ma ( $2\sigma$ , decay-const. errs included, MSWD 1.08, Probability of concordance = 0.30; Fig. 15). Single spot  $^{206}\text{Pb}/^{207}\text{Pb}$  ages range between  $2010 \pm 17$  Ma and  $1909 \pm 53$  Ma with an average age of  $1985 \pm 11$  Ma (95% confident decay-const. errs included, MSWD 1.6, Probability of concordance = 0.15; Fig. 15). Zircons from sample NP380 (Ignimbrite) show slightly older single spot  $^{206}\text{Pb}/^{207}\text{Pb}$  ages between  $2023 \pm 31$  Ma and  $1981 \pm 24$  Ma with an average age of  $1998 \pm 5.9$  Ma (95% confident decay-const. errs included, MSWD 0.74, Probability of concordance = 0.68; Fig. 14). Analyses are slightly discordant (up to 4%) providing an upper intercept at  $1998 \pm 7.7$  Ma (95% confident decay-const. errs included, MSWD 0.74). Zircons from sample NP396 (Banded lava) provide 5 discordant ages and 8 concordant analyses, which provide ~~for~~ an upper intercept at  $1994 \pm 8.2$  Ma (95% confident decay-const. errs included, MSWD 1.40) and a concordia age at  $1997 \pm 7.0$  Ma ( $2\sigma$ , decay-const. errs included, MSWD 5.70, Probability of concordance = 0.02; Fig. 15). Single spot  $^{206}\text{Pb}/^{207}\text{Pb}$  ages range between  $2014 \pm 14$  Ma and  $1973 \pm 8$  Ma with an average age of  $1994 \pm 8.7$  Ma (95% confident decay-const. errs included, MSWD 1.6, Probability of concordance = 0.12; Fig. 14). Pooling together the analyses of the Tapajós samples provides an average age of  $1991 \pm 12$  Ma ( $2\sigma$ , MSWD 1.50, Probability of concordance = 0.06). Zircons from sample XU08 (Lava flow) provide a concordia age at  $1882 \pm 6.4$  Ma ( $2\sigma$ , decay-const. errs included, MSWD 2.70, Probability of concordance = 0.10; Fig. 16). Single spot  $^{206}\text{Pb}/^{207}\text{Pb}$  ages range between  $1899 \pm 10$  Ma and  $1875 \pm 13$  Ma, with an average at

1884 ±5.2 Ma (95% confident decay-const. errs included, MSWD 0.60, Probability of concordance = 0.82).

## 107. Discussion

### 10.1. Subduction-related to extensional setting

The geochemistry of the TMP samples presented in this work display a high-K calc-alkaline signature (Fig. 12); ~~most of them are related to a volcanic are setting (fig. 14), although few samples display a geochemical signature that vary from the trend and they majorly~~ fall into the A-type intra-plate granite field and tectonic discriminant diagrams suggest a late- to post-collisional setting for the TMP volcanism (Fig. 14). This interpretation is also supported by enrichment in low-HSFE and the high-LILE, Th, U and LREE contents of our samples, which suggest a strong crustal component in the parent melt, consistent with a subduction/post orogenic geodynamic setting (Fig. 12), and the high HSFE which shifted the TMP volcanics composition in the A-type granites showing however FeO/MgO which are low and comparable with I- and S-types granites (Fig. 14). Similar features are: ~~These two distinct signatures are also well~~ reported in previous works (Lamarão et al., 1999; Lamarão et al., 2002) for volcanics in the Tapajós region, which are grouped into the Vila Riozinho (VR) and Maraes Aldeida (MA) formations, respectively. The Vila Riozinho rocks are intermediate to felsic in composition (Lamarão et al., 2002) with a calc-alkaline signature, while the rhyolites and ignimbrites of Moraes Almeida are slightly enriched in silica compared to the rhyolites of Vila Riozinho and are geochemically similar to evolved A-type granites (Lamarão et al., 2002). Our results show similarities with these data, suggesting that our specimens could be part of the VR and/or MA formations. The identification of two volcanic series has important implications for the understanding of the magmatic evolution of the Amazonian craton in late Paleoproterozoic. A model for the evolution of the TMP involves a first stage of subduction-related magmatism followed by an intracontinental magmatism related to a distensional event (Lamarão et al., 2002). Geochronological analyses by Lamarão et al. (2002) yielded ages of ca. 2 Ga for the VR rocks and ca. 1.88-1.87 Ga for the MA volcanism. The three new U-Pb geochronological analyses reported in this study yielded ages of ca. 2000 Ma (fig. 15) are, concordant with the ages presented by Lamarão et al. (2002) for the VR magmatism, thus suggesting that the TMP rocks could be part of the VR volcanic sequence. However, TMP rocks are geochemically more evolved with

Formatted: Indent: First line: 0 cm

Formatted: No underline, Font color: Text 1

Formatted: Normal, No bullets or numbering

Formatted: Font: Not Italic, No underline, Font color: Auto

Formatted: Font color: Text 1

respect to VR in terms of SiO<sub>2</sub> (63.8-76.6 wt.% and 54.4-71.8 wt.%, respectively), K<sub>2</sub>O (2.3-7.1 wt.% and 2.1-5.8 wt.%, respectively) and REE abundances (Fig. 12) and are more similar to MA rocks (Fig-s. 11, 12 and 13). In particular, REE patterns of the TMP samples are comparable with the rocks of the MA formation (Fig. 12) while they are more enriched in REE with respect to VR rocks. Conversely, TMP rocks are enriched in Ba (Fig. 12), while ~~MA~~ are depleted, and have compositions for Rb/Zr and Nb, considered as a proxy for arc maturity (Brown et al., 1984), similar to VR and different from MA (Rb/Zr between 0.3-1.1 in TMP, 0.2-0.7 in VR and 0.2-1.7 in MA; Lamarão et al., 2002). Thus, according to geochronological and petrological data, we proposed that the TMP rocks in this study ~~represent the more felsic and evolved facies of the VR magmatism and~~ must be ascribed ~~at this~~ to the VRs formation. Geochemical differences in our rocks and VR volcanics could be explained by a more evolved character of the TMP rocks. The ~~The~~ evidences of plagioclase fractionation from the parent melts of the TMP (negative Eu and Sr anomalies, Fig. 12) and their absence in less evolved VR rocks reinforce this interpretation, and suggest fractional crystallization as the prominent process controlling the VR magmatism evolution. However, we want to point out that due to the large area covered by the presented investigation (Fig. 2), together with the VR area, the geochemical variations between our rocks (TMP) and VR could be the result of local/regional heterogeneities in the magmatism. This hypothesis is supported by the intermediate characteristics of the TMP samples with respect to the VR and MA volcanics (Figs 11, 12 and 13).

Recently, new authors (Juliani et al., 2014) suggest the geochemical and geochronological signature of the MA ~~(TMP)~~ formation could be correlated to the felsic Santa Rosa (SR) formation cropping out in the SFX region. Our new U-Pb geochronological analyses on one rock sample from the SR formation yielded an average age of  $1884 \pm 5.2$  Ma (Fig. 168) that is consistent with previous Pb-Pb ages on other locations. Giuliani and Fernandes (2010) published two Pb-Pb ages on zircons of  $1879 \pm 2$  Ma and  $1884 \pm 1.7$  for a rhyolite and an ash tuff, respectively. Recently Antonio et al. (2017) publishes the first U-Pb ages on zircons for the Santa Rosa Formation with  $1877.4 \pm 4.3$  Ma for a rhyolite and  $1895 \pm 11$  Ma for a dike. All geochronological results support a ca. 1880 Ma age for the emplacement of these rocks.

The southern Amazonian craton, as well as other ~~P~~recambrian terrains worldwide (Condie, 2002; Hoffman, 1988; Zhao et al., 2002), are considered to be



characterized by a series of orogenic to post-orogenic events from 2.0 up to 1.88 Ga. The amalgamation of cratonic blocks worldwide established connections between South America and West Africa and other cratonic terrains such as Western Australia and South Africa, Laurentia and Baltica, Siberia and Laurentia, Laurentia and Central Australia, etc (Zhao et al., 2002). These late-Paleoproterozoic collisional processes likely formed the controversial supercontinent Columbia (Zhao et al., 2004). This period also coincides with a major peak in orogenic gold resources (Goldfarb et al., 2001, Juliani et al., 2014) and understanding the geodynamic of this period is crucial for economic interests. Antonio et al. (2017) highlight that for the period 1.88 Ga, many cratonic terrain have been characterized by extensive magmatism. These authors report as examples the 1880 Ma NE-trending Ghost dike swarm and the 1880 Ma Circum-Superior LIP in the Canadian shield (Minifie et al., 2013), the 1880 Ma Southern Bastar- Cuddapah LIP in India (French et al., 2008), the Mashonaland sills and the Post-Waterberg dolerites in Kalahari craton (Hanson et al., 2004), an extensive A-type magmatism in Baltica and in Siberia. The A-type affinity of the 1.88 Ga rocks is widely described by other authors in different regions into the Amazonian craton (Ferron et al., 2010; Pierosan et al., 2011; Fernandes et al., 2011; Klein et al., 2012; Barreto et al., 2014; Teixeira et al., 2018). Currently, the significance of the 1.88 Ga A-type magmatism in the Amazonian craton is still matter of debate, also due to the extremely large aerial cover which interested several different domains with different basements and geologic evolutions. For example, studies on the Carajas region suggest that the 1.88 Ga anorogenic magmatism in this domain was provoked by delamination and fusion of the Archean basement by a mantle plume which originated an extensional setting (Dell'Agnol et al., 2005; Silva et al., 2016; Teixeira et al., 2018; Teixeira et al., 2019).

Conversely, the geochemical features of the TMP and SFX magmatism presented in this work and in literature (Lamarão et al., 2002, 2005; Fernandes et al., 2011) mainly support an extensional regime of these regions related to a late- to post-collisional event, being possibly related to the end of the subduction process.-

~~According to these authors we suggest that the A-type rocks emplaced during the period 1.88 Ga in both TMP and SFX are related to an intraplate environment in an extensional regime.~~ The transition from convergent (syn/post-orogenic) to extensional tectonic setting could register the beginning of the taphrogenesis that marked the Amazonian Craton throughout the Mesoproterozoic (Brito Neves, 1999; Lamarão et

**Formatted:** Font: (Default) Times New Roman, No underline, Font color: Text 1

**Formatted:** Font: (Default) Times New Roman, Font color: Text 1, English (United States)

**Formatted:** Font: (Default) Times New Roman, No underline, Font color: Auto

**Formatted:** Font: (Default) Times New Roman, No underline

**Formatted:** Font: (Default) Times New Roman, No underline, Font color: Auto

**Formatted:** Font: (Default) Times New Roman, No underline

**Formatted:** Font: (Default) Times New Roman, No underline, Font color: Auto

al., 2002). The ca. 1.88 Ga felsic magmatism in different provinces of the Amazonian craton could represent the oldest magmatism related to this event. It should be mentioned that in term of textural features, the products emitted during the transition between the post-collisional to extensive events don't display substantial variations. In other words, the lithofaciological signature of the volcanic and volcanoclastic rocks that characterized the 2 Ga VR event (subduction related) is similar for those products erupted during the 1.88-1.87 Ga extensional volcanism that characterized the MA and SR events. Moreover, the post-orogenic to extensional setting emphasizes the continental setting where the studied volcanic products have been emitted. Following the idea of Roverato et al. (2017) for the Late-Paleoproterozoic andesitic Sobreiro Formation, we stress the lack of any evidences in favour of subaqueous eruptions for the emitted felsic products such as pillow lavas as well as hyaloclastites. This suggests the subaerial character of the volcanism and its emitted products acted in both regions.

## 107.2. Eruptive style and emplacement

The study areas are widely characterized by volcanic deposits whose eruptive style is hard to differentiate. Distinguishing between banded lavas and high grade ignimbrites is, sometime, extremely challenging (Henry and Wolff, 1992; Manley, 1995). This is made even more complicated when the investigated deposits are ancient and the outcrops intensely eroded, such as those Precambrian terrains investigated here (Lenhardt et al., 2012; Roverato et al., 2016; Lenhardt et al., 2017). Evidences in the field show that a great volume of the volcanic activity is represented by the emission of lava flows and/or high-grade to rheomorphic ignimbrites, although an important amount of other fragmental products of different type (Lf mAL, mLA, l-g/m-g/h-gwAL) are also well represented in both regions. High-grade welded and rheomorphic (up to lava-like) ignimbrites share similar features with lavas, displaying banding and ductile folds formed by the elongation of fiamme and vesicles (Schmincke and Swanson, 1967; Chapin and Lowell, 1979; Wolff and Wright, 1981; Branney et al., 1992; Sumner and Branney, 2002; Pioli and Rosi, 2005; Andrews and Branney, 2011; Brown and Bell, 2013). Although the ignimbrites investigated here have a fragmental derivation their origin largely differ from those characteristic of fallout deposits that form by a sustained column explosive-driven eruption. High-grade welded and rheomorphic ignimbrites are correlated with highly explosive plinian-type eruptions

**Formatted:** Font: (Default) Times New Roman, No underline

**Formatted:** Font: (Default) Times New Roman, No underline

**Formatted:** Font: (Default) Times New Roman, No underline, Font color: Auto

**Formatted:** Font: (Default) Times New Roman, No underline, Font color: Auto

**Formatted:** Indent: First line: 0 cm

**Formatted:** Font: Not Italic, No underline

**Formatted:** Font: Not Italic, No underline



which produce, during their column collapse stage, large PDC. In addition, high-grade  
 rheomorphism of silicic products, either deriving from an explosive or effusive  
 eruption, are favored by high temperature low-viscosity emplacement conditions and  
 the presence of some residual water. The high temperatures condition of our deposits is  
 also confirmed by the pervasive presence of spherulites and lithophysae formed during  
 the slow-cooling regimes of large silica-rich lavas and welded ignimbrites (Lofgren,  
 1971; Breitzkreuz, 2013). The eruptive scenario showed in figure 17 giving origin to the  
 frequent eruption of large volume and high discharge rate lava flows and ignimbrites  
 was likely characterized by fissure-fed and caldera collapses systems as those  
 described by previous authors (Legros et al., 2000; Aguirre et al., 2003; Cas et al.,  
 2011; Lesti et al., 2011; Lenhardt et al., 2012; Willcock et al., 2013). Eruptions fed by  
 extensive fissures of large size, in fact, appear to be the most favourable volcanic  
 systems to minimize cooling during emplacement and produce an alternance of low-  
 height sustained column eruptions feeding PDC and eruptions characterized by the  
 effusion of low viscosity lava flows, coulees and domes, while maintaining high  
 discharge rates (e.g. Bachmann et al., 2000; Aguirre-Diaz & Labarthe-Hernandez,  
 2003; Polo et al., 2018a, b; Simões et al., 2017). The sustained fountaining and  
 entrainment of air in the eruptive jet is strongly influenced by the geometry of the  
 conduit (Legros et al., 2000) as well as the transition from sustained to collapsing  
 eruptive column. A wide-geometry conduit would impede much air entrainment into  
 the pyroclastic fountain and, at the same time, would favors magmatic escape of  
 volcanic gases, favoring the low fountaining and promoting a “boil-over” style  
 eruption (Branney and Kokelaar, 1992, 2002; Lenhardt et al., 2017) with high  
 discharge rate. Moreover, the low air injection would inhibit the dilution of the  
 eruptive material making it thermodynamically isolated from the surrounding  
 environment (Lesti et al., 2011), preserving the high temperatures and enhancing the  
 agglutination of fragments (welding) (e.g. Quane and Russell, 2004; Russell and  
 Quane 2005; Giordano et al., 2005). When the low-altitude pyroclastic fountaining or  
 the emission of high temperature lavas would be maintained for long time the high  
 flow-mobility is ensured (Sulpizio et al., 2014). If the material supply from the vent  
 continues for long time and with high discharge rate, the mobility could be maintained  
 even on very low slope angles (Sulpizio et al., 2014; Giordano et al., 2017; Kolzenburg  
 et al., 2017), and flowing various kilometers up to hundreds of kilometers far from the  
 vent (Aguirre-Diaz et al., 2008; Cas et al., 2011; Giordano et al., 2017). This could

explain the presence of large silicic volcanic areas characteristic of the ancient Amazonian volcanism (Roverato et al., 2016). Although, volcanoclastic rocks seem to be volumetrically less important in the study areas than the lava flows and/or rheomorphic ignimbrites the recognition of fragmental rocks during our field campaigns is important to understand their significance into our paleogeographic reconstruction (Fig. 17). An idealized deposit sequence of a caldera forming eruption displays an air-fall deposit overlain by an ignimbrite (Druitt and Sparks, 1984) and the transition from the sustained column phase to the pyroclastic flow phase is often accompanied by a strong increase in the discharge rate (Bursik and Woods, 1996). The stratigraphic sequence of figure 11 shows this association of a possible air-fall deposit (Lf dsAL) linked with pyroclastic flow-dominated deposits (Lf mAL and *m-gwLA*). In some cases, pyroclastic eruptions commonly precede lava emplacement (Fink 1983; Heiken and Wohletz 1987). The sequence presented in figure 7 shows a low-grade welded ignimbrite deposit (Lf *l-gwAL*) overlaid by a thick banded body that we are interpreting here as a lava flow. At the base of the banded lava is a breccia (Lf mLB) consisting of clasts of a mix of lava textural types, including massive, vesicular, flow banded and flow-folded, glassy, pumiceous and devitrified. Autobrecciation in lavas or rheomorphic ignimbrites occurs when more rigid layers and the external parts are broken in response to the applied shear stress locally exceeding the tensile strength (Fink and Manley; 1987). Some polymictic breccia deposits (Lf mLA) are characterized by lithic angular clasts and devitrified fragments that could point to co-ignimbritic breccias with short transport of the emitted material. These deposits could be also related to collapse-caldera-breccias falling down into the caldera ring during the roof subsidence (Fig. 8). Air-fall (sA) and dilute pyroclastic flow (xsA) deposits (surge type) crop out in both regions. These, linked with the glassy and lithic pyroclastic material described above, are evidence of intense explosive phases from more sustained column eruptions of smaller intra-caldera volcanic centers and/or associated to events of caldera collapse (Fig. 17).

#### 107.2.1 The sedimentary response

Sets of small basins intra-calderas and probable relatively immature shallow marine deposits are interpreted as forming part of a tectonically unstable setting of a young extensional environment that characterized the southern Amazonian craton during the Paleoproterozoic. Reworked sediments can accumulate into volcano-

Formatted: Font: Not Italic, No underline

Formatted: Font: Not Italic

tectonic depressions created by the eruption, which often collects an intra-caldera lake  
 (Heiken et al., 2000 Németh et al., 2009, Manville et al., 2009). The sedimentation into  
 intra-volcano shallow-water lacustrine basins would have be facilitated (Fig. 17). The  
 alternation of subaerial to shallow-water sedimentation displayed by the alternation of  
 Lf mS and csG is indicative of this volcano-tectonic depressions, which could be also  
 interpreted as immature marine depressions. Subaerial and subaqueous talus coarse-  
 grained up to finer grained turbidites (dsSt) and suspension deposits formed during  
 quiescent periods into lakes or pounds is also inferred (Bacon et al., 2002). Silica-rich  
 accumulations into shallow water basins (Chipera et al., 2008; Manville et al., 2009)  
 deriving from hydrothermal activity in a dynamic volcanic context is also thought to be  
 responsible for the formation of chert accumulation (Lf bChS). Post caldera uplifting  
 (Fig. 17), resurgence or central volcanism could also contribute to produce new  
 sediments to be reworked and transported. Fluvial erosion and reworking of primary  
 deposits produced wide range of different sediments from localized cross-bedded,  
 well-sorted sand (Lf xsS) and gravel (Lf xsSG) beds to massive clast-supported sand  
 and gravel (Lf csGS, csG) and cobble (Lf csGC) deposits. Fluvial deposits occur  
 throughout all successions, representing periods of stream and river reworking and re-  
 establishment after an eruptive phase (Zernack et al., 2011; Roverato et al., 2017).  
 Debris-flows, hyperconcentrated flows, sheet-floods and active sandy braided river  
 systems existed and the probable absence of vegetation during the Precambrian  
 (Oberholzer and Eriksson, 2000; Roverato et al., 2017) permitted that copious rainfalls  
 easily reworked the available sediments.

## 119. Conclusion

This study is the result of the lithofaciological analysis carried out during the  
 2013, 2014 and 2015 field campaigns in the Amazon Craton in the TMP and SFX  
 regions and the successive geochemical and geochronological analysis of samples  
 collected in the field. This work constitutes a further step ahead toward the  
 comprehension of significance, chronostratigraphic distribution and the dynamic of  
 eruption and emplacement of felsic volcanic products in the region. Our results  
 complete previous studies and confirm that products present in the Amazonia Craton  
 could be related either to caldera-type systems (e.g. Lamarão et al., 2002; Juliani et al.,  
 2005; Lamarão et al., 2005; Pierosan et al., 2011) and to fissure-fed eruptive

environment following the model proposed by Aguirre-Diaz and Labarthe-Hernandez (2003) for the “Sierra Madre Occidental” formation and by Juliani and Fernandes (2010) for the Xingu region. The two models are in fact very similar only differing for the size of the hypothesized magma chambers and the shape of the fissural vents. The described volcano-sedimentary sequences that were characterized by the emission of large volcanic felsic products were likely formed in a late- to post-orogenic (~ 2 Ga) to extensional regimes (~ 1.88 Ga).

~~Here we also image that an ideal late-convergent to extensional geotectonic environment was likely similar to that proposed in our discussion paragraph, where a post-orogenic to extensional regime for the period ~1.88 Ga was characterized by the emission of large volcanic felsic products. With this contribution we want also stress the importance of the results obtained by investigating the lithofaciological character of the deposits instead of only carrying out geochemical studies.~~

#### Acknowledgments

This work was supported by the project CAPES/CNPq 402564/2012-0 (Programa Ciências sem Fronteiras) to Caetano Juliani and Matteo Roverato. M. Roverato acknowledges the grant of the Brazilian CAPES/ CNPq Programa Ciências Sem Fronteiras, Atração de Jovem Talento 402564/2012-0. We acknowledge the CNPq/CT-Mineral (Proc. 550.342/ 2011-7) and the INCT-Geociam (573733/2008-2) — (CNPq/MCT/ FAPESPA/PETROBRAS). Furthermore, the first author would like to thank Jeovaci Jr. Martins da Rocha, Diego Felipe Gomez Gutierrez, Lucas Villela Cassini for the help in the field and Carlos Marcelo Diaz Fernandez for the help ~~in the field~~ and very useful discussions. Dr. Giordano acknowledges the financial support for this research from the CAPES project (proposal 302827) of the Ciências Sem Fronteiras program (Brazil) and the local research funds (2012, 2013, 2014) of the University of Turin (Ex60-2015). We are indebted to ~~-----~~ Nils Lenhardt and Roberto Dall’Agnol----- for the dedication in reviewing this manuscript and important comments and reviews, which improved considerably this work., -----

#### References

Aguirre-Diaz, G.J., Labarthe-Hernández, G., 2003. Fissure ignimbrites: fissure-source

Formatted: Indent: First line: 0.75 cm

- 1054 origin for voluminous ignimbrites of the Sierra Madre Occidental and its  
1055 relationship with Basin and Range faulting. *Geology* 31, 773-776.
- 1056 Aguirre-Díaz, G.J., Labarthe-Hernández, G., Tristán-González, M., Nieto-Obregón, J.,  
1057 Isaac Gutiérrez-Palomares, I., 2008. The ignimbrite flare-up and graben calderas  
1058 of the Sierra Madre Occidental, Mexico. In: Martí, J., Gottsman, J. (Eds.), *Caldera*  
1059 *Volcanism: Analysis, Modelling and Response*. *Developments in Volcanology* 10,  
1060 143-180.
- 1061 Almeida, F.F.M., Hasui, Y., Brito Neves, B.B., Fuck, R.A., 1981. Brazilian structural  
1062 provinces: an introduction. *Earth Science Reviews* 17, 1-29.
- 1063 Almeida, M.E., Brito, M.F.L., Ferreira, A.L., Monteiro, M.A.S., 2000. Projeto Especial  
1064 Província Mineral do Tapajós. *Geologia e recursos minerais da Folha Vila Mamãe*  
1065 *Anã (SB.21-V-D). Estados do Pará e Amazonas*. CPRM, Brasília. [CD-ROM].
- 1066 Amaral, G., 1974. *Geologia Pré-Cambriana da Região Amazônica*. Tese de Livre  
1067 Docência, IG/USP (212 pp.).
- 1068 Anders, E., Ebihara, M., 1982. Solar system abundances of the elements. *Geochim.*  
1069 *Cosmochim. Ac.* 46, 2363-2380.
- 1070 Andrews, G.D.M., Branney, M.J., 2011. Emplacement and rheomorphic deformation  
1071 of a large, lava-like rhyolitic ignimbrite: Grey's Landing, southern Idaho.  
1072 *Geological Society of America Bulletin* 123, 725-743.
- 1073 Antonio, P., D'Agrella-Filho, M.S., Trindade, R.I.F., Nédélec, A., de Oliveira, D.C., da  
1074 Silva, F.F., Roverato M., Lana, C., 2017. Turmoil before the boring billion:  
1075 Paleomagnetism of the 1880–1860 Ma Uatumã event in the Amazonian craton.  
1076 *Gondwana Research* 49, 106-129.
- 1077 Araújo, O.J.B., Maia, R.G.N., Jorge, João, X.S., Costa, J.B.S., 1988. A  
1078 megaestruturação arqueana da folha Serra dos Carajás. In: SBG (Ed.), *Congresso*  
1079 *Latinoamericano de Geologia*, seventh ed. Belém. 324-333.
- 1080 Bacon, C.R., Gardner, J.V., Mayer, L.A., Buktenica, M.W., Dartnell, P., Ramsey,  
1081 D.W., Robinson, J.E., 2002. Morphology, volcanism, and mass wasting in Crater  
1082 Lake, Oregon. *Geological Society of America bulletin* 114, 675-692.
- 1083 Bahia, R.B.C., Quadros, M.L.E.S., 2000. *Geologia e recursos minerais da Folha*  
1084 *Caracol SB.21-X-C. Estados do Pará e Amazonas*. Escala 1:250.000. Brasília:  
1085 CPRM, 2000. 1 CD ROM.
- 1086 Barreto, C.J.S., Lafonb, J.M., da Rosa Costac L.T., Fernandes-Limad, E., 2014.  
1087 Palaeoproterozoic (~1.89 Ga) felsic volcanism of the Iricoumé Group, Guyana

- 1088 Shield, South America: geochemical and Sm-Nd isotopic constraints on sources  
1089 and tectonic environment. *International Geology Review*, 2014.  
1090 <http://dx.doi.org/10.1080/00206814.2014.930800>
- 1091 Best, M.G., Christiansen, E.H., 1997. Origin of broken phenocrysts in ash-flow tuffs.  
1092 *GSA Bulletin*, 109 (1), 63-73.
- 1093 Blatt, H., Middleton, G., Murray, R., 1980. *Origin of Sedimentary Rocks*. Prentice-  
1094 Hall, Englewood Cliffs, 634.
- 1095 Branney, M.J., Kokelaar, B.P., 1992. A reappraisal of ignimbrite emplacement:  
1096 progressive aggradation and changes from particulate to non-particulate flow  
1097 during emplacement of high-grade ignimbrite. *Bull. Volcanol.* 54, 504-520.
- 1098 Breitzkreuz, C., 2013. Spherulites and lithophysae—200 years of investigation on high  
1099 temperature crystallization domains in silica-rich volcanic rocks. *Bull. Volcanol.*  
1100 75:705.
- 1101 Brito-Neves, B.B., 2011. The Paleoproterozoic in the South-American continent:  
1102 Diversity in the geologic time. *Journal of South American Earth Sciences* 32, 270-  
1103 286.
- 1104 Brown, D.J., Bell, B.R., 2013. The emplacement of a large, chemically zoned,  
1105 rheomorphic, lava-like ignimbrite: the Sgurr of Eigge Pitchstone, NW Scotland.  
1106 *Journal of the Geological Society* 170, 753-767.
- 1107 Brown, G.C., Thorpe, R.S., Webb, P.C., 1984. The geochemical characteristics of  
1108 granitoids in contrasting arcs and comments on magma sources. *Journal of the*  
1109 *Geological society* 141, 413-426.
- 1110 Bursik, M.I., Woods, A.W., 1996. The dynamics and thermodynamics of large ash  
1111 flows. *Bull. Volcanol.* 58, 175-193.
- 1112 Capuzzo, N., Wetzel, A., 2004. Facies and basin architectural of the Late  
1113 Carboniferous Salvan-Dorénaz continental basin (Western Alps,  
1114 Switzerland/France). *Sedimentology* 51, 675-697.
- 1115 Cas, R.A.F., Wright, J.V., 1987. *Volcanic Successions, Modern and Ancient*. Unwin  
1116 Hyman, Boston. 528.
- 1117 Cas, R.A.F., Wright, H.M.N., Folkes, C.B., Lesti, C., Porreca, M., Giordano, G.,  
1118 Viramonte, J.G., 2011. The flow dynamics of an extremely large volume  
1119 pyroclastic flow, the 2.08-Ma Cerro Galán Ignimbrite, NW Argentina, and  
1120 comparison with other flow types. *Bull. Volcanol.* 73, 1583-1609.

- 1121 Chipera, S.J., Goff, F., Goff, C.J., Fittipaldo, M., 2008. Zeolitization of intracaldera  
1122 sediments and rhyolitic rocks in the 1.25 Ma lake of Valles caldera, New Mexico,  
1123 USA. *Journal of Volcanology and Geothermal Research* 178, 317-330.
- 1124 Collinson, J.D., 1966. Antidune bedding in the Namurian of Derbyshire, England:  
1125 *Geologie en Mijnbouw* 45, 262-264.
- 1126 Collinson, J.D., Thompson, D.B., 1982 *Sedimentary structures*: London, Allen and  
1127 Unwin, 194.
- 1128 Condie, K.C., 2000. Episodic continental growth models: after thoughts and  
1129 extensions. *Tectonophysics* 322, 153-162.
- 1130 Condie, K.C., 2002. Continental growth during a 1.9-Ga superplume event. *Journal of*  
1131 *Geodynamics* 34, 249-264.
- 1132 Costa, J.B.S., Hasui, Y. 1997. Evolução geológica da Amazônia. In: M.L. Costa &  
1133 R.S. Angélica (Ed.), *Contribuições à geologia da Amazônia*, 16-90.
- 1134 Da Cruz, R.S., Fernandes, C.M.D., Villas, R.N.N., Juliani, C., Monteiro, L.V.S.,  
1135 Almeida, T.I.R., Lagler, B., Carneiro, C.C., Misas, C.M.E., 2015. A study of the  
1136 hydrothermal alteration in Paleoproterozoic volcanic centers, São Felix do Xingu  
1137 region, Amazonian Craton, Brazil, using short-wave infrared spectroscopy. *J.*  
1138 *Volc. Geoth. Res.* 304, 324-335.
- 1139 Dall'Agnol, R., Lafon, J.M., Macambira, M.J.B., 1994. Proterozoic anorogenic  
1140 magmatism in the Central Amazonian Craton: geochronological and geochemical  
1141 aspects. *Mineral. Petrol.* 50, 113-138.
- 1142 Dall'Agnol, R., Costi, H.T., Leite, A.A.S., Magalhães, M.S., Teixeira, N.P., 1999.  
1143 Rapakivi granites from Brazil and adjacent areas. *Precambrian Research* 95, 9-39.
- 1144 Dall'Agnol, R., Teixeira, N.P., Rämö, O.T., Moura, C.A.V., Macambira, M.J.B.,  
1145 Oliveira, D.C., 2005. Petrogenesis of the paleoproterozoic, rapakivi, A-type granites  
1146 of the Archean Carajás metallogenic province, Brazil. *Lithos* 80, 101-129.
- 1147 Dall'Agnol, R., da Cunha, I.R.V., Guimarães, F.V., de Oliveira, D.C., Teixeira,  
1148 M.F.B., Feio, G.R.L., Lamarão, C.N., 2017. Mineralogy, geochemistry, and  
1149 petrology of Neoproterozoic ferroan to magnesian granites of Carajás province,  
1150 Amazonian Craton: The origin of hydrated granites associated with charnockites.  
1151 *Lithos* 277, 3-32.
- 1152 Druitt, T.H., Sparks, R.S.J., 1984. On the formation of calderas during ignimbrite  
1153 eruptions. *Nature* 310, 679-681.
- 1154 Echeverri-Misas, C.M., 2010. Geologia e gênese do depósito de Au-(Cu) do Palito,

Formatted: Font: 12 pt, No underline, Font color: Auto

Formatted: Font: 12 pt, No underline, Font color: Auto

Formatted: Font: 12 pt, No underline, Font color: Auto

Formatted: Font: 12 pt, No underline, Font color: Auto

Formatted: Font: 12 pt, No underline, Font color: Auto



- 1155 Província Aurífera do Tapajós. Dissertação de Mestrado, IG/USP.
- 1156 Eriksson, P.G., Engelbrecht, J.P., Res, M., Harmer, R.E., 1994. The Bushy Bend lavas,  
1157 a new volcanic member of the Pretoria Group, Transvaal Sequence. S. Afr. J.  
1158 Geol. 97, 1-7.
- 1159 Faraco, M.T.L., Carvalho, J.M.A., Klein, E.L., 1997. Carta metalogenética da  
1160 Província Aurífera do Tapajós, in: Costa, M.L.C., Ange´lica, R.S. (Eds.),  
1161 Contribuições à Geologia da Amazônia. Sociedade Brasileira de Geologia,  
1162 Belém, Brazil 1, 423-437.
- 1163 Fernandes, C.M.D., Juliani, C., Monteiro, L.V.S., Lagler, B., Misas, C.M.E., 2011.  
1164 High-K calc-alkaline to A-type fissure-controlled volcano-plutonism of the São  
1165 Félix do Xingu region, Amazonian craton, Brazil: Exclusively crustal sources or  
1166 only mixed Nd model ages? Journal of South America Earth Science 32 (4), 351-  
1167 368.
- 1168 Ferrari, L., Orozco-Esquivel, T., Manea, V.C., Manea, M., 2012. The dynamic history  
1169 of the Trans-Mexican Volcanic Belt and the Mexico subduction zone.  
1170 Tectonophysics 522-523, 122-149.
- 1171 Ferreira, A.L., Almeida, M.E., Brito, M.F.L., Monteiro, M.A.S., 2000. Projeto Especial  
1172 Província Mineral do Tapajós. Geologia e recursos minerais da Folha  
1173 Jacareacanga (SB.21-Y-B). Estados do Pará e Amazonas. Escala 1:250.000. Nota  
1174 explicativa e mapas, CPRM, Brasília. [CD ROM].
- 1175 Ferron, J.M.T.M., Bastos-Neto, A.C., Lima, E.F., Nardi, L.V.S., Costi, H.T., Pierosan,  
1176 R., Prado, M., 2010. Petrology, geochemistry, and geochronology of  
1177 Paleoproterozoic volcanic and granitic rocks (1.89–1.88 Ga) of the Pitinga  
1178 Province, Amazonian Craton, Brazil. Journal of South American Earth Sciences  
1179 29, 483-497.
- 1180 Fink, J., 1983. Structure and emplacement of a rhyolitic obsidian flow: little Glass  
1181 Mountain, Medicine Highland, northern California. GSA Bull. 94, 362-380.
- 1182 Fink, J.H., Manley, C.R., 1987. Origin of pumiceous and glassy textures in rhyolite  
1183 flows and domes: Geological Society of America Special Paper 212, 77-88.
- 1184 Fisher, R.V., 1961. Proposed classification of volcanoclastic sediments and rocks.  
1185 Geological Society of America Bulletin 72, 1409-1414.
- 1186 French, J.E., Heaman, L.M., Chacko, T., Srivastava, R.K., 2008. 1891–1883 Ma  
1187 Southern Bastar–Cuddapah mafic igneous events, India: a newly recognized large  
1188 igneous province. Precambrian Research 160, 308-322.



- Giordano, D., La Felice, S., Arzilli, F., De Cristofaro, S.P., Masotta, M., Polo L.  
(2017). Il vulcanismo effusivo acido del Monte Amiata: stima delle condizioni  
pre- e sin-eruttive ed implicazioni vulcanologiche. Effusive acidic volcanism of  
Monte Amiata: estimates of pre- and syn-eruptive conditions and volcanological  
implications. Monografia Il Vulcano di Monte Amiata, ISBN 978-88-99742-32-4,  
171-193.
- Giordano, D., Nichols, A.R.L., Dingwell, D.B., 2005. Glass transition temperatures of  
natural hydrous melts: a relationship with shear viscosity and implications for the  
welding process. Jour. Volc Geoth. Res. 142, 105-118.
- [Giovanardi, T., Girardi, V.A.V., Correia, C.T., Sinigoi, S., Tassinari, C.C.G.,  
Mazzucchelli, M., 2015. U-Pb zircons SHRIMP data from the Cana Brava  
Layered Complex: New constraints for the mafic-ultramafic intrusions of Northern  
Goiás, Brazil. Open Geosci 7, 197-206.](#)
- Goldfarb, R., Groves, D., Gardoll, S., 2001. Rotund versus skinny orogens: well-  
nourished or malnourished gold? Geology 29, 539-542.
- Gutscher, M.A., Maury, R., Eissen, J.P., Bourdon, E., 2000. Can slab melting be  
caused by flat subduction? Geology 28, 535-538.
- Hanson, R.E., Gose, W.A., Crowley, J.L., Ramezani, J., Bowring, S.A., Bullen, D.S.,  
Hall, R.P., Pancake, J.A., Mukwakwami, J., 2004. Paleoproterozoic intraplate  
magmatism and basin development on the Kaapvaal Craton: age, paleomagnetism  
and geochemistry of ~1.93 to ~1.87 Ga post-Waterberg dolerites. South African  
Journal of Geology 107, 233-254.
- Hasui, Y., Haraly, N.L.E., Schobbenhaus, C., 1993. Megaestruturação Pré-Cambriana  
do território brasileiro baseada em dados geofísicos e geológicos. Geociências 12,  
7-31.
- Heiken, G., Wohletz, K., 1987. Tephra deposits associated with silicic domes and lava  
flows. GSA Special Paper 212.
- Heiken, G., Krier, D., McCormick, T., Snow, M.G., 2000. Intracaldera volcanism and  
sedimentation — Creede caldera, Colorado. In: Bethke, P.M., Hay, R.L. (Eds.),  
Ancient Lake Creede: Its volcano-tectonic setting, history of sedimentation, and  
relation to mineralization in the Creede Mining District. Geological Society of  
America Special Paper, 346. Boulder, Colorado, 127-157.
- Hofmann, A.W., 1988. Chemical differentiation of the Earth: The relationship between  
mantle, continental crust and oceanic crust. EPSL 90, 297-314.

- 1223 Hollocher, K., Robinson, P., Walsh, E., Roberts, D., 2012. Geochemistry of
- 1224 amphibolite-facies volcanics and gabbros of the Støren Nappe in extensions west
- 1225 and southwest of Trondheim, Western Gneiss Region, Norway: a key to
- 1226 correlations and paleotectonic settings. *American Journal of Science* 312, 357-
- 1227 416.
- 1228 Juliani, C., 2002. Alteração hidrotermal e metalogênese em sistemas vulcano-
- 1229 plutônicos paleoproterozóicos na Província Aurífera do Tapaj, Cráton Sul
- 1230 Amazônico, Pará. Tese de Livre-Docência, IG/USP.
- 1231 Juliani, C., Vasquez, M.L., Klein, E.L., Villas, R.N., Echeverri-Misas, C.M., Santiago,
- 1232 E.S.B., Monteiro, L.V.S., Carneiro, C.C., Fernandes, C.M.D., Usero, G., 2014.
- 1233 Metalogenia da Província Tapajós. In: Silva M.G.; Jost H.; Kuyumajian R.M.
- 1234 (Org.). *Metalogênese das Províncias Tectônicas Brasileiras*. 1 ed. : CPRM —
- 1235 Serviço Geológico do Brasil 1, 51-90.
- 1236 Juliani, C., Rye, R.O., Nunes, C.M.D., Snee, L.W., Correa Silva, R.H., Monteiro,
- 1237 L.V.S., Bettencourt, J.S., Neumann, R., Neto, A.A., 2005. Paleoproterozoic high
- 1238 sulphidation mineralization in the Tapajós gold province, Amazonian Craton,
- 1239 Brazil: geology, mineralogy, alunite argon age, and stable-isotope constraints.
- 1240 *Chemical Geology* 215, 95-125.
- 1241 Juliani, C., Fernandez C.M.D., 2010. Well-preserved Late Paleoproterozoic volcanic
- 1242 centers in the São Félix do Xingu region, Amazonian Craton, Brazil. *Journal of*
- 1243 *Volcanology and Geothermal Research* 191, 167-179.
- 1244 Kay, S.M., Godoy, E., Kurtz, A., 2005. Episodic arc migration, crustal thickening,
- 1245 subduction erosion, and magmatism in the south\_central Andes. *Geological*
- 1246 *Society of America Bulletin* 117, 67-88.
- 1247 Klein, E.L., Almeida, M.E., and Costa, L.T.R., 2012. The 1.89-1.87 Ga Uatumã Silicic
- 1248 Large Igneous Province, northern South America: Large Igneous Provinces
- 1249 Commission: <http://www.largeigneousprovinces.org/12nov> (accessed 12 January
- 1250 2012).
- 1251 Klein, E.L., Santos, R.A., Fuzikawa, K., Angélica, R.S., 2001. Hydrothermal fluid
- 1252 evolution and structural control of the brittle-style Guarim lode-gold
- 1253 mineralisation, Tapajós Province, Amazonian Craton, Brazil. *Miner. Depos.* 36,
- 1254 149-164.
- 1255 Klein, E.L., Vasquez, M.L., Rosa-Costa, L.T., Carvalho, J.M.A., 2002. Geology of
- 1256 Paleoproterozoic gneiss- and granitoid-hosted gold mineralization in Southern

- 1257 Tapajós Gold Province, Amazonian Craton, Brazil. *Intern. Geol. Rev.*, 44, 544-  
1258 558.
- 1259 Klein, E.L., Rosa-Costa, L.T., Carvalho, J.M.A., 2004. Estudo de inclusões fluidas em  
1260 veio de quartzo aurífero do prospecto Patinhas, Província Aurífera do Tapajós,  
1261 Cráton Amazônico. *RBG* 34, 59-66.
- 1262 Lagler, B., Juliani, C., Pessoa, F.F., Fernandes, C.M.D., 2011. Petrografia e  
1263 geoquímica das sequências vulcânicas Paleoproterozóicas na região de Vila  
1264 Tancredo, São Félix do Xingu (PA). In: *SBGq, Congr. Bras. Geoquí.*, 13, e Simp.  
1265 Países do Mercosul, 3, Gramado, RS. Anais, [CD-ROM].
- 1266 Lamarão, C.N., Dall'Agnol, R., Lafon, J.M., Lima, E.F., 1999. As associações  
1267 vulcânicas e plutônicas de Vila Riozinho e Morais Almeida, Província Aurífera do  
1268 Tapajós, SW do estado do Pará. In: *Simpósio sobre Vulcanismo e Ambientes*  
1269 *Associados. 1, Gramado\*/RS, Boletim de resumos*, 93 (in Portuguese).
- 1270 Lamarão, C.N., Dall'agnol, R., Lafon, J.M., Lima, E.F., 2002. Geology, geochemistry,  
1271 and Pb-Pb zircon geochronology of the Paleoproterozoic magmatism of Vila  
1272 Riozinho, Tapajós Gold Province, Amazonian craton, Brazil. *Prec. Res.* 119, 189-  
1273 223.
- 1274 Lamarão, C.N., Dall'agnol, R., Pimentel, M.M., 2005. Nd isotopic composition of  
1275 Paleoproterozoic volcanic rocks of Vila Riozinho: Implications for the crustal  
1276 evolution of the Tapajós gold province, Amazon craton. *J. South Am. Earth Sci.*  
1277 18, 277-292.
- 1278 Legros, F., Kelfoun, K., 2000. On the ability of pyroclastic flows to scale topographic  
1279 obstacles. *J. Volcanol. Geotherm. Res.* 98, 235-241.
- 1280 Lenhardt, N., Hornung, J., Hinderer, M., Böhnelt, H., Torres-Alvarado, I.S., Trauth, N.,  
1281 2011. Build-up and depositional dynamics of an arc front volcanoclastic complex:  
1282 the Miocene Tepoztlan Formation (Transmexican Volcanic Belt, Central Mexico).  
1283 *Sedimentology* 58, 785-823.
- 1284 Lenhardt, N., Eriksson, P., Catuneanu, O., Bumby, A.J., 2012. Nature of and controls  
1285 on volcanism in the ca. 2.32-2.06 Ga Pretoria Group, Transvaal Supergroup,  
1286 Kaapvaal Craton, South Africa. *Precambrian Research* 214-215, 106-123.
- 1287 Lenhardt, N., Masango S.M., Jolayemi, O.O., Lenhardt, S.Z., Peeters, G.J., Eriksson,  
1288 P.G., 2017. The Palaeoproterozoic (~2.06 Ga) Rooiberg Group, South Africa:  
1289 Dominated by extremely high-grade lava-like and rheomorphic ignimbrites? New  
1290 observations and lithofacies analysis. *Journal of African Earth Sciences* 131, 213-

- 232.
- Lesti, C., Porreca, M., Giordano, G., Mattei, M., Cas, R.A.F., Wright, H.M.N., Folkes, C.B., Viramonte, J., 2011. High-temperature emplacement of the Cerro Galán and Toconquis Group ignimbrites (Puna plateau, NW Argentina) determined by TRM analyses. *Bull. Volcanol.* 73, 1535-1565.
- Lofgren, G., 1971. Spherulite textures in glassy and crystalline rocks. *J. Geophys. Res.* 76, 5635-5648.
- Ludwig, K.R., 2009. Isoplot 4.1. A geochronological toolkit for Microsoft Excel. Berkeley Geochronology Center special publication 4, 76.
- Macambira, E.M.B., 1997. Geologia e aspectos metalogenéticos dos elementos do grupo de platina no complexo máfico-ultramáfico da serra da Onça – sul do Pará. Tese de Mestrado, UFPA, Belém, Pará, Brasil.
- Macambira, E.M.B., Vale, A.G., 1997. Programa Levantamentos Geológicos Básicos do Brasil. São Félix do Xingu. Folha SB-22-Y-B. Estado do Pará, CPRM, Brasília (in Portuguese).
- Manea, V.C., Pérez-Gussinyé, M., Manea, M., 2012. Chilean flat-slab subduction controlled by overriding plate thickness and trench rollback. *Geology* 40 (1), 35-38.
- Manville, V., Németh, K., Kano, K., 2009. Source to sink: A review of three decades of progresss in the understanding of volcanoclastic processes, deposits, and hazards. *Sedimentary Geology* 220, 136-161.
- McPhie, J., Doyle, M., Allen, S.R., 1993. Volcanic textures: A guide to the interpretation of textures in volcanic rocks, Centre for Ore Deposit and Exploration Studies. University of Tasmania, 198.
- Miall, A.D., 1996. The Geology of Fluvial Deposits: Sedimentary Facies, Basin Analysis, and Petroleum Geology. Springer-Verlag, New York. 582.
- Minifie, M.J., Kerr, A.C., Ernst, R.E., Hastie, A.R., Ciborowski, T.J.R., Desharnais, G., Millar, I.L., 2013. The northern and southern sections of the western ca. 1880 Ma Circum-Superior Large Igneous Province, North America: the Pickle Crow dyke connection? *Lithos* 174, 217-235.
- Monteiro, L.V.S., Xavier, R.P., de Carvalho, E.R., Hitzman, M.W., Johnson, C.A., de Souza Filho, C.R., Torresi, I., 2008. Spatial and temporal zoning of hydrothermal alteration and mineralization in the Sossego iron oxide-copper-gold deposit, Carajás Mineral Province, Brazil: paragenesis and stable isotope constraints.

**Formatted:** Normal, Left, Indent:  
Left: 0 cm, Hanging: 0.75 cm,  
Line spacing: 1.5 lines, No  
widow/orphan control, Don't adjust  
space between Latin and Asian  
text, Don't adjust space between  
Asian text and numbers

- [Miner Deposita 43, 129-159.](#)
- Mori, L., Gómez-Tuena, A., Cai, Y., Goldstein, S., 2007. Effects of prolonged flat subduction on the Miocene magmatic record of the central Trans-Mexican Volcanic Belt. *Chemical Geology* 244, 452-473.
- [Mori, P.E., Reeves, S., Correia, C.T., Haukka, M., 1999. Development of a fused glass disc XRF facility and comparison with the pressed powder pellet technique at Instituto de Geociências. Rev. Bras. Geociências, 29, 441-446.](#)
- Mueller, W.U., Concoran, P.L., 1998. Late-orogenic basins in the Archaean Superior Province, Canada: characteristics and inferences. *Sedimentary Geology* 120, 177-203.
- Mueller, W.U., Chown, E.H., Thurston, P.C., 2000a. Processes in physical volcanology and volcanoclastic sedimentation: modern and ancient. *Precambrian Research* 101, 81-85.
- [Navarro, M.S., Andrade, S., Ulbrich, H.H.G.J., Gomes, C.B., Girardi, V.A.V., 2008. The analysis of rare earth elements with ICP-MS in basaltic and related rocks: testing the efficiency of sample decomposition procedures. Geostand. Geoanal. Res. 32\(2\),167-180.](#)
- Németh, K., Cronin, S.J., Stewart, R.B., Charley, D., 2009. Intra- and extra- caldera volcanoclastic facies architecture of a frequently active mafic island-arc volcano, Ambryn Island, Vanuatu. *Sedimentary Geology* 220, 256-270.
- Oberholzer, J.D., Eriksson, P.G., 2000. Subaerial volcanism in the Palaeoproterozoic Heekpoort Formation (Transvaal Supergroup), Kaapvaal craton. *Precambrian Research* 101, 193-210.
- Pearce, J.A., Harris, N.B.W., and Tindle, A.G., 1984. Trace element discrimination diagrams for the tectonic interpretation of granitic rocks. *Journal of Petrology* 25, 956-983.
- [Pearce, 1996.....](#)
- Pessoa M.R., Santiago A.F., Andrade A.F., Barreto E.L., Nascimento J.O., Santos J.O.S., Oliveira J.R., Lopes R.C., Prazeres W.V. 1977. Projeto Jamanxim. CPRM/DNPM, 1-3, 614.
- Pierosan, R., Lima, E.F., Nardi, L.V.S., Bastos Neto, A.C., Campos, C.P., Jarvis, K., Ferron, J.M.T.M., Prado, M., 2011. Geochemistry of Palaeoproterozoic volcanic rocks of the Iricoumé Group, Pitinga Mining District, Amazonian craton, Brazil: *International Geology Review* 53, 946-979.

- 1359 Pinho, S.C.C., Fernandes, C.M.D., Teixeira, N.P., Paiva Jr., A.L., Cruz, V.L.,  
1360 Lamarão, C.N., Moura, C.A.V., 2006. O magmatismo paleoproterozóico da região  
1361 de São Félix do Xingu, Província Estanífera do Sul do Pará: Petrografia e  
1362 geocronologia. *Revista Brasileira de Geociências* 36, 793-802.
- 1363 Pioli, L., Rosi, M., 2005. Rheomorphic structures in a high-grade ignimbrite: the  
1364 Nuraxi tuff, Sulcis volcanic district (SW Sardinia, Italy). *Journal of Volcanology  
and Geothermal Research* 142, 11-28.
- 1366 Polo, L.A., Giordano, D., Janasi, V., Freitas-Guimaraes, L., 2017(a). Effusive silicic  
1367 volcanism in the Paraná Magmatic Province, South Brazil: Physico-chemical  
1368 conditions of storage and eruption and considerations on the rheological behaviour  
1369 during emplacement. *J. Volcanol. Geoth. Res.* 355, 115-135.
- 1370 Polo L.A., Janasi V., Giordano D., Lima E.F., Cañon-Tapia E., Roverato M., 2017(b).  
1371 Effusive silicic volcanism in the Paraná Magmatic Province, South Brazil:  
1372 Evidence for locally-fed lava flows and domes from detailed field work. *J.  
1373 Volcanol. Geoth. Res.* 355, 204-218.
- 1374 Quane, S. L., Russell, J. K., 2005. Welding: Insights from high-temperature analogue  
1375 experiments. *Journal of Volcanology and Geothermal Research* 142 (1-2), 67-87.
- 1376 Reis, N.R., Almeida, M.E., Ferreira, A.L., Riker, S.R., 2006. *Geologia e Recursos  
1377 Minerais do Estado do Amazonas. Sistema de Informações Geográficas  
1378 1:1.000.000. CPRM, Manaus, 144.*
- 1379 Rino, S., Tsuyoshi, K., Windley, B.F., Katayama, I., Motoki, A., Hirata, T., 2004.  
1380 Major episodic increases of continental crustal growth determined from zircon  
1381 ages of river sands; implications for mantle overturns in the Early Precambrian.  
1382 *Physics of the Earth and Planetary Interiors* 146, 369-394.
- 1383 Roverato, M., Capra, L., Sulpizio, R., Norini, G., 2011. Stratigraphic reconstruction of  
1384 two debris avalanche deposits at Colima Volcano (Mexico): insights into pre-  
1385 failure conditions and climate influence. *J. Volc. Geoth. Res.* 207 (1), 33-46.
- 1386 Roverato, M., Cronin, S., Procter, J., Capra, L., 2014. Textural features as indicators of  
1387 debris avalanche transport and emplacement, Taranaki volcano. *Geol. Soc. Am.  
1388 Bull.* B30946-1
- 1389 Roverato, M., 2016. The Montesbelos mass-flow (southern Amazonian craton, Brazil):  
1390 a Paleoproterozoic volcanic debris avalanche deposit? *Bull. Volcanol.* 78, 49.
- 1391 Roverato, M., Giordano, D., Echeverri-Misas, CM., Juliani, C., 2016.  
1392 Paleoproterozoic felsic volcanism of the Tapajós Mineral Province, Southern

- Amazon Craton, Brazil. *Journal of Volcanology and Geothermal Research* 310, 98-106.
- Roverato, M., Juliani, C., Marcelo Dias-Fernandes, C., Capra, L., 2017. Paleoproterozoic andesitic volcanism in the southern Amazonian craton, the Sobreiro Formation: new insights from lithofacies analysis of the volcanoclastic sequences. *Precambrian Research* 289, 18-30.
- Russell, J. K., Quane, S. L., 2005. Rheology of welding: Inversion of field constraints. *Journal of Volcanology and Geothermal Research* 142 (1-2), 173-191.
- Santos, J.O.S., Hartmann, L.A., Gaudette, H.E., Groves, D.I., McNaughton, N.J., Fletcher, I.R., 2000. A new understanding of the provinces of the Amazon craton based on integration of field mapping and U-Pb and Sm-Nd geochronology. *Gondwana Research* 3, 453-488.
- Santos, J.O.S., Groves D.I., Hartmann L.A., Moura M.A., McNaughton, N.J. 2001. Gold deposits of the Tapajós and Alta Floresta Domains, Tapajós-Parima orogenic belt, Amazon Craton, Brazil. *Mineralium Deposita* 36, 278-299.
- Santos, J.O.S., 2003. Geotectônica dos Escudos da Guiana e Brasil Central. In: L.A. Bizzi, C. Schobbenhaus, R.M. Vidotti, J.H. Gonçalves (Eds.). *Geologia, tectônica e recursos minerais do Brasil. Texto, mapas e SIG. CPRM - Serviço Geológico do Brasil, Brasília* 169-226.
- Santos, J.O.S., Van Breemen, O.B., Groves, D.I., Hartmann, L.A., Almeida, M.E., McNaughton, N.J., Fletcher, I.R., 2004. Timing and evolution of multiple Paleoproterozoic magmatic arcs in the Tapajós Domain, Amazon Craton: constraints from SHRIMP and TIMS zircon, baddeleyite and titanite U-Pb geochronology. *Prec. Res.* 13, 73-109.
- Silva, F.S., Oliveira, D.C., Antonio, P.Y., D'Agrella-Filho, M., Lamarão, C.N., 2016. Bimodal magmatism of the Tucuma area, Carajás Province: U-Pb geochronology, classification and processes. *J. S. Am. Earth Sci.* 72, 95-114.
- Simões, M.S., Lima, E.F., Sommer, C.A., Rossetti, L.M.M., 2017. Structures and lithofacies of inferred silicic conduits in the Paraná-Etendeka LIP, southernmost Brazil. *Journal of Volcanology and Geothermal Research* 355, 319-336.
- Sulpizio, R., Mele, D., Dellino, P., La Volpe, L., 2007. Deposits and physical properties of pyroclastic density currents during complex Subplinian eruptions: the AD 472 (Pollena) eruption of Somma-Vesuvius, Italy. *Sedimentology* 54, 607-635.



- Sumner, J.M., Branney, M.J. 2002. The emplacement history of a remarkable heterogeneous, chemically zoned, rheomorphic and locally lava-like ignimbrite: 'TL' on Gran Canaria. *Journal of Volcanology and Geothermal Research* 115, 109-138.
- Tassinari, C.C.G., Macambira, M.J.B., 1999. Geochronological provinces of the Amazonian craton. *Episodes* 22, 174-182.
- ~~Teixeira, W., Tassinari, C.C.G., Cordani, U.G., Kawashita, K., 1989. A review of the geochronology of the Amazonian craton: tectonic implications. *Precambrian Res.* 42, 213-227.~~
- ~~Teixeira, M.F.B., Dall'Agnol, R., Santos, J.O.S., Oliveira, D.C., Lamarão, C.N., McNaughton, N.J., 2018. Crystallization ages of Paleoproterozoic A-type granites of Carajás province, Amazon craton: Constraints from U-Pb geochronology of zircon and titanite. *J. of South American Earth Sciences* 88, 312-331.~~
- Teixeira, N.P., Bettencourt, J.S., Moura, C.A.V., Dall'Agnol, R., Macambira, E.M.B., 2002. Archean crustal sources for Paleoproterozoic tin-mineralized granites in the Carajas Province, SSE Para, Brazil: Pb-Pb geochronology and Nd isotope geochemistry. *Precambrian Research* 119, 257-275.
- ~~Teixeira, W., Tassinari, C.C.G., Cordani, U.G., Kawashita, K., 1989. A review of the geochronology of the Amazonian craton: tectonic implications. *Precambrian Res.* 42, 213-227.~~
- ~~Teixeira, W., Nelson, J.R., Bettencourt, J.S., Klein, E.L., Oliveira, D.C., 2019. Intraplate Proterozoic magmatism in the Amazonian Craton reviewed: geochronology, crustal tectonics and global matches. In book: *Dyke Swarms of the World: A Modern Perspective*. DOI:10.1007/978-981-13-1666-1\_4~~
- Van Kranendonk, M.J., 2006. Volcanic degassing, hydrothermal circulation and the flourishing of early life on Earth: a review of the evidence from c. 3490-3240 Ma rocks of the Pilbara Supergroup, Pilbara Craton, Western Australia. *Earth Science Rev.* 74, 197-240.
- Vasquez, M.L., Klein, E.L., Macambira, M.J.B., Santos, A., Bahia, R.B.C., Ricci, P., dos, S.F., Quadros, M.L.E.S., 2000. Geochronology of granitoids, mafic intrusions and mineralizations of the Tapajós Gold Province - Amazonian Craton - Brazil. In: *Inter. Geol. Congr. 31, Abstracts, [CD-ROM]*.
- Vasquez, M.L., Sousa, C.S., Carvalho, J.M.A., 2008. Mapa Geológico e de Recursos

Formatted: Font color: Auto

Formatted: Font: (Default) Times New Roman, 11 pt, No underline



- Minerais do Estado do Pará, escala 1:1.000.000. Programa Geologia do Brasil, Belém, CPRM.
- Vasquez, M.L., Dreher, A.M. 2011. Uma avaliação da estratigrafia dos eventos magmáticos de 1900-1860 Ma do Cráton Amazônico. In: SBG, Simp. Geol. Amaz. 12, Bol. Res. [CD ROM].
- Walker, G.P.L., 1983. Ignimbrite types and ignimbrite problems. J. Volcanol. Geotherm. Res. 17, 65-88.
- Went, D.J., 2016 Alluvial fan, braided river and shallow-marine turbidity current deposits in the Port Lazo and Roche Jagu formations, Northern Brittany: relationships to andesite emplacements and implications for age of the Plourivo-Plouézec Group. Geol. Mag. 1-24, Cambridge University Press 2016.
- White, J.D.L., Houghton, B.F., 2006. Primary volcanoclastic rocks. Geological Society of America Bulletin 34, 677-680.
- Willcock, M.A.W., Cas, R.A.F., Giordano, G., Morelli, C., 2013. The eruption, pyroclastic flow behaviour, and caldera in-filling processes of the extremely large volume (N1290 km<sup>3</sup>), intra- to extra-caldera, Permian Ora (Ignimbrite) Formation, Southern Alps, Italy. J. Volcanol. Geotherm. Res. 265, 102-126.
- [Williams, I.S., 1998. U-Th-Pb geochronology by ion microprobe. In: McKibben, M.A., Shanks, W.C.P., Ridley, W.I. \(eds\) Applications of Microanalytical Techniques to Understanding Mineralizing Processes, Rev Econ Geol vol 7. Soc. Econ. Geol., Littleton, 1-35.](#)
- Wolff, J.A., Wright, J.V., 1981. Rheomorphism of welded tuffs. Journal of Volcanology and Geothermal Research 10, 13-34.
- Zanchetta, G., Sulpizio, R., Di Vito, M.A., 2004. The role of volcanic activity and climate in alluvial fan growth at volcanic areas: an example from southern Campania (Italy). Sedimentary Geology 168, 249-280.
- Zernack, A.V., Cronin, S.J., Neall, V.E., Procter, J.N., 2011. A medial to distal volcanoclastic record of an andesitic stratovolcano: detailed stratigraphy of the ring-plain succession of south-west Taranaki, New Zealand: International Journal of Earth Sciences 100, 1937-1966.
- Zhao, G., Cawood, P.A., Wilde, S.A., Sun, M., 2002. Review of global 2.1–1.8 Ga orogens: implications for a pre-Rodinia supercontinent. Earth-Science Reviews 59, 125-162.
- Zhao, G., Sun, M., Wilde, S.A., Li, S., 2004. A Paleo-Mesoproterozoic supercontinent:

assembly, growth and breakup. Earth-Science Reviews 67, 91-123.

#### Figure Captions

Figure 1: location map of the northern South America and the Amazonian ~~Ceraton~~ and divided into several ~~its~~ geochronological provinces and other domains according to Santos et al. (2000); TMP = Tapajós Mineral Province, SFX = São Felix do Xingú Region. ; G = Guyana, GF = French Guyana, S = Suriname.

Figure 2: distribution map of the outcrops analyzed during the field campaigns in both regions a) Tapajós Mineral Province (TMP) and b) São Felix do Xingú region (SFX); PW=distribution of the Santa Rosa formation inferred during the present work; F=distribution of the Santa Rosa formation inferred by Fernandes et al. (2011); BIF=Banded Iron Formation; red and white dot refers to primary andesitic deposits analyzed in Roverato et al. (2017). In both figures are reported the outcrops described in the paper.

Figure 3: massive and banded lavas and rheo-ignimbrite (?) deposits. a) Np173 (7°33'52.31" S, 55°10'58.80" W), b) Xu23 (6°41'08.65" S, 52°25'55.67" W), c) Xu101 (6°52'12.82" S, 52°09'16.12" W), d) Xu52 (6°28'19.32" S, 51°50'08.90" W), e), f), g) Np396 (6°32'41.06" S, 55°23'59.37" W); see Fig. 2 for the outcrops location. For the lithofacies description and more details see the text.

Figure 4: massive primary volcanoclastic rocks with different proportion of ash, lapilli and blocks. All the deposits are interpreted to be emplaced from pyroclastic density currents except (f) that is interpreted as a basal-breccia of a lava body. a) Xu104 (6°52'22.96" S, 52°08'15.91" W), -b) Np183 (7°32'04.13" S, 55°08'50.02" W), c) Np93 (6°44'16.60" S, 55°27'12.96" W), d) Xu29 (6°41'42.51" S, 52°01'23.06" W), e) Xu07 (6°41'56.36" S, 52°08'42.27" W) f) Xu192 (6°31'31.92" S, 53°02'36.60" W); see Fig. 2 for the outcrops location. For the lithofacies description see the text and

Table 1.

Figure 5: microphotographs of different massive ash and lapilli ignimbrite deposits in

thin section: a) broken crystals suggesting the fragmental character of the rock; b) detail of a devitrified juvenile ~~-(?)~~ fragment displaying axiolitic fabric; c) banded sub-millimetric to millimetric lithic fragments immersed in a devitrified groundmass.

Figure 6: reconstructed schematic stratigraphic column and associated photographs representing the evolution of ignimbrite deposits cropping out in the TMP (Np183; 7°32'04.13" S, 55°08'50.02" W); note the increase of welding from the base to the top.

Figure 7: schematic stratigraphic column and relative photographs of a >150 m thick felsic banded lava(s) cropping out in SFX (Xu192; 6°31'31.92" S, 53°02'36.60" W) overlying a basal breccia (Lf ~~m~~LB) and an ignimbrite deposit characterized by a low grade of welding (Lf *l-gw*LA).

Figure 8: stratified primary volcanoclastic rocks, a) related to sedimentation by highly dilute ash-cloud (Np130; 6°54'16.09" S, 55°10'59.38" W) and, b) attribute to pyroclastic surge-type depositional condition from dilute currents (XU162; 6°32'28.39" S, 52°25'26.07" W); see Fig. 2 for the outcrops location. Relative thin section microphotographs (~~c~~b/d) showing micrometric shards. For the lithofacies description see the text and Table 1.

Figure 9: massive sedimentary rocks. ~~-(a)~~ The alternation of lithofacies *csG* and *mS* indicates changes in energy conditions of sedimentation belonging to a subaqueous-subaerial fan-delta interface (Np146; 6°42'58.24" S, 55°28'53.49" W); ~~d~~Detail of centimeters ripples of Lf *mS* (Np89; 6°54'39.36" S, 55°26'12.28 W); ~~(c)~~ Lf *csG* is also associated to Lf *xsSG* (see stratified rocks in section 6.2) (Np27; 8°08'18.43" S, 54°54'37.33" W); ~~(d)~~ ~~Np27, /e/f~~ (e) Xu209 (6°13'55.26" S, 52°42'29.25" W), f) Np158 (7°03'33.79" S, 55°24'11.84" W); ~~t~~The rounded and clast supported character of these lithofacies is linked with fluvial/alluvial deposition by debris-flow dominated processes; see Fig. 2 for the outcrops location. For a more detailed lithofacies description see the text and Table 1.

Figure 10: stratified sedimentary rocks. ~~(a)~~ The quartzitic sandy cross-bedded lithofacies is interpreted as formed in fluvial channel or around margins of immature marine basins (?) (Xu 201; 6°16'12.95" S, 52°52'18.84" W); ~~(b)~~ ~~t~~The cross-stratified

Formatted: Font: Not Italic, No underline

water reworked lithofacies is linked with stream-dominated fluvial/alluvial settings  
 (Np82; 8°03'40.79" S, 54°50'43.52" W); ~~-(c)-~~ The silty sedimentation likely belong to  
 a lacustrine environment characterized by small turbidities (Np158; 7°03'33.79" S,  
 55°24'11.84" W); ~~-(d)-~~ The top of the photographs shows the Lf *bChs* interpreted as  
 inorganic precipitation of silica (chert) in a closed lake basin; white arrows show  
 fragments of the chert deposit eroded by low-energy sandy stream flows or local  
 lacustrine turbidites (Np90; 6°49'50.20" S, 55°28'15.47" W); see Fig. 2 for the  
 outcrops location. For a more detailed lithofacies description see the text and Table 1.

Figure 11: sketch of a wide (300 x 80 m) outcrop in the TMP (Np407; 6°40'35.21" S,  
 55°21'14.63" W). The stratigraphic sequence is tilted showing sub-vertical contacts of  
 the different deposits. The sequence is interpreted displaying at the base banded (or  
 rheo-ignimbrite) and massive lava flows passing to fragmental deposits to the top. (a)  
 ignimbrite medium-grade welded; b) the diffuse-stratified lithofacies indicates tractive  
 processes usually attribute to pyroclastic surge-type depositional condition from dilute  
 currents; c) sedimentary clast-supported deposit (see descriptions in chapter 4.3); d)  
 non-welded lapilli to ash ignimbrite; e) banded lava or highly reomorphic ignimbrite  
 (lava-like). For a more detailed lithofacies description see the text and Table 1.

Figure 12: classification diagrams for the Tapajos volcanics (TMP-V) and lava flow  
 (TMP-LF). TAS diagram with limits of alkaline series from Kuno (1968), dashed line,  
 and Irvine and Baragar (1971), solid line. AFM diagram with alkaline field from Irvine  
 and Baragard (1971). SiO<sub>2</sub> vs K<sub>2</sub>O classification diagram (Ewart, 1982). Literature  
 values are from: VR (a) Vila Rozinho and MA (a) Moraes Almeida volcanic sequences  
 from Lamarão et al. (2002); SF (b) Sobreiro Formation and; SRF (b) Santa Rosa  
 Formation from Fernandes et al. (2011).

Figure 13: REE and spider-diagrams of volcanics and lava flow rocks from the Tapajos  
 region (TMP-V and TMP-LF). REE data are normalized to Chondrite I (CI; values  
 from Ander and Ebihara, 1982) and trace elements are normalized to Mid Ocean Ridge  
 Basalt (MORB; values from Hoffman, 1988). Literature values are from: VR (a) Vila  
 Rozinho and MA (a) Moraes Almeida volcanic sequences are average values from  
 Lamarão et al. (2002); SRF (b) Santa Rosa Formation from Fernandes et al. (2011)

divided in -V volcanoclastics and -LF lava flow. Due to the lack of literature data, comparison of VR (a) and MA (a) is reported only for REE diagram.

Figure 14: tectonic affinity discriminant diagrams for the Tapajos volcanics (TMP-V) and lava flow (TMP-LF). Zr+Nb+Ce+Y (ppm) vs FeO<sub>tot</sub>/MgO (wt.%) diagram. Yb vs Ta diagram. La/Yb vs Nb/La diagram. Th-Ta-Hf/3 diagram. Literature values are from: VR (a) Vila Rozinho and MA (a) Moraes Almeida volcanic sequences from Lamarão et al. (2002); SF (b) Sobreiro Formation and SRF (b) Santa Rosa Formation from Fernandes et al. (2011).

Figure 15: geochronological U-Pb data from Tapajos zircons. Average <sup>206</sup>Pb/<sup>207</sup>Pb age (errors are calculated as 2σ) of the three samples. Probability density plot of <sup>206</sup>Pb/<sup>207</sup>Pb ages. Calculated concordia age for sample NP396 (lava flow) and NP183 (ignimbrite).

Figure 16: geochronological U-Pb data from Xingu zircons. Calculated concordia age for ignimbrite sample XU-08. Probability density plot of <sup>206</sup>Pb/<sup>207</sup>Pb ages.

Figure 17: pelegeographic reconstruction of the fissural and calderic volcanic activity during the Late-Paleoproterozoic in the southern part of the Amazonian craton. In the foreground is shown a section of a caldera and a post-caldera ignimbrite uplift that could facilitate the production of new sediments to be reworked and transported. The rising magma could form sporadic intra-caldera domes and volcanic centers as also shown in the background calderas. Reworked sediments can accumulate into volcano-tectonic depressions, which often collects intra-caldera lakes. In the background a fissure-fed volcanism is the responsible of the emission of lava flows and/or high-grade to rheomorphic ignimbrites. Fluvial deposits that occur throughout all successions represent periods of stream and river reworking. The area is punctuated by little scoria cones and maars that contribute to the amount of the fragmental products well represented in the study regions.

Tables

Table 1: Summary of the main characteristics of volcaniclastic lithofacies of the primary and secondary felsic products analyzed and their interpretation.

Table 2: Major and trace element bulk rock composition of Tapajos samples. Class identify the lithological features of the rocks: VC: volcanoclastic; I: ignimbrite; R: rhyolite; Type identify the geochemical affinity according to the granite classification (Zr+Nb+Ce+Y (ppm) vs  $\text{FeO}_{\text{tot}}/\text{MgO}$  (wt.%) diagram, Fig. 14): I is for I-type granites and A is for A-type granites; b.d.l. is below detection limits; Mg# is calculated as  $\text{Mg}^{2+}/(\text{Fe}^{2+} + \text{Mg}^{2+})$ ; (\*) major elements analyses already published in Roverato et. (2016).

~~Table 2: Major and trace element bulk rock composition of Tapajos samples. VC: volcanoclastic; I: ignimbrite; R: rhyolite; b.d.l. is below detection limits; Mg# is calculated as  $\text{Mg}^{2+}/(\text{Fe}^{2+} + \text{Mg}^{2+})$ ; (\*) major elements analyses already published in Roverato et. (2016).~~

1     **The 2.0-1.88 Ga Paleoproterozoic evolution of the southern Amazonian Craton**  
2     **(Brazil): an interpretation inferred by lithofaciological, geochemical and**  
3     **geochronological data.**  
4  
5  
6  
7     Roverato<sup>\*1,2</sup> M., Giordano<sup>3,4</sup> D., Giovanardi<sup>5</sup> T., Juliani<sup>2</sup> C., Polo<sup>2</sup> L.  
8  
9  
10  
11         1. YachayTech University, School of Geological Sciences and Engineering, Hacienda San José,  
12             Urcuquí, Ecuador.  
13  
14         2. Instituto de Geociências (IGC), Universidade de São Paulo, INCT – Geociam, SP, 05508080,  
15             Brazil.  
16  
17         3. Università degli studi di Torino, Dipartimento di Scienze della Terra, via Valperga Caluso 35,  
18             10125, Torino, Italy.  
19  
20         4. Centro Nazionale delle Ricerche (CNR), Istituto di Geoscienze e Georisorse (IGG), via G.  
21             Moruzzi 1, 56124, Pisa, Italy.  
22  
23         5. Università di Modena e Reggio Emilia, Dipartimento di Scienze Chimiche e Geologiche, 41125,  
24             Modena, via Campi 103, Italy.  
25  
26  
27  
28  
29     \*Corresponding author: matteoroverato1809@gmail.com  
30  
31  
32  
33     **Keywords:** Paleoproterozoic volcanism; Amazonian craton; Fissure eruption; Felsic  
34     volcanism; Lithofacies analyses  
35  
36  
37  
38  
39  
40         **Abstract**  
41  
42         The study of Paleoproterozoic rocks is crucial for understanding Earth's  
43     tectonic evolution during the time when most of the modern crust and ore deposits  
44     were formed. The rocks of the Brazilian Amazonian Craton record some of the most-  
45     complete and best-preserved Paleoproterozoic magmatic and volcanic episodes on  
46     Earth. Following previous investigations, we present new lithofaciological and  
47     stratigraphic records of the felsic rocks of the Tapajós Mineral Province (TMP) (~ 2-  
48     1.88 Ga) and the São Felix do Xingú region (SFX) (~ 1.88 Ga) which, combined with  
49     new petrological and geochronological data, help providing a more complete  
50     understanding of the tectonic, magmatic and volcanological evolution of the  
51     Amazonian Craton. This magmatism/volcanism is thought to be formed in a late-/post-  
52     orogenic to extentional regime confirmed by the new geochemical data presented here.  
53  
54  
55  
56  
57  
58  
59  
60  
61  
62  
63  
64  
65

The transition from late-convergent to extensional tectonic setting could register the beginning of the taphrogenesis that marked the Amazonian Craton throughout the Mesoproterozoic. The volcanological approach of this contribution can serve as a strategy for the modelling of the evolution of Precambrian volcano-sedimentary basins around the world. The large amount of rocks analyzed are divided into primary and secondary volcanoclastic products depending on if they resulted from a direct volcanic activity (pyroclastic) or processes that reworked pyroclastic fragments. Furthermore, the deposits are subdivided into massive and stratified, depending on their primary mechanisms of transport and emplacement. By confirming the results from previous studies, our study permits to depict a more precise paleo-environmental picture of the processes that occurred in the Amazonian Craton during the Late-Paleoproterozoic. In particular, the presence of large regional-scale fissural systems and caldera collapses produced large silicic explosive volcanic eruptions, also accompanied by the emission of large volume effusive products. Although studies on the Amazonian Craton are still scarce and controversial, the present study provides new evidence that this volcanism may have formed one of the largest Silicic Large Igneous Provinces (SLIP) on earth. Our data also confirm that at least two major Paleoproterozoic periods of formation of volcanic rocks exist in the Amazonian craton. This point is of great relevance for any future interpretation of the geological evolution of this craton.

## 1. Introduction

The Proterozoic Eon (2500 – 541 Ma) is the longest and youngest part of the Precambrian Supereon. This Eon represents the time just before the proliferation of oxygen accumulation and complex life on Earth. This period was likely the most tectonically active in Earth's history. In fact, it is also the period during which the largest portion of the modern crust (43%) and mineral ores were produced (Condie, 2000). Studies by Condie (2000) and Rino et al. (2004) suggest that crust production took place episodically, forming predominantly granitoidal crust and secondary volcanic and metamorphic rocks, some of which are extraordinarily well preserved. The Amazonian Craton (AC) is one of the largest preserved Precambrian terrains in the world ( $4.6 \times 10^6 \text{ km}^2$ ) (Almeida et al., 1981). It occupies approximately half of the Brazilian territory and it is the location of important mineral resources such as gold, iron, copper, and tin, among others (e.g. Faraco et al., 1997; Bahia and Quadros, 2000; Juliani, 2002; Klein et al., 2002, 2004; Reis et al., 2006; Klien and Carvalho, 2008;



Monteiro et al., 2008; Juliani et al., 2014, Dall’Agnol et al., 2017). Although the geological investigation of the AC has recently seen a renewed interest of the national and international scientific community, mainly because of the massive presence of ore deposits, a general consensus related to the interpretation of its complex Paleoproterozoic evolution is still missing. Ancient volcanic regions represent a challenge for the understanding of emplacement dynamics especially when the stratigraphic relationships are difficult to decipher or blurred by erosion or vegetation cover. The present work constitutes the natural prosecution of previous investigations, carried out by our research group (Juliani et al., 2005, 2010, 2014; Fernandes et al., 2011; da Cruz et al., 2015; Roverato, 2016; Roverato et al., 2016, 2017), which are devoted to characterize the dynamics of emplacement of Precambrian volcanic rocks and their relationships to sedimentary facies. The study area comprises of the Tapajós Mineral Province (TMP) and the São Felix do Xingú (SFX) region, Pará state, northern Brazil. This contribution provides a means to interpret the volcanic processes active in this region during the Precambrian, mainly based on field observation and detailed lithofacies analyses. In addition, new geochemical and geochronological data are provided. Our study demonstrates how powerful is the approach of rock structure and texture characterization to the interpretation of the eruptive processes that governed the emplacement of volcanic and volcanoclastic sequences. The detailed lithofacies characterization and the stratigraphic reconstruction are important in this area and constitute a powerful key-tool to appropriately interpret the evolution of Precambrian volcano-sedimentary basins. Such an approach would turn to be useful when employed to investigate ancient terrains associated both to the ancient Amazonian felsic volcanism and Precambrian terrains in general.

## 2. Geological evolution of the southern portion of the Amazonian craton

The AC (Almeida et al., 1981) is located in the northern part of South America and is divided into two Precambrian shields, the Central-Brazil (or Guaporé, southern portion) and Guiana Shields (northern portion), which are separated by the Phanerozoic Amazonian Sedimentary Basin (Fig. 1) (Almeida et al., 1981). The entire craton has become tectonically stable before the end of the Precambrian (Dall’Agnol et al., 1994).

It has also been considered (Amaral, 1974; Hasui et al., 1993; Costa and Hasui, 1997) as a large Archean platform that had been reworked and reactivated during the

ca. 2100 Ma Trans-Amazonian event. Alternative proposals based on geochronological and isotopic data (Teixeira et al., 1989; Tassinari and Macambira, 1999; Santos et al., 2000) divided the craton into several, predominantly NW-oriented, geochronological provinces, which have been interpreted as successive continental accretionary events, followed by granitic magmatism and tectonic reworking (Santos, 2003; Vasquez et al., 2008).

In a recent review Teixeira et al. (2019) report that the AC is the host of four LIP-scale (or SLIP) magmatic events discriminated by the Orocaima, Uatumã, Avanavero and Rincón del Tigre events. The igneous rocks described in the present manuscript are widely attributed to the Uatumã event (Dall'Agnol et al., 1999; Lamarão et al., 1999). The studied region is located between TMP and SFX, which is considered to be related to a continental arc, with a NE-SW arc migration as suggested by Juliani and Fernandes (2010), Fernandes et al. (2011) and Roverato et al. (2017). According to these authors a migration from the Serra do Cachimbo graben (in TMP where the subduction trench is located) towards the SFX could be explained by a change in the subducting angle of the oceanic plate beneath the continental plate. This is in agreement with the flat-subduction plate settings proposed by previous authors in other parts of the world (Ferrari et al., 2012; Gutscher et al., 2000; Kay et al., 2005; Mori et al., 2007; Manea et al., 2012).

## 2.1. The TMP (Tapajós Mineral Province)

The TMP (Fig. 2a) is primarily situated in the Tapajós–Parima geochronological/tectonic province (Santos et al., 2000) with the eastern part belonging to the Amazonia Central geochronological/tectonic province (Fig. 1). Based on Sm–Nd data and U–Pb ages (2100–1870 Ma), Santos et al. (2001, 2004) and Vasquez et al. (2008), identified several different domains for the Tapajós–Parima geochronological province and consider the TMP as a sequence of continental magmatic arcs (Ferreira et al., 2000; Santos et al., 2000, 2004; Vasquez et al., 2000; Klein et al., 2001; Lamarão et al., 1999, 2002). Late Paleoproterozoic volcanism of the Tapajós domain is represented by the Vila Riozinho Formation, formed by ca. 2000–1990 Ma intermediate to acid volcanic rocks (Lamarão et al., 2002), and by the Iriri Group that can be divided into the Bom Jardim (Almeida et al., 2000), Salustiano (1870 ± 0.008 Ma; Juliani et al., 2005) and Aruri (Pessoa et al., 1977) formations.

The Bom Jardim Formation (1898 ± 5 Ma, Santos et al., 2001) consists of

mafic to intermediate high-K to shoshonitic calc-alkaline rocks while the latter formations are characterized by rhyolites, dacites and their pyroclastic and epiclastic derivatives. Juliani et al. (2005) considered the Bom Jardim volcanism as a preliminary step of the Iriri event representing pre-caldera volcanism followed by the Salustiano and Aruri caldera-related felsic activity. Post-caldera volcanism is characterized by ring-felsic volcanic structures that produced A-type (Vasquez and Dreher, 2011) rhyolitic lavas and volcanoclastic deposits. Lamarão et al. (2002, 2005) described the felsic A-type Moraes Almeida volcanic sequence ( $1890 \pm 6$  Ma rhyolite,  $1875 \pm 4$  Ma ignimbrite) represented by lavas and ignimbrites as part of the Iriri Group. Juliani et al. (2014) consider these last A-type rocks as similar in composition and age to the Santa Rosa Formation that crops out in the São Felix do Xingú region (SFX), which is considered to have formed by the same fissural-type volcanism (Juliani and Fernandes, 2010; Fernandes et al., 2011; Roverato et al., 2016). Preliminary data indicate that these rocks, for both TMP and SFX, display a very low grade of metamorphism, falling into the prehnite-pumpellyite field (Echeverri-Misas, 2010; Lagler et al., 2011; Fernandes et al., 2011).

## 2.2. The SFX (São Felix do Xingú region)

According to the work of Santos (2003) and Vasques et al. (2008) the SFX region belongs to the Amazonia Central province (Fig. 1). The study area (Fig. 2b) is located near to São Felix do Xingú city, which corresponds to the southern portion of the Carajás Province. The Paleoproterozoic volcanic sequences in the SFX comprise the basal Sobreiro and upper Santa Rosa formations (Macambira and Vale, 1997; Juliani and Fernandes, 2010), which are crosscut by the Sn-bearing A-type granitoids of the Velho Guilherme Suite (Teixeira et al., 2002). Antonio et al. (2017) published the first U-Pb ages on zircons for the Santa Rosa Formation with  $1877.4 \pm 4.3$  Ma for a rhyolite and  $1895 \pm 11$  Ma for a dike. Recent geochronological data on a felsic porphyritic dike belonging to the Velho Guilherme suite yielded an age of  $1857 \pm 8.4$  Ma (Shrimp U/Pb zircon analyses; Roverato, 2016). Other available geochronological data yielded ca.  $1880 \pm 6$  Ma (TIMS Pb–Pb in zircon) for the Sobreiro Formation and ca.  $1879 \pm 2$  Ma (TIMS Pb–Pb in zircon) for the Santa Rosa Formation (Fernandes et al., 2011; Pinho et al., 2006; Teixeira et al., 2002). Despite their similar ages, their geochemical compositions, geological features and eruption styles point to their non-cogeneticity (Fernandes et al., 2011). The Sobreiro Formation (SF) comprises basaltic

172 andesite, andesite and less dacite massive lava flows and volcanoclastic rocks with  
173 high-K calc-alkaline signature (Fernandes et al., 2011; Roverato et al., 2017).  
174 According to da Cruz et al. (2015) late- to post-magmatic hydrothermal alteration in  
175 these rocks is responsible for a secondary paragenesis characterized by epidote,  
176 chlorite, carbonate, clinozoisite, sericite, quartz, albite, hematite and pyrite. The Santa  
177 Rosa Formation (SRF) is described by Fernandes et al. (2011) as characterized by four  
178 lithological facies with A-type signature: (i) rhyolitic lava flow and thick dikes of  
179 banded rhyolite and ignimbrite; (ii) highly rheomorphic felsic ignimbrite associated  
180 with un-welded ash tuff; (iii) felsic crystal tuff, lapilli-tuff and co-ignimbritic breccias;  
181 (iv) granitic porphyry stocks and dikes and subordinate equigranular granitic  
182 intrusions.

### 184 3. Lithofacies analyses

185 Lithofaciological analyses were carried out in the course of this study in order  
186 to understand the geodynamic evolution of the study area. Here we report on the  
187 lithofacies analysis of rocks recognized during our field campaigns (and after in  
188 petrological thin section) at the TMP and SFX provinces. Within the study area (TMP  
189 and SFX), massive to banded lava flows and rheomorphic ignimbrites (Fig. 3) as well  
190 as felsic volcanoclastic rocks of various origin (Figs. 4-8, 11) are frequently found.  
191 Reworked (secondary) volcanoclastic rocks (Fig. 9,10) and sedimentary alluvial/coastal  
192 clastic deposits (epiclastic) are also widely distributed in both TMP and SFX areas.  
193 Primary volcanoclastic rocks are here defined as those fragmental products formed  
194 during a syn-eruptive explosion, which were deposited regardless of whether their  
195 transport occurs through air, water, granular debris or a combination of them (McPhie  
196 et al., 1993; White and Houghton, 2006; Manville et al., 2009; Roverato et al., 2017).  
197 On the other hand, all the units deposited as a consequence of a reworking process of  
198 pre-existing volcanic units are defined here as secondary volcanoclastic rocks. We also  
199 introduce into this group all those epiclastic products that constitute sediments that had  
200 been reworked before, independent of their source and composition. Table 1 shows a  
201 description and interpretation of the volcanoclastic lithofacies, both primary and  
202 secondary, for the deposits identified in the study areas.

### 204 4. Lava flows and rheo-ignimbrites

205 As already discussed by Roverato et al. (2016), the absence of unequivocal

vitroclastic textures complicates the distinction between volcanoclastic and layered lava  
 flows in general and, more in particular, for the ancient volcanic rocks investigated  
 here. Lava flows found in the TMP and SFX provinces have both massive and banded  
 structures (Fig. 3) while still maintaining, in some cases, glassy (obsidian) and  
 aphanitic to porphyritic texture. Their composition varies from trachytic to rhyolitic with  
 various content of alkalis (see section 8). The phenocryst assemblage consists mainly  
 of plagioclase, quartz, Fe–Ti oxides and accessory-amount of zircon and apatite.  
 Plagioclase and bipiramidal quartz crystals (Fig. 3a), with a maximum size of 3-4 mm,  
 range from euhedral to anhedral, showing moderate to intense resorption. Plagioclase  
 shows sieve texture indicating non-equilibrium conditions likely determined by  
 magmatic transport. K-feldspar is also present as anhedral crystals in the groundmass  
 often associated with sericite as alteration phase. Samples are generally affected by  
 variable intensity of hydrothermal alteration. Plagioclase phenocrysts, in particular,  
 present diffuse potassic and minor propylitic alterations. Abundant spherulites and  
 lithophysae of variable size, from millimetric to decimetric, were recognized in almost  
 every sample and are thus common in these rocks (Fig. 3b, c). The spherulites  
 (radiating fibers of K-feldspar and cristobalite), ranging from few millimeters to 2 cm,  
 are typically associated with perlitic fractures. Their content can vary from 10 vol% to  
 70% in the investigated rocks. A large amount of the spherulites developed into  
 lithophysae commonly reaching 10-12 cm as a consequence of cooling and degassing  
 processes. In the obsidian-type lavas (Fig. 3c), the groundmass is characterized by a  
 micro-granophiric-like devitrification texture characterized by crystallization of  
 amorphous quartz and alkali feldspar, a process that occurred after the emplacement of  
 lava bodies. Several rocks show textures that are not easy to be associated to either  
 lava flows or flows of fragmented material which underwent rheomorphism (Fig. 3d-  
 g). Both banded lavas and rheo-ignimbrites display folds (Fig. 3d-g, see also Fig. 11e)  
 and sub-parallel bands on mm- to dm-scale, planar to wavy (Fig. 3e, see also Fig. 6 and  
 7) (parataxitic fabric), that deform and flattened around lithic fragments and crystals  
 which alignment suggests the flow direction. In thin sections, the bands are  
 characterized by extremely flattened vitroclastic textures with the former glass  
 completely replaced by a mixture of quartz and feldspar (Roverato et al., 2016).

## 5. Primary volcanoclastic rocks

We consider primary volcanoclastic rocks those dense, scoriaceous and

pumiceous products of fragmental character emplaced by explosive processes. With pyroclastic we refer to fragmental material generated by any kind of explosive volcanic activity and transported as ash-fall and pyroclastic density currents (Manville et al., 2009), which deposition occurs by suspension settling, from traction, by en masse freezing, or any combination of these (White and Houghton, 2006). Depending on the mechanism of transport and the eruptive style these clastic rocks were distinguished into two different categories, i.e. massive and stratified; and they can vary from well sorted, poorly sorted or unsorted. The rocks are predominantly rhyolitic in composition (Fernandes et al., 2011, Roverato et al., 2016) and there is no significant geochemical difference from the lava flows. Nine main lithofacies (Lf) have been recognized for the volcaniclastic rocks: six of them are massive and three are stratified.

## 5.1. Massive

Six massive lithofacies (mAL, mLA, mLB, *l-gwLA*, *m-gwLA* and *h-gwLA*) were recognized during our field campaign, three of them belong to the welded ignimbrites sub-group (Table 1). By using the granulometric classification proposed by Fisher (1961), ash is defined as any fragment with size <2 mm, lapilli are fragments with size between 2 to 64 mm and blocks (or bombs) have sizes > 64 mm. Massive lithofacies includes all those deposits that display a massive coherent structure. Outcrops of such kind of lithofacies are constituted by a high percentage of ash up to block-rich textures. Most of the observed samples appear to have been affected by devitrification processes of the juvenile pyroclastic fragments and matrix. The presence of juvenile material linked with other observed textures such as broken crystals (Best and Christiansen, 1997) and eutaxitic fabric allows us to confirm that the rocks belonging to lithofacies mAL, mLA, *l-gwLA*, *m-gwLA* and *h-gwLA* are fragmental and pyroclastic in origin. We discuss the meaning of Lf mLB below in section 5.1.2.

### 5.1.1. Lf mAL; mLA (massive Ash to Lapilli; massive Lapilli *and* Ash)

Description: the ash to lapilli (mAL) and lapilli *and* ash (mLA) deposits (Fig. 4a-e, Fig.6) are heterolithologic, matrix supported, containing angular to sub-rounded medium to coarse devitrified lapilli (displaying axiolitic fabric), banded fragments, occasional (or absent) lithics and angular-shaped broken crystals of plagioclase, bipiramidal quartz and rare oxides (Fig. 5). In mLA, clasts < 25 cm in size are randomly immersed in the groundmass (Fig 4d and 4e, 11d). Some of them are altered

by carbonate minerals. Groundmass of mAL and mLA is formed by K-feldspar and quartz crystals, devitrified ash fragments and sericite crystals as phase of alteration (Fig. 5).

Interpretation: the general massive aspect and the poor sorting of mAL and mLA point to a laminar granular flow transport regime and the fine content suggests the deposition from a dilute fluid escape-dominated flow-boundary zone in which turbulent shear-induced tractional segregation is suppressed (Branney and Kokelaar, 2002; Sulpizio et al., 2007, Roverato et al., 2017). These lithofacies are interpreted as ash flow deposits suggesting the deposition from a pyroclastic density current (PDC) (Lenhardt et al., 2011; Sulpizio et al., 2014; Roverato et al., 2017). The coarser lithofacies mLA (fig. 4e) could be related to proximal co-ignimbritic breccias as result of deposition by denser pyroclastic granular flows (Branney and Kokelaar, 2002). The angular aspect of the clasts indicates short-period transport.

#### 5.1.2. Lf mLB (massive Lapilli and Block)

Description: this lithofacies (fig. 4f, fig.7) represents monolithologic coarse-grained rocks having high-clast content (clast:matrix ratios up to 3:1). Angular/sub-angular coarse lapilli and blocks up to 50-60 cm of devitrified banded or massive lava fragments are immersed in a devitrified fine lapilli and coarse ash matrix.

Interpretation: the blocky and monolithologic coarse-grained aspect of the lithofacies mLB and its position underneath thick flow-deposits is attributed to the basal auto-brecciation of lava flows and/or rheo-ignimbrite flows. Despite the lithofacies is likely a consequence of an effusive volcanic activity (in the lava-flow case) it is considered anyway as part of the volcanoclastic group due to its fragmental character.

#### 5.1.3. Lf *l*-gwLA; *m*-gwLA; *h*-gwLA (welded Ignimbrites)

Description: all massive deposits displaying welding characteristics have been grouped in the “welded ignimbrites” group (Table 1), following the idea of “grade of welding” (Walker, 1983) (i.e. the amount of welding and compaction exhibited by deposits). The rocks are matrix-supported with sub-rounded to angular lapilli and ash lithic clasts, euhedral, subhedral and broken crystals (plagioclase and less quartz) and deformed devitrified juvenile fragments (*fiamme*). Slightly- (low-grade, *l*-gwLA), medium- (medium-grade, *m*-gwLA), well-stretched (high-grade, *h*-gwLA) *fiamme*

(Fig. 6), as well as, devitrified shards define the eutaxitic fabric (Roverato et al., 2016). These fragments varying from millimetric to 3–4 cm in size are immersed in a homogeneous micro-granophiric-like devitrified groundmass (see Roverato et al., 2016 for details). Figure 6 shows a stratigraphic column representing a 35 m thick sequence of ignimbrite deposits found in the TMP, displaying very low-grade to high-grade welded fabric where the grade of welding increases toward the top of the succession. The very top of the sequence is characterized by columnar jointing.

Interpretation: the massive aspect and the poor sorting of the lithofacies *l-gwLA*, *m-gwLA* and *h-gwLA* point to a laminar granular flow transport regime, interpreted to be deposited from a pyroclastic density current (PDC). The welded character of these lithofacies is indicative of hot PDC emplacement and compaction that result into the low- up to high-grade eutaxitic fabric. This process is favored by loading-compaction, low-viscosity fragments, high temperature (i.e. > 900°C), cooling of gas-permeable fragments (pumices) and dissolved water (Branney and Kokelaar, 2002; Roverato et al., 2016 and references therein).

## 5.2. Stratified

These lithofacies, although commonly associated with ignimbrites, are not very spread in the studied areas. We also didn't find any alternation between massive and stratified deposits even if this association is a common occurrence in PDC deposits (Sulpizio et al., 2014; Roverato et al., 2017), alternating dilute (stratified deposits resulting) and concentrated (massive deposits resulting) regimes during transport (Sulpizio et al., 2014). Just one example has been found in TMP and is reported in the stratigraphic reconstruction of fig.11.

### 5.2.1 Lf sA; xsA; dsAL (stratified Ash; cross-stratified Ash; diffusely stratified Ash to lapilli)

Description: the stratified samples and outcrops analyzed comprise well sorted very fine to fine ash organized in millimetric to sub-millimetric parallel (sA) or cross-stratified (xsA) layers, with sharp or gradational changes in grain size (Fig. 8). The fragments are represented by devitrified shards, crystals (plagioclase), and rare (or absent) lithics (fig. 8d) immersed in a devitrified groundmass. Diffuse-stratified lithofacies dsAL display a coarser character with coarse lithic and devitrified ash and lapilli fragments forming well developed parallel continuous meter-long stratification



(or very-low angle cross-stratification) at centimeter scale (fig. 11b), with gradational changes in grain-size. The sorting varies from well to moderate.

Interpretation: the fine parallel layering of shards material displayed by lithofacies sA is interpreted here as being deposited under the product of sedimentation by the upper and highly dilute ash-cloud that accompany a pyroclastic-density current. We don't exclude the direct sedimentation from tephra fall-out activity. Cross-stratified (Lf xsA) and diffuse-stratified (Lf dsAL) deposits indicate tractive processes usually attribute to pyroclastic surge-type depositional condition from dilute currents (Cas and Wright 1987; Lenhardt et al., 2011; Roverato et al., 2017). We interpreted these as pyroclastic surge deposits although Lf dsAL could also be the product of coarse ash fall-out processes. Pyroclastic surge deposits usually display small volume and rarely reach more than 10 km from their source (Lenhardt et al., 2011). Conversely, fall-out deposits could emplace tens of kilometers from their source.

## 6. Secondary volcanoclastic/epiclastic rocks

The nomenclature of Fisher et al. (1961) is applied also for the secondary volcanoclastic rocks as follow: silt ( $2 < \phi < 64 \mu\text{m}$ ), sand ( $64 \mu\text{m} < \phi < 2 \text{ mm}$ ), gravel ( $2 < \phi < 64 \text{ mm}$ ), cobble ( $64 < \phi < 256 \text{ mm}$ ). These rocks are considered as the product of reworking and erosive processes. The clasts belonging to this group show a wide range of composition, size and shape variations. Based on their component, texture and fabric, we recognized five massive, both matrix- and clast-supported, and four stratified lithofacies (fig. 9).

### 6.1. Massive

#### 6.1.1. Lf mS (massive Sand)

Description: this lithofacies consists of reddish moderately to well-sorted, massive, fine- to medium grained sand forming parallel strata intercalated to clast-supported conglomerate deposits (Lf csG) (fig. 9a). The sandstone strata extend tens of meters and present thinness between 0.4-0.8 m. Lf mS is predominantly composed of quartz, feldspar and minor rock fragments. Contacts between mS and csG are sharp with rare slightly erosional surfaces. The tops of the sandstone are characterized by the presence of centimeters ripples (fig. 9b).

Interpretation: the massive sand (mS) and the small ripples found at the top of the strata indicate low energy under tractional currents in shallow water conditions

(Collison and Thompson, 1982; Lenhardt et al., 2011). The alternation of Lf csG and mS indicates changes in energy conditions of sedimentation. We interpret these oscillations as belonging to a subaqueous-subaerial fan-delta interface setting where continental supply of material alternates to under-water sand accumulation (Lf mS).

#### 6.1.2. Lf csG (clast supported Gravel)

Description: this lithofacies (Fig. 9a, c, d) is massive, clast to matrix supported, with heterolithologic felsic rounded high-spherical coarse gravel with a sandy inter-clast matrix. Clasts are mainly characterized by massive and banded medium- to coarse-size felsic lava fragments (and rare quartz; size does not exceed 5 cm) and present rounded with low- to high-sphericity. We found lithofacies csG also associated to xsSG (see below section 6.2.2.) (Fig. 9c, 10b).

Interpretation: lithofacies csG is dominated by water flow processes where matrix plays a secondary role. The clast-supported character and less matrix content indicates that water removed the finer particles during transport and deposition. Lf csG display rounded clasts and well-sorting indicative of good selection during transport and emplacement. The rounded character of csG and the presence of matrix in the deposits suggest a laminar debris-flow regime in medial reaches of stream-dominated fluvial/alluvial fans (Mueller and Corcoran, 1998).

#### 6.1.3. Lf csGS (clast supported Gravel to Sand)

Description: Lf csGS (Fig. 9e, 11c) is massive, moderately well-sorted and clast-supported. Clasts (gravel to sand) present sub-rounded to sub-angular with low/medium sphericity with maximum size of 2-3 cm. The rocks belonging to this lithofacies are mainly formed by massive felsic lava fragments with different color and crystallinity.

Interpretation: Lf csGS is dominated by water flow processes where matrix plays a secondary role. The clast-supported character and less matrix content indicates that water removed the finer particles during transport and deposition. This lithofacies represents deposition within a debris-flow dominated fluvial/alluvial environment. Poor sorting, clast-supported and sub-angular clasts point to deposition by localized laminar hyperconcentrated-flows in volcanic fans fringing flanks of volcanic edifices. Single cross-beds are usually ca. 1 cm thick

#### 6.1.4. Lf csGC (clast supported Gravel and Cobble)

Description: Lithofacies csGC (Fig. 9f) is massive, low-sorted and clast-supported. The clast population is characterized by sub-rounded, low/medium sphericity, massive felsic porphyritic fragments with maximum size up to 20 cm. This lithofacies has an interstitial matrix characterized by medium to coarse sand.

Interpretation: Lf csGC is dominated by water flow processes where matrix plays a secondary role. The clast-supported character and less matrix content indicates that water removed the finer particles during transport and deposition. This lithofacies represents deposition within a debris-flow dominated alluvial environment. Poor sorting, clast-supported and sub-angular clasts likely points to deposition by localized non-cohesive debris-flows.

### 6.2. Stratified

#### 6.2.1 Lf xsS (cross-stratified Sand)

Description: lithofacies cross-stratified Sand (Fig. 10a) consist of white to brownish low-angle cross-stratified coarse quartzitic sandstone. The sandstones are characterized by lobe to sheet-shaped bodies. Major bedsets are recognized ranging in thickness from 0.5 to 1.5 m, composed of fine-grained sandstone dominated by medium-angle cross strata (18-20°). Single cross-beds are usually 0.7-1cm thick. The outcrops displaying this lithofacies extend tens of meters with sharp upper and lower contact.

Interpretation: the cross-stratification of xsS is interpreted as formed in fluvial channels attesting the deposition from crested dune bed-forms that formed under condition of lower flow regime (Collinson, 1996; Miall, 1996; Capuzzo and Wetzel, 2004; Went, 2016). The deposition of medium-angle cross-bedding within large-scale examples of beds indicates that these larger beds are likely a product of bar migration. The beds are interpreted as channel-fill deposits (Lenhardt et al., 2017) related to a fluvial environment likely associated to meandering or braided rivers. Shoreline deposition developed around margins of immature marine basins is also considered.

#### 6.2.2. Lf xsSG (cross-stratified Sand and Gravel)

Description: Lf xsSG (Fig. 10b) is characterized by crystal-lithic fine to coarse sand and fine gravel (max 5-6 mm in size) organized in cross-bedded stratification. Clasts display medium roundness and sphericity and are mostly composed by felsic

fragments. Stratification is defined by alternating of well to poorly sorted, fine to coarse millimeters-thick strata. The finer black layers are formed by sub-millimetric hematite sand.

Interpretation: Lf xsSG correspond to cross-stratified water reworked deposits. The cross-stratified thicker fine gravelly strata, alternated with sandy layers laterally discontinuous, were interpreted as different pulses as the result of rapid deposition from hyperconcentrated flows (Zanchetta et al., 2004) in a stream-dominated fluvial/alluvial setting. Alternation with csG (Fig. 9c) represents difference of energy condition.

#### 6.2.3. Lf dsSt (diffusely layered Silt)

Description: this lithofacies consists of parallel, lenticular, truncated, and locally low-angle cross-stratified multicolor millimetric well-sorted fine- to very fine-grained sand and silt strata (Fig. 10c). Within the sandy bedset, a thinning- and fining-upward trend may be distinguished. Small and straight groove marks have been detected and reduced tiny slump folding is also presence in some parts.

Interpretation: lithofacies dsSt displays diffuse fine stratification with tiny ripples, suggesting transport and sedimentation in shallow water. The thin sheet-shaped is interpreted as flood sediments (Lenhardt et al., 2011). These deposits are interpreted to have been formed in low energy lacustrine environment or ponds (Collinson, 1996; Roverato et al., 2017) characterized by small turbidities successions affected by scouring and tiny deformations (slumps) of the sediments.

#### 6.2.4. Lf bChS (bedded Chert and Sand)

Description: the bedded chert lithofacies (with sand) (bChS) (Fig. 10d) crops out in both regions and it is characterized by outcrops that can be traced on strike for hundreds of meters. The facies consist of thin laminated pinkish chert (layers < 1mm in thickness) with darker laminae intercalated, formed predominantly by hematite (Lenhardt et al., 2017). The layers are composed by microcrystalline quartz. In some portions, these lithofacies are associated with fine to medium sand composed mainly by quartz and less volcanic fragments.

Interpretation: this lithofacies is interpreted as inorganic precipitation of silica in a closed lake basin mainly due to its association with volcanic rocks and fine sandstone (Blatt et al., 1980; Eriksson et al., 1994). The picture in figure 10d shows

elongated ripped-up millimetric fragments of chert immersed in the sandstone eroded by low-energy stream flow or local lacustrine turbidites. As suggests by Lenhardt et al. (2017) the chert may have formed during repeated pulses of hydrothermal fluids that circulated into the lake water during hiatuses in the volcanism (Van Kranendonk, 2006).

## 7. Analytical methods for geochemistry and geochronology

A total of 19 new samples (9 volcanoclastics and 10 lava flows) from the Tapajós region (associated with the data published in Roverato et al., 2016; Table 2) were analysed for bulk rock major and trace elements. Major element bulk rock analyses were performed by X-ray fluorescence, using a wavelength dispersive Philips PW 2400 spectrometry, using fused glass disks according to procedures described by Mori et al. (1999). Accuracy was greater than 2%. Trace element analyses in selected samples were performed by Inductively Coupled Plasma-Mass Spectrometry (ICP-MS) using the procedure described by Navarro et al. (2008). Accuracy, determined with respect to the reference standards BHVO-2 and BR, was 0.5–2%.

Zircon grains were examined with a FEI-QUANTA 250 scanning electron microscope equipped with secondary-electron and cathodoluminescence (CL) detectors at the Instituto de Geociências - Centro de Pesquisas Geocronológicas - Universidade de São Paulo (IGc-CPGeo-USP); the most common conditions used in CL analysis were 60  $\mu$ A of emission current, 15.0 kV of accelerating voltage, 7  $\mu$ m of beam diameter, 200  $\mu$ s of acquisition time, and a resolution of 2048x1887 pixels and 345 dpi. Selected samples were analyzed for U-Pb isotopes using a SHRIMP-IIe also at IGc-CPGeo-USP, following the analytical procedures of Williams (1998) as reported by Giovanardi et al. (2015). Correction for common Pb is based on the measured  $^{204}\text{Pb}$ , and the typical error for the  $^{206}\text{Pb}/^{238}\text{U}$  ratio is less than 2%; U abundance and U-Pb ratios were calibrated against the TEMORA-II standard. The dataset consists of 56 new U-Pb SHRIMP-II analyses and is reported in Table 3. Thirty-five analyses were performed on zircon grains from the Tapajós region as follow: 11 analyses on sample NP380-C, 11 analyses on sample NP183 and 13 analyses on sample NP396-B. Eleven analyses were performed on zircon grains from Xingú sample XU08. For all samples,  $^{207}\text{Pb}/^{235}\text{U}$  and  $^{206}\text{Pb}/^{238}\text{U}$  concordia ages (with 95% of confidence level and  $2\sigma$  error) are calculated using Isoplot 4.1 software (Ludwig, 2009).

512

## 513 8. Geochemistry of the TMP samples

514 Independently of their nature (lavas or volcanoclastic), the rocks of the TMP  
515 follow a typical calc-alkaline trend (Fig. 12). They are mostly rhyolitic in composition  
516 (Table 2), with four exceptions which fall in the trachytic field. In addition, their low  
517 LOI values (0.32-3.51%) and the low FeO content (0.78 – 3.26%) together with the  
518 negative correlation FeO vs SiO<sub>2</sub> appears to indicate that the investigated volcanic  
519 rocks neither underwent significant alteration processes nor they belong to sedimentary  
520 suites which commonly contain water rich clay minerals. TMP volcanoclastic and lava  
521 flows show similar negative correlation between TiO<sub>2</sub>, Al<sub>2</sub>O<sub>3</sub>, MgO, FeO, CaO, Na<sub>2</sub>O  
522 and P<sub>2</sub>O<sub>5</sub> with SiO<sub>2</sub>. A negative correlation between K<sub>2</sub>O and SiO<sub>2</sub> also exists for the  
523 volcanoclastic, but not for the lava flows. The similar trends observed suggest that both  
524 these kind of rocks are originated by similar magmatic sources. Such a conclusion is  
525 supported by similar variation paths, although with different values, of minor and trace  
526 elements (Fig. 13). In particular, TMP lava flows show LREE enrichment  
527 ((La/Yb)<sub>N</sub>=10.68-21.45; normalization to Chondrite I from Anders & Ebihara, 1982)  
528 and a negative Eu anomaly which increases from trachytes ((Eu/Eu\*)<sub>N</sub>=0.89-0.78) to  
529 rhyolites ((Eu/Eu\*)<sub>N</sub>=0.69-0.31) (Fig. 13). The Eu negative anomaly, shown from all  
530 the samples, is expression of feldspar fractionation. On the other hand, volcanoclastics  
531 rocks show similar LREE enrichment ((La/Yb)<sub>N</sub>=11.12-28.10) and negative Eu  
532 anomaly ((Eu/Eu\*)<sub>N</sub>=0.97-0.37) (Fig. 13). In addition, volcanoclastics have higher  
533 LREE abundances with respect to lavas (La between 35.5-91.3 ppm and between 40.5-  
534 71.9 ppm, respectively) while they have similar MREE and HREE contents (Yb  
535 between 1.56-3.43 ppm and between 1.83-4.11 ppm, respectively). Volcanoclastics  
536 commonly show higher Rb (121-272.9 ppm) and Pb (4.5-137.1 ppm) with respect to  
537 lavas (Rb=96.1-232 ppm and Pb=2.7-45.8 ppm). Volcanoclastics are enriched in LILE,  
538 Th and U with respect to MORB (Fig. 13; normalization to MORB from Hoffman,  
539 1988), with the exception of Sr, which commonly show a pronounced negative  
540 anomaly ((Sr/Sr\*)<sub>N</sub>=0.55-0.05). The Sr negative anomaly is consistent with feldspar  
541 fractionation. Negative anomalies are also present for Nb and Ta, while Ba and Pb are  
542 commonly enriched (Fig. 13). Lavas show a similar trace pattern, but higher values  
543 dispersion (Fig. 13). The Ba enrichment is less pronounced with respect to  
544 volcanoclastics (Ba between 75-1965 ppm and 310-2245 ppm, respectively) and the  
545 Nb/Ta ratio show higher dispersion (3.29-14.63 and 6.73-13.9, respectively), indicating

more limited fractionation of feldspar. Geochemical affinity of Tapajós volcaniclastics and lava flows suggests that the magmatism occurred in active continental setting (Fig. 14). Using the tectonic discriminant diagrams of  $Zr+Nb+Ce+Y$  (ppm) vs  $FeO_{tot}/MgO$  (wt.%),  $Yb$  vs  $Ta$  and  $Th-Ta-Hf/3$  (Wahlen et al., 1987; Pearce et al., 1984; Wood, 1980), the magmatism in the Tapajos region appears related to a syn- to post-collisional setting with few samples falling into the intraplate field (Fig. 14). According to the refined diagram  $Nb+Y$  vs  $Rb$  of Pearce (1996), all the Tapajos volcanics, together with the majority of volcanic rocks from the Sobreiro formation (Fernandes et al., 2011) are consistent with a late- to post-collisional setting (Fig. 14).

## 9. U-Pb zircon Geochronology

Zircons from Tapajos samples are colorless, sometimes fractured and euhedral to sub-euhedral. They can contain inclusions of apatite or spinel and display commonly low emission in Cathodoluminescence (CL). All crystals show magmatic oscillatory zoning and commonly a dark core which, in most cases, appears to be homogenous. Nonetheless, in few cases an inner core with discordant and partially reabsorbed domains is recognized. Some of the zircons also show a bright CL rim with transgressive or sub-concordant contacts with the inner oscillatory zoning. Zircons from sample XU08 from the Xingu region are colourless, rarely fractured and sub-euhedral. Inclusions of apatite or spinel are also observed sometimes. Crystals are medium in CL emissions and commonly show a homogeneous core and a concordant magmatic oscillatory zoning. Few zircons show a core with discordant zoning. No transgressive bright CL rims were recognized. Analyses were carried out on zircons that do not show transgressive or resorption features and discordant inner cores. Zircons from sample NP183 (Ignimbrite) provide 4 discordant and 7 concordant analyses that provide an upper intercept at  $1984 \pm 8.5$  Ma (95% confident decay-const. errs included, MSWD 1.09) and a concordia age at  $1986 \pm 8.2$  Ma ( $2\sigma$ , decay-const. errs included, MSWD 1.08, Probability of concordance = 0.30; Fig. 15). Single spot  $^{206}Pb/^{207}Pb$  ages range between  $2010 \pm 17$  Ma and  $1909 \pm 53$  Ma with an average age of  $1985 \pm 11$  Ma (95% confident decay-const. errs included, MSWD 1.6, Probability of concordance = 0.15; Fig. 15). Zircons from sample NP380 (Ignimbrite) show slightly older single spot  $^{206}Pb/^{207}Pb$  ages between  $2023 \pm 31$  Ma and  $1981 \pm 24$  Ma with an average age of  $1998 \pm 5.9$  Ma (95% confident decay-const. errs included, MSWD 0.74,

Probability of concordance = 0.68; Fig. 15). Analyses are slightly discordant (up to 4%) providing an upper intercept at  $1998 \pm 7.7$  Ma (95% confident decay-const. errs included, MSWD 0.74). Zircons from sample NP396 (Banded lava) provide 5 discordant ages and 8 concordant analyses, which provide an upper intercept at  $1994 \pm 8.2$  Ma (95% confident decay-const. errs included, MSWD 1.40) and a concordia age at  $1997 \pm 7.0$  Ma ( $2\sigma$ , decay-const. errs included, MSWD 5.70, Probability of concordance = 0.02; Fig. 15). Single spot  $^{206}\text{Pb}/^{207}\text{Pb}$  ages range between  $2014 \pm 14$  Ma and  $1973 \pm 8$  Ma with an average age of  $1994 \pm 8.7$  Ma (95% confident decay-const. errs included, MSWD 1.6, Probability of concordance = 0.12; Fig. 15). Pooling together the analyses of the Tapajós samples provides an average age of  $1991 \pm 12$  Ma ( $2\sigma$ , MSWD 1.50, Probability of concordance = 0.06). Zircons from sample XU08 (Lava flow) provide a concordia age at  $1882 \pm 6.4$  Ma ( $2\sigma$ , decay-const. errs included, MSWD 2.70, Probability of concordance = 0.10; Fig. 16). Single spot  $^{206}\text{Pb}/^{207}\text{Pb}$  ages range between  $1899 \pm 10$  Ma and  $1875 \pm 13$  Ma, with an average at  $1884 \pm 5.2$  Ma (95% confident decay-const. errs included, MSWD 0.60, Probability of concordance = 0.82).

## 10. Discussion

### 10.1. Subduction-related to extensional setting

The geochemistry of the TMP samples presented in this work display a high-K calc-alkaline signature (Fig. 12); they mainly fall into the A-type intra-plate granite field and tectonic discriminant diagrams suggest a late- to post-collisional setting for the TMP volcanism (Fig. 14). This interpretation is also supported by enrichment in LILE, Th, U and LREE of our samples, which suggest a strong crustal component in the parent melt consistent with a subduction/post orogenic geodynamic setting (Figs. 12, 13, 14), and the high HSFE which shifted the TMP volcanics composition in the A-type granites showing however FeO/MgO which are low and comparable with I- and S-types granites (Fig. 14). Similar features are reported in previous works (Lamarão et al., 1999; Lamarão et al., 2002) for volcanics in the Tapajós region, which are grouped into the Vila Riozinho (VR) and Maraes Aldeida (MA) formations, respectively. The VR rocks are intermediate to felsic in composition (Lamarão et al., 2002) with a calc-alkaline signature, while the rhyolites and ignimbrites of MA are slightly enriched in silica compared to the rhyolites of VR and are geochemically similar to evolved A-type granites (Lamarão et al., 2002). Our results show similarities with these data,



suggesting that our specimens could be part of the VR and/or MA formations. The identification of two volcanic series has important implications for the understanding of the magmatic evolution of the Amazonian craton in late Paleoproterozoic. A model for the evolution of the TMP involves a first stage of subduction-related magmatism followed by an intracontinental magmatism related to a distensional event (Lamarão et al., 2002). Geochronological analyses by Lamarão et al. (2002) yielded ages of ca. 2 Ga for the VR and ca. 1.88-1.87 Ga for the MA volcanisms. The three new U-Pb geochronological analyses reported in this study yielded ages of ca. 2000 Ma (fig. 15) are concordant with the ages presented by Lamarão et al. (2002) for the VR magmatism, thus suggesting that the TMP rocks could be part of the VR volcanic sequence. However, TMP rocks are geochemically more evolved with respect to VR in terms of SiO<sub>2</sub> (63.8-76.6 wt.% and 54.4-71.8 wt.%, respectively), K<sub>2</sub>O (2.3-7.1 wt.% and 2.1-5.8 wt.%, respectively) and REE abundances and are more similar to MA rocks (Figs. 11, 12 and 13). In particular, REE patterns of the TMP samples are comparable with the rocks of the MA formation (Fig. 12) while they are more enriched in REE with respect to VR rocks. Conversely, TMP rocks are enriched in Ba (Fig. 12), while MA are depleted, and have compositions for Rb/Zr ratio and Nb, considered as a proxy for arc maturity (Brown et al., 1984), similar to VR and different from MA (Rb/Zr between 0.3-1.1 in TMP, 0.2-0.7 in VR and 0.2-1.7 in MA; Lamarão et al., 2002). Thus, according to geochronological and petrological data, we proposed that the TMP rocks in this study must be ascribed to the VR formation. Geochemical differences in our rocks and VR volcanics could be explained by a more evolved character of the TMP rocks. The evidences of plagioclase fractionation from the parent melts of the TMP (negative Eu and Sr anomalies, Fig. 12) and their absence in less evolved VR rocks reinforce this interpretation, and suggest fractional crystallization as the prominent process controlling the VR magmatism evolution. However, we want to point out that due to the large area covered by the presented investigation (Fig. 2), together with the VR area, the geochemical variations between our rocks (TMP) and VR could be the result of local/regional heterogeneities in the magmatism. This hypothesis is supported by the intermediate characteristics of the TMP samples with respect to the VR and MA volcanoclastic material (Figs 11, 12 and 13).

Recently, new authors (Juliani et al., 2014) suggest the geochemical and geochronological signature of the MA formation could be correlated to the felsic Santa Rosa formation (SRF) cropping out in the SFX region. Our new U-Pb geochronological

analyses on one rock sample from the SRF yielded an average age of  $1884 \pm 5.2$  Ma (Fig. 16) that is consistent with previous Pb-Pb ages on other locations. Juliani and Fernandes (2010) published two Pb-Pb ages on zircons of  $1879 \pm 2$  Ma and  $1884 \pm 1.7$  for a rhyolite and an ash tuff, respectively. Recently Antonio et al. (2017) publishes the first U-Pb ages on zircons for the Santa Rosa Formation with  $1877.4 \pm 4.3$  Ma for a rhyolite and  $1895 \pm 11$  Ma for a dike. All geochronological results support a ca. 1880 Ma age for the emplacement of these rocks.

The southern Amazonian craton, as well as other Precambrian terrains worldwide (Condie, 2002; Hoffman, 1988; Zhao et al., 2002), are considered to be characterized by a series of orogenic to post-orogenic events from 2.0 up to 1.88 Ga. The amalgamation of cratonic blocks worldwide established connections between South America and West Africa and other cratonic terrains such as Western Australia and South Africa, Laurentia and Baltica, Siberia and Laurentia, Laurentia and Central Australia, etc (Zhao et al., 2002). These late-Paleoproterozoic collisional processes likely formed the controversial supercontinent Columbia (Zhao et al., 2004). This period also coincides with a major peak in orogenic gold resources (Goldfarb et al., 2001; Juliani et al., 2014) and understanding the geodynamic of this period is crucial for economic interests. Antonio et al. (2017) highlight that for the period 1.88 Ga, many cratonic terrains have been characterized by extensive magmatism. These authors report as examples the 1880 Ma NE-trending Ghost dike swarm and the 1880 Ma Circum-Superior LIP in the Canadian shield (Minifie et al., 2013), the 1880 Ma Southern Bastar- Cuddapah LIP in India (French et al., 2008), the Mashonaland sills and the Post-Waterberg dolerites in Kalahari craton (Hanson et al., 2004), an extensive A-type magmatism in Baltica and in Siberia. The A-type affinity of the 1.88 Ga rocks is widely described by other authors in different regions into the Amazonian craton (Ferron et al., 2010; Pierosan et al., 2011; Fernandes et al., 2011; Klein et al., 2012; Barreto et al., 2014; Teixeira et al., 2018). Currently, the significance of the 1.88 Ga A-type magmatism in the AC is still matter of debate, also due to the extremely large aerial cover which interested several different domains with different basements and geologic evolutions. For example, studies on the Carajas region suggest that the 1.88 Ga anorogenic magmatism in this domain was provoked by delamination and fusion of the Archean basement by a mantle plume which originated an extensional setting (Dell'Agnol et al., 2005; Silva et al., 2016; Teixeira et al., 2018; Teixeira et al., 2019).

Conversely, the geochemical features of the TMP and SFX magmatism

presented in this work and in literature (Lamarão et al., 2002, 2005; Fernandes et al., 2011) mainly support an extensional regime of these regions related to a late- to post-collisional event, being possibly related to the end of the subduction process. The transition from convergent (late-/post-orogenic) to extensional tectonic setting could register the beginning of the taphrogenesis that marked the Amazonian Craton throughout the Mesoproterozoic (Brito Neves, 1999; Lamarão et al., 2002). The ca. 1.88 Ga felsic magmatism in different provinces of the Amazonian craton could represent the oldest magmatism related to this event.

It should be mentioned that in term of textural features, the products emitted during the transition between the late-/post-collisional to extensive events don't display substantial variations. In other words, the lithofaciological signature of the volcanic and volcanoclastic rocks that characterized the 2 Ga VR event (subduction related) is similar for those products erupted during the 1.88-1.87 Ga extensional volcanism that characterized the MA and SRF events. Moreover, the post-orogenic to extensional setting emphasizes the continental setting where the studied volcanic products have been emitted. Following the idea of Roverato et al. (2017) for the Late-Paleoproterozoic andesitic Sobreiro Formation, we stress the lack of any evidences in favour of subaqueous eruptions for the emitted felsic products such as pillow lavas as well as hyaloclastites. This suggests the subaerial character of the volcanism and its emitted products acted in both regions.

## 10.2. Eruptive style and emplacement

The study areas are widely characterized by volcanic deposits whose eruptive style is hard to differentiate. Distinguishing between banded lavas and high grade ignimbrites is, sometime, extremely challenging (Henry and Wolff, 1992; Manley, 1995). This is made even more complicated when the investigated deposits are ancient and the outcrops intensely eroded, such as those Precambrian terrains investigated here (Lenhardt et al., 2012; Roverato et al., 2016; Lenhardt et al., 2017). Evidences in the field show that a great volume of the volcanic activity is represented by the emission of lava flows and/or high-grade to rheomorphic ignimbrites, although an important amount of other fragmental products of different type (Lf mAL, mLA, *l-g/m-g/h-gwAL*) are also well represented in both regions. High-grade welded and rheomorphic (up to lava-like) ignimbrites share similar features with lavas, displaying banding and

ductile folds formed by the elongation of fiamme and vesicles (Schmincke and Swanson, 1967; Chapin and Lowell, 1979; Wolff and Wright, 1981; Branney et al., 1992; Sumner and Branney, 2002; Pioli and Rosi, 2005; Andrews and Branney, 2011; Brown and Bell, 2013). Although the ignimbrites investigated here have a fragmental derivation their origin largely differ from those characteristic of fallout deposits that form by a sustained column explosive-driven eruption. High-grade welded and rheomorphic ignimbrites are correlated with highly explosive plinian-type eruptions which produce, during their column collapse stage, large PDC. In addition, high-grade rheomorphism of silicic products, either deriving from an explosive or effusive eruption, are favored by high temperature low-viscosity emplacement conditions and the presence of some residual water. The high temperatures condition of our deposits is also confirmed by the pervasive presence of spherulites and lithophysae formed during the slow-cooling regimes of large silica-rich lavas and welded ignimbrites (Lofgren, 1971; Breitzkreuz, 2013). The eruptive scenario showed in figure 17 giving origin to the frequent eruption of large volume and high discharge rate lava flows and ignimbrites was likely characterized by fissure-fed and caldera collapses systems as those described by previous authors (Legros et al., 2000; Aguirre et al., 2003; Cas et al., 2011; Lesti et al., 2011; Lenhardt et al., 2012; Willcock et al., 2013). Eruptions fed by extensive fissures of large size, in fact, appear to be the most favourable volcanic systems to minimize cooling during emplacement and produce an alternance of low-height sustained column eruptions feeding PDC and eruptions characterized by the effusion of low viscosity lava flows, coulees and domes, while maintaining high discharge rates (e.g. Bachmann et al., 2000; Aguirrez-Diaz & Labarthe-Hernandez, 2003; Polo et al., 2018a, b; Simões et al., 2017). The sustained fountaining and entrainment of air in the eruptive jet is strongly influenced by the geometry of the conduit (Legros et al., 2000) as well as the transition from sustained to collapsing eruptive column. A wide-geometry conduit would impede much air entrainment into the pyroclastic fountain and, at the same time, would favors magmatic escape of volcanic gases, favoring the low fountaining and promoting a “boil-over” style eruption (Branney and Kokelaar, 1992, 2002; Lenhardt et al., 2017) with high discharge rate. Moreover, the low air injection would inhibit the dilution of the eruptive material making it thermodynamically isolated from the surrounding environment (Lesti et al., 2011), preserving the high temperatures and enhancing the agglutination of fragments (welding) (Quane and Russell, 2004; Russell and Quane

2005; Giordano et al., 2005). When the low-altitude pyroclastic fountaining or the emission of high temperature lavas would be maintained for long time the high flow-mobility is ensured (Sulpizio et al., 2014). If the material supply from the vent continues for long time and with high discharge rate, the mobility could be maintained even on very low slope angles (Sulpizio et al., 2014; Giordano et al., 2017; Kolzenburg et al., 2017), and flowing various kilometers up to hundreds of kilometers far from the vent (Aguirre-Diaz et al., 2008; Cas et al., 2011; Giordano et al., 2017). This could explain the presence of large silicic volcanic areas characteristic of the ancient Amazonian volcanism (Roverato et al., 2016). Although, volcanoclastic rocks seem to be volumetrically less important in the study areas than the lava flows and/or rheomorphic ignimbrites the recognition of fragmental rocks during our field campaigns is important to understand their significance into our paleogeographic reconstruction (Fig. 17). An idealized deposit sequence of a caldera forming eruption displays an air-fall deposit overlain by an ignimbrite (Druitt and Sparks, 1984) and the transition from the sustained column phase to the pyroclastic flow phase is often accompanied by a strong increase in the discharge rate (Bursik and Woods, 1996). The stratigraphic sequence of figure 11 shows this association of a possible air-fall deposit (Lf dsAL) linked with pyroclastic flow-dominated deposits (Lf mAL and *m-gwLA*). In some cases, pyroclastic eruptions commonly precede lava emplacement (Fink 1983; Heiken and Wohletz 1987). The sequence presented in figure 7 shows a low-grade welded ignimbrite deposit (Lf *l-gwAL*) overlaid by a thick banded body that we are interpreting here as a lava flow. At the base of the banded lava is a breccia (Lf mLB) consisting of clasts of a mix of lava textural types, including massive, vesicular, flow banded and flow-folded, glassy, pumiceous and devitrified. Autobrecciation in lavas or rheomorphic ignimbrites occurs when more rigid layers and the external parts are broken in response to the applied shear stress locally exceeding the tensile strength (Fink and Manley; 1987). Some polymictic breccia deposits (Lf mL) are characterized by lithic angular clasts and devitrified fragments that could point to co-ignimbritic breccias with short transport of the emitted material. These deposits could be also related to collapse-caldera-breccias falling down into the caldera ring during the roof subsidence. Air-fall (sA) and dilute pyroclastic flow (xsA) deposits (surge type) crop out in both regions. These, linked with the glassy and lithic pyroclastic material described above, are evidence of intense explosive phases from more sustained column eruptions of smaller intra-caldera volcanic centers and/or associated

to events of caldera collapse (Fig. 17).

#### 10.2.1 The sedimentary response

Sets of small basins intra-calderas and probable relatively immature shallow marine deposits are interpreted as forming part of a tectonically unstable setting of a young extensional environment that characterized the southern Amazonian craton during the Paleoproterozoic. Reworked sediments can accumulate into volcano-tectonic depressions created by the eruption, which often collects an intra-caldera lake (Heiken et al., 2000; Németh et al., 2009; Manville et al., 2009). The sedimentation into intra-volcano shallow-water lacustrine basins would have been facilitated (Fig. 17). The alternation of subaerial to shallow-water sedimentation displayed by the alternation of Lf mS and csG is indicative of this volcano-tectonic depressions, which could be also interpreted as immature marine depressions. Subaerial and subaqueous talus coarse-grained up to finer grained turbidites (dsSt) and suspension deposits formed during quiescent periods into lakes or ponds is also inferred (Bacon et al., 2002). Silica-rich accumulations into shallow water basins (Chipera et al., 2008; Manville et al., 2009) deriving from hydrothermal activity in a dynamic volcanic context is also thought to be responsible for the formation of chert accumulation (Lf bChS). Post caldera uplifting (Fig. 17), resurgence or central volcanism could also contribute to produce new sediments to be reworked and transported. Fluvial erosion and reworking of primary deposits produced wide range of different sediments from localized cross-bedded, well-sorted sand (Lf xsS) and gravel (Lf xsSG) beds to massive clast-supported sand and gravel (Lf csGS, csG) and cobble (Lf csGC) deposits. Fluvial deposits occur throughout all successions, representing periods of stream and river reworking and re-establishment after an eruptive phase (Zernack et al., 2011; Roverato et al., 2017). Debris-flows, hyperconcentrated flows, sheet-floods and active sandy braided river systems existed and the absence of vegetation during the Precambrian (Oberholzer and Eriksson, 2000; Roverato et al., 2017) permitted that copious rainfalls easily reworked the available sediments.

#### 11. Conclusion

This study is the result of the lithofaciological analysis carried out during the 2013, 2014 and 2015 field campaigns in the Amazon Craton in the TMP and SFX regions and the successive geochemical and geochronological analysis of samples

collected in the field. This work constitutes a further step ahead toward the comprehension of significance, chronostratigraphic distribution and the dynamic of eruption and emplacement of felsic volcanic products in the region. Our results complete previous studies and confirm that products present in the Amazonia Craton could be related either to caldera-type systems (e.g. Lamarão et al., 2002; Juliani et al., 2005; Lamarão et al., 2005; Pierosan et al., 2011) and to fissure-fed eruptive environment following the model proposed by Aguirre-Diaz and Labarthe-Hernandez (2003) for the “Sierra Madre Occidental” formation and by Juliani and Fernandes (2010) for the Xingu region. The two models are in fact very similar only differing for the size of the hypothesized magma chambers and the shape of the fissural vents. The described volcano-sedimentary sequences that were characterized by the emission of large volcanic felsic products were likely formed in a late-/post-orogenic (~ 2 Ga) to extensional regimes (~ 1.88 Ga).

## Acknowledgments

This work was supported by the project CAPES/CNPq 402564/2012-0 (Programa Ciências sem Fronteiras) to Caetano Juliani and Matteo Roverato. M. Roverato acknowledges the grant of the Brazilian CAPES/ CNPq Programa Ciências Sem Fronteiras, Atração de Jovem Talento 402564/2012-0. We acknowledge the CNPq/CT-Mineral (Proc. 550.342/ 2011-7) and the INCT-Geociam (573733/2008-2) — (CNPq/MCT/ FAPESPA/PETROBRAS). Furthermore, the first author would like to thank Jeovaci Jr. Martins da Rocha, Diego Felipe Gomez Gutierrez, Lucas Villela Cassini for the help in the field and Carlos Marcelo Diaz Fernandez for the help and very useful discussions. Dr. Giordano acknowledges the financial support for this research from the CAPES project (proposal 302827) of the Ciências Sem Fronteiras program (Brazil) and the local research funds (2012, 2013, 2014) of the University of Turin (Ex60-2015). We are indebted to Nils Lenhardt and Roberto Dall’Agnol for the dedication in reviewing this manuscript and important comments and reviews, which improved considerably this work.

## References

Aguirre-Diaz, G.J., Labarthe-Hernández, G., 2003. Fissure ignimbrites: fissure-source

850 origin for voluminous ignimbrites of the Sierra Madre Occidental and its  
 851 relationship with Basin and Range faulting. *Geology* 31, 773-776.  
 852 Aguirre-Diaz, G.J., Labarthe-Hernández, G., Tristán-González, M., Nieto-Obregón, J.,  
 853 Isaac Gutiérrez-Palomares, I., 2008. The ignimbrite flare-up and graben calderas  
 854 of the Sierra Madre Occidental, Mexico. In: Martí, J., Gottsman, J. (Eds.), *Caldera*  
 855 *Volcanism: Analysis, Modelling and Response*. *Developments in Volcanology* 10,  
 856 143-180.  
 857 Almeida, F.F.M., Hasui, Y., Brito Neves, B.B., Fuck, R.A., 1981. Brazilian structural  
 858 provinces: an introduction. *Earth Science Reviews* 17, 1-29.  
 859 Almeida, M.E., Brito, M.F.L., Ferreira, A.L., Monteiro, M.A.S., 2000. Projeto Especial  
 860 Província Mineral do Tapajós. Geologia e recursos minerais da Folha Vila Mamãe  
 861 Anã (SB.21-V-D). Estados do Pará e Amazonas. CPRM, Brasília. [CD-ROM].  
 862 Amaral, G., 1974. Geologia Pré-Cambriana da Região Amazônica. Tese de Livre  
 863 Docência, IG/USP (212 pp.).  
 864 Anders, E., Ebihara, M., 1982. Solar system abundances of the elements. *Geochim.*  
 865 *Cosmochim. Ac.* 46, 2363-2380.  
 866 Andrews, G.D.M., Branney, M.J., 2011. Emplacement and rheomorphic deformation  
 867 of a large, lava-like rhyolitic ignimbrite: Grey's Landing, southern Idaho.  
 868 *Geological Society of America Bulletin* 123, 725-743.  
 869 Antonio, P., D'Agrella-Filho, M.S., Trindade, R.I.F., Nédélec, A., de Oliveira, D.C., da  
 870 Silva, F.F., Roverato M., Lana, C., 2017. Turmoil before the boring billion:  
 871 Paleomagnetism of the 1880–1860 Ma Uatumã event in the Amazonian craton.  
 872 *Gondwana Research* 49, 106-129.  
 873 Araújo, O.J.B., Maia, R.G.N., Jorge, João, X.S., Costa, J.B.S., 1988. A  
 874 megaestruturação arqueana da folha Serra dos Carajás. In: SBG (Ed.), *Congresso*  
 875 *Latinoamericano de Geologia*, seventh ed. Belém. 324-333.  
 876 Bacon, C.R., Gardner, J.V., Mayer, L.A., Buktenica, M.W., Dartnell, P., Ramsey,  
 877 D.W., Robinson, J.E., 2002. Morphology, volcanism, and mass wasting in Crater  
 878 Lake, Oregon. *Geological Society of America bulletin* 114, 675-692.  
 879 Bahia, R.B.C., Quadros, M.L.E.S., 2000. Geologia e recursos minerais da Folha  
 880 Caracol SB.21-X-C. Estados do Pará e Amazonas. Escala 1:250.000. Brasília:  
 881 CPRM, 2000. 1 CD ROM.  
 882 Barreto, C.J.S., Lafonb, J.M., da Rosa Costac L.T., Fernandes-Limad, E., 2014.  
 883 Palaeoproterozoic (~1.89 Ga) felsic volcanism of the Iricoumé Group, Guyana



884 Shield, South America: geochemical and Sm-Nd isotopic constraints on sources  
885 and tectonic environment. *International Geology Review*, 2014.  
886 <http://dx.doi.org/10.1080/00206814.2014.930800>  
887 Best, M.G., Christiansen, E.H., 1997. Origin of broken phenocrysts in ash-flow tuffs.  
888 *GSA Bulletin*, 109 (1), 63-73.  
889 Blatt, H., Middleton, G., Murray, R., 1980. *Origin of Sedimentary Rocks*. Prentice-  
890 Hall, Englewood Cliffs, 634.  
891 Branney, M.J., Kokelaar, B.P., 1992. A reappraisal of ignimbrite emplacement:  
892 progressive aggradation and changes from particulate to non-particulate flow  
893 during emplacement of high-grade ignimbrite. *Bull. Volcanol.* 54, 504-520.  
894 Breitzkreuz, C., 2013. Spherulites and lithophysae—200 years of investigation on high  
895 temperature crystallization domains in silica-rich volcanic rocks. *Bull. Volcanol.*  
896 75:705.  
897 Brito-Neves, B.B., 2011. The Paleoproterozoic in the South-American continent:  
898 Diversity in the geologic time. *Journal of South American Earth Sciences* 32, 270-  
899 286.  
900 Brown, D.J., Bell, B.R., 2013. The emplacement of a large, chemically zoned,  
901 rheomorphic, lava-like ignimbrite: the Sgurr of Eigge Pitchstone, NW Scotland.  
902 *Journal of the Geological Society* 170, 753-767.  
903 Brown, G.C., Thorpe, R.S., Webb, P.C., 1984. The geochemical characteristics of  
904 granitoids in contrasting arcs and comments on magma sources. *Journal of the*  
905 *Geological society* 141, 413-426.  
906 Bursik, M.I., Woods, A.W., 1996. The dynamics and thermodynamics of large ash  
907 flows. *Bull. Volcanol.* 58, 175-193.  
908 Capuzzo, N., Wetzel, A., 2004. Facies and basin architectural of the Late  
909 Carboniferous Salvan-Dorénaz continental basin (Western Alps,  
910 Switzerland/France). *Sedimentology* 51, 675-697.  
911 Cas, R.A.F., Wright, J.V., 1987. *Volcanic Successions, Modern and Ancient*. Unwin  
912 Hyman, Boston. 528.  
913 Cas, R.A.F., Wright, H.M.N., Folkes, C.B., Lesti, C., Porreca, M., Giordano, G.,  
914 Viramonte, J.G., 2011. The flow dynamics of an extremely large volume  
915 pyroclastic flow, the 2.08-Ma Cerro Galán Ignimbrite, NW Argentina, and  
916 comparison with other flow types. *Bull. Volcanol.* 73, 1583-1609.

- 917 Chipera, S.J., Goff, F., Goff, C.J., Fittipaldo, M., 2008. Zeolitization of intracaldera  
918 sediments and rhyolitic rocks in the 1.25 Ma lake of Valles caldera, New Mexico,  
919 USA. *Journal of Volcanology and Geothermal Research* 178, 317-330.
- 920 Collinson, J.D., 1966. Antidune bedding in the Namurian of Derbyshire, England:  
921 *Geologie en Mijnbouw* 45, 262-264.
- 922 Collinson, J.D., Thompson, D.B., 1982 *Sedimentary structures*: London, Allen and  
923 Unwin, 194.
- 924 Condie, K.C., 2000. Episodic continental growth models: after thoughts and  
925 extensions. *Tectonophysics* 322, 153-162.
- 926 Condie, K.C., 2002. Continental growth during a 1.9-Ga superplume event. *Journal of*  
927 *Geodynamics* 34, 249-264.
- 928 Costa, J.B.S., Hasui, Y. 1997. Evolução geológica da Amazônia. In: M.L. Costa &  
929 R.S. Angélica (Ed.), *Contribuições à geologia da Amazônia*, 16-90.
- 930 Da Cruz, R.S., Fernandes, C.M.D., Villas, R.N.N., Juliani, C., Monteiro, L.V.S.,  
931 Almeida, T.I.R., Lagler, B., Carneiro, C.C., Misas, C.M.E., 2015. A study of the  
932 hydrothermal alteration in Paleoproterozoic volcanic centers, São Felix do Xingu  
933 region, Amazonian Craton, Brazil, using short-wave infrared spectroscopy. *J.*  
934 *Volc. Geoth. Res.* 304, 324-335.
- 935 Dall'Agnol, R., Lafon, J.M., Macambira, M.J.B., 1994. Proterozoic anorogenic  
936 magmatism in the Central Amazonian Craton: geochronological and geochemical  
937 aspects. *Mineral. Petrol.* 50, 113-138.
- 938 Dall'Agnol, R., Costi, H.T., Leite, A.A.S., Magalhães, M.S., Teixeira, N.P., 1999.  
939 Rapakivi granites from Brazil and adjacent areas. *Precambrian Research* 95, 9-39.
- 940 Dall'Agnol, R., Teixeira, N.P., Rämö, O.T., Moura, C.A.V., Macambira, M.J.B.,  
941 Oliveira, D.C., 2005. Petrogenesis of the paleoproterozoic, rapakivi, A-type granites  
942 of the Archean Carajás metallogenic province, Brazil. *Lithos* 80, 101-129.
- 943 Dall'Agnol, R., da Cunha, I.R.V., Guimarães, F.V., de Oliveira, D.C., Teixeira,  
944 M.F.B., Feio, G.R.L., Lamarão, C.N., 2017. Mineralogy, geochemistry, and  
945 petrology of Neoproterozoic ferroan to magnesian granites of Carajás province,  
946 Amazonian Craton: The origin of hydrated granites associated with charnockites.  
947 *Lithos* 277, 3-32.
- 948 Druitt, T.H., Sparks, R.S.J., 1984. On the formation of calderas during ignimbrite  
949 eruptions. *Nature* 310, 679-681.
- 950 Echeverri-Misas, C.M., 2010. Geologia e gênese do depósito de Au-(Cu) do Palito,

- 951 Província Aurífera do Tapajós. Dissertação de Mestrado, IG/USP.
- 952 Eriksson, P.G., Engelbrecht, J.P., Res, M., Harmer, R.E., 1994. The Bushy Bend lavas,  
953 a new volcanic member of the Pretoria Group, Transvaal Sequence. S. Afr. J.  
954 Geol. 97, 1-7.
- 955 Faraco, M.T.L., Carvalho, J.M.A., Klein, E.L., 1997. Carta metalogenética da  
956 Província Auréfera do Tapajós, in: Costa, M.L.C., Ange`lica, R.S. (Eds.),  
957 Contribuições à Geologia da Amazônia. Sociedade Brasileira de Geologia,  
958 Belém, Brazil 1, 423-437.
- 959 Fernandes, C.M.D., Juliani, C., Monteiro, L.V.S., Lagler, B., Misas, C.M.E., 2011.  
960 High-K calc-alkaline to A-type fissure-controlled volcano-plutonism of the São  
961 Félix do Xingu region, Amazonian craton, Brazil: Exclusively crustal sources or  
962 only mixed Nd model ages? Journal of South America Earth Science 32 (4), 351-  
963 368.
- 964 Ferrari, L., Orozco-Esquivel, T., Manea, V.C., Manea, M., 2012. The dynamic history  
965 of the Trans-Mexican Volcanic Belt and the Mexico subduction zone.  
966 Tectonophysics 522-523, 122-149.
- 967 Ferreira, A.L., Almeida, M.E., Brito, M.F.L., Monteiro, M.A.S., 2000. Projeto Especial  
968 Província Mineral do Tapajós. Geologia e recursos minerais da Folha  
969 Jacareacanga (SB.21-Y-B). Estados do Pará e Amazonas. Escala 1:250.000. Nota  
970 explicativa e mapas, CPRM, Brasília. [CD ROM].
- 971 Ferron, J.M.T.M., Bastos-Neto, A.C., Lima, E.F., Nardi, L.V.S., Costi, H.T., Pierosan,  
972 R., Prado, M., 2010. Petrology, geochemistry, and geochronology of  
973 Paleoproterozoic volcanic and granitic rocks (1.89–1.88 Ga) of the Pitinga  
974 Province, Amazonian Craton, Brazil. Journal of South American Earth Sciences  
975 29, 483-497.
- 976 Fink, J., 1983. Structure and emplacement of a rhyolitic obsidian flow: little Glass  
977 Mountain, Medicine Highland, northern California. GSA Bull. 94, 362-380.
- 978 Fink, J.H., Manley, C.R., 1987. Origin of pumiceous and glassy textures in rhyolite  
979 flows and domes: Geological Society of America Special Paper 212, 77-88.
- 980 Fisher, R.V., 1961. Proposed classification of volcanoclastic sediments and rocks.  
981 Geological Society of America Bulletin 72, 1409-1414.
- 982 French, J.E., Heaman, L.M., Chacko, T., Srivastava, R.K., 2008. 1891–1883 Ma  
983 Southern Bastar–Cuddapah mafic igneous events, India: a newly recognized large  
984 igneous province. Precambrian Research 160, 308-322.

- 985 Giordano, D., La Felice, S., Arzilli, F., De Cristofaro, S.P., Masotta, M., Polo L.  
 986 (2017). Il vulcanismo effusivo acido del Monte Amiata: stima delle condizioni  
 987 pre- e sin-eruttive ed implicazioni vulcanologiche. Effusive acidic volcanism of  
 988 Monte Amiata: estimates of pre- and syn-eruptive conditions and volcanological  
 989 implications. Monografia Il Vulcano di Monte Amiata, ISBN 978-88-99742-32-4,  
 990 171-193.
- 991 Giordano, D., Nichols, A.R.L., Dingwell, D.B., 2005. Glass transition temperatures of  
 992 natural hydrous melts: a relationship with shear viscosity and implications for the  
 993 welding process. Jour. Volc Geoth. Res. 142, 105-118.
- 994 Giovanardi, T., Girardi, V.A.V., Correia, C.T., Sinigoi, S., Tassinari, C.C.G.,  
 995 Mazzucchelli, M., 2015. U-Pb zircons SHRIMP data from the Cana Brava  
 996 Layered Complex: New constraints for the mafic-ultramafic intrusions of Northern  
 997 Goiás, Brazil. Open Geosci 7, 197-206.
- 998 Goldfarb, R., Groves, D., Gardoll, S., 2001. Rotund versus skinny orogens: well-  
 999 nourished or malnourished gold? Geology 29, 539-542.
- 1000 Gutscher, M.A., Maury, R., Eissen, J.P., Bourdon, E., 2000. Can slab melting be  
 1001 caused by flat subduction? Geology 28, 535-538.
- 1002 Hanson, R.E., Gose, W.A., Crowley, J.L., Ramezani, J., Bowring, S.A., Bullen, D.S.,  
 1003 Hall, R.P., Pancake, J.A., Mukwakwami, J., 2004. Paleoproterozoic intraplate  
 1004 magmatism and basin development on the Kaapvaal Craton: age, paleomagnetism  
 1005 and geochemistry of ~1.93 to ~1.87 Ga post-Waterberg dolerites. South African  
 1006 Journal of Geology 107, 233-254.
- 1007 Hasui, Y., Haraly, N.L.E., Schobbenhaus, C., 1993. Megaestruturação Pré-Cambriana  
 1008 do território brasileiro baseada em dados geofísicos e geológicos. Geociências 12,  
 1009 7-31.
- 1010 Heiken, G., Wohletz, K., 1987. Tephra deposits associated with silicic domes and lava  
 1011 flows. GSA Special Paper 212.
- 1012 Heiken, G., Krier, D., McCormick, T., Snow, M.G., 2000. Intracaldera volcanism and  
 1013 sedimentation — Creede caldera, Colorado. In: Bethke, P.M., Hay, R.L. (Eds.),  
 1014 Ancient Lake Creede: Its volcano-tectonic setting, history of sedimentation, and  
 1015 relation to mineralization in the Creede Mining District. Geological Society of  
 1016 America Special Paper, 346. Boulder, Colorado, 127-157.
- 1017 Hofmann, A.W., 1988. Chemical differentiation of the Earth: The relationship between  
 1018 mantle, continental crust and oceanic crust. EPSL 90, 297-314.

- 1019 Hollocher, K., Robinson, P., Walsh, E., Roberts, D., 2012. Geochemistry of  
1020 amphibolite-facies volcanics and gabbros of the Støren Nappe in extensions west  
1021 and southwest of Trondheim, Western Gneiss Region, Norway: a key to  
1022 correlations and paleotectonic settings. *American Journal of Science* 312, 357-  
1023 416.
- 1024 Juliani, C., 2002. Alteração hidrotermal e metalogênese em sistemas vulcano-  
1025 plutônicos paleoproterozóicos na Província Aurífera do Tapaj, Cráton Sul  
1026 Amazônico, Pará. Tese de Livre-Docência, IG/USP.
- 1027 Juliani, C., Vasquez, M.L., Klein, E.L., Villas, R.N., Echeverri-Misas, C.M., Santiago,  
1028 E.S.B., Monteiro, L.V.S., Carneiro, C.C., Fernandes, C.M.D., Usero, G., 2014.  
1029 Metalogenia da Província Tapajós. In: Silva M.G.; Jost H.; Kuyumajian R.M.  
1030 (Org.). *Metalogênese das Províncias Tectônicas Brasileiras*. 1 ed. : CPRM —  
1031 Serviço Geológico do Brasil 1, 51-90.
- 1032 Juliani, C., Rye, R.O., Nunes, C.M.D., Snee, L.W., Correa Silva, R.H., Monteiro,  
1033 L.V.S., Bettencourt, J.S., Neumann, R., Neto, A.A., 2005. Paleoproterozoic high  
1034 sulphidation mineralization in the Tapajós gold province, Amazonian Craton,  
1035 Brazil: geology, mineralogy, alunite argon age, and stable-isotope constraints.  
1036 *Chemical Geology* 215, 95-125.
- 1037 Juliani, C., Fernandez C.M.D., 2010. Well-preserved Late Paleoproterozoic volcanic  
1038 centers in the São Félix do Xingu region, Amazonian Craton, Brazil. *Journal of*  
1039 *Volcanology and Geothermal Research* 191, 167-179.
- 1040 Kay, S.M., Godoy, E., Kurtz, A., 2005. Episodic arc migration, crustal thickening,  
1041 subduction erosion, and magmatism in the south\_central Andes. *Geological*  
1042 *Society of America Bulletin* 117, 67-88.
- 1043 Klein, E.L., Almeida, M.E., and Costa, L.T.R., 2012. The 1.89-1.87 Ga Uatumã Silicic  
1044 Large Igneous Province, northern South America: Large Igneous Provinces  
1045 Commission: <http://www.largeigneousprovinces.org/12nov> (accessed 12 January  
1046 2012).
- 1047 Klein, E.L., Santos, R.A., Fuzikawa, K., Angélica, R.S., 2001. Hydrothermal fluid  
1048 evolution and structural control of the brittle-style Guarim lode-gold  
1049 mineralisation, Tapajós Province, Amazonian Craton, Brazil. *Miner. Depos.* 36,  
1050 149-164.
- 1051 Klein, E.L., Vasquez, M.L., Rosa-Costa, L.T., Carvalho, J.M.A., 2002. Geology of  
1052 Paleoproterozoic gneiss- and granitoid-hosted gold mineralization in Southern

- 1053 Tapajós Gold Province, Amazonian Craton, Brazil. *Intern. Geol. Rev.*, 44, 544-  
1054 558.
- 1055 Klein, E.L., Rosa-Costa, L.T., Carvalho, J.M.A., 2004. Estudo de inclusões fluidas em  
1056 veio de quartzo aurífero do prospecto Patinhas, Província Aurífera do Tapajós,  
1057 Cráton Amazônico. *RBG* 34, 59-66.
- 1058 Lagler, B., Juliani, C., Pessoa, F.F., Fernandes, C.M.D., 2011. Petrografia e  
1059 geoquímica das sequências vulcânicas Paleoproterozóicas na região de Vila  
1060 Tancredo, São Félix do Xingu (PA). In: *SBGq, Congr. Bras. Geoquí.*, 13, e Simp.  
1061 Países do Mercosul, 3, Gramado, RS. *Anais*, [CD-ROM].
- 1062 Lamarão, C.N., Dall'Agnol, R., Lafon, J.M., Lima, E.F., 1999. As associações  
1063 vulcânicas e plutônicas de Vila Riozinho e Morais Almeida, Província Aurífera do  
1064 Tapajós, SW do estado do Pará. In: *Simpósio sobre Vulcanismo e Ambientes*  
1065 *Associados*. 1, Gramado\*/RS, *Boletim de resumos*, 93 (in Portuguese).
- 1066 Lamarão, C.N., Dall'agnol, R., Lafon, J.M., Lima, E.F., 2002. Geology, geochemistry,  
1067 and Pb-Pb zircon geochronology of the Paleoproterozoic magmatism of Vila  
1068 Riozinho, Tapajós Gold Province, Amazonian craton, Brazil. *Prec. Res.* 119, 189-  
1069 223.
- 1070 Lamarão, C.N., Dall'agnol, R., Pimentel, M.M., 2005. Nd isotopic composition of  
1071 Paleoproterozoic volcanic rocks of Vila Riozinho: Implications for the crustal  
1072 evolution of the Tapajós gold province, Amazon craton. *J. South Am. Earth Sci.*  
1073 18, 277-292.
- 1074 Legros, F., Kelfoun, K., 2000. On the ability of pyroclastic flows to scale topographic  
1075 obstacles. *J. Volcanol. Geotherm. Res.* 98, 235-241.
- 1076 Lenhardt, N., Hornung, J., Hinderer, M., Böhnell, H., Torres-Alvarado, I.S., Trauth, N.,  
1077 2011. Build-up and depositional dynamics of an arc front volcanoclastic complex:  
1078 the Miocene Tepoztlan Formation (Transmexican Volcanic Belt, Central Mexico).  
1079 *Sedimentology* 58, 785-823.
- 1080 Lenhardt, N., Eriksson, P., Catuneanu, O., Bumby, A.J., 2012. Nature of and controls  
1081 on volcanism in the ca. 2.32-2.06 Ga Pretoria Group, Transvaal Supergroup,  
1082 Kaapvaal Craton, South Africa. *Precambrian Research* 214-215, 106-123.
- 1083 Lenhardt, N., Masango S.M., Jolayemi, O.O., Lenhardt, S.Z., Peeters, G.J., Eriksson,  
1084 P.G., 2017. The Palaeoproterozoic (~2.06 Ga) Rooiberg Group, South Africa:  
1085 Dominated by extremely high-grade lava-like and rheomorphic ignimbrites? New  
1086 observations and lithofacies analysis. *Journal of African Earth Sciences* 131, 213-

- 1087 232.
- 1088 Lesti, C., Porreca, M., Giordano, G., Mattei, M., Cas, R.A.F., Wright, H.M.N., Folkes,  
 1089 C.B., Viramonte, J., 2011. High-temperature emplacement of the Cerro Galán and  
 1090 Toconquis Group ignimbrites (Puna plateau, NW Argentina) determined by TRM  
 1091 analyses. *Bull. Volcanol.* 73, 1535-1565.
- 1092 Lofgren, G., 1971. Spherulite textures in glassy and crystalline rocks. *J. Geophys. Res.*  
 1093 76, 5635-5648.
- 1094 Ludwig, K.R., 2009. Isoplot 4.1. A geochronological toolkit for Microsoft Excel.  
 1095 Berkeley Geochronology Center special publication 4, 76.
- 1096 Macambira, E.M.B., 1997. Geologia e aspectos metalogenéticos dos elementos do  
 1097 grupo de platina no complexo máfico-ultramáfico da serra da Onça – sul do Pará.  
 1098 Tese de Mestrado, UFPA, Belém, Pará, Brasil.
- 1099 Macambira, E.M.B., Vale, A.G., 1997. Programa Levantamentos Geológicos Básicos  
 1100 do Brasil. São Félix do Xingu. Folha SB-22-Y-B. Estado do Pará, CPRM, Brasília  
 1101 (in Portuguese).
- 1102 Manea, V.C., Pérez-Gussinyé, M., Manea, M., 2012. Chilean flat-slab subduction  
 1103 controlled by overriding plate thickness and trench rollback. *Geology* 40 (1), 35-  
 1104 38.
- 1105 Manville, V., Németh, K., Kano, K., 2009. Source to sink: A review of three decades  
 1106 of progresss in the understanding of volcanoclastic processes, deposits, and  
 1107 hazards. *Sedimentary Geology* 220, 136-161.
- 1108 McPhie, J., Doyle, M., Allen, S.R., 1993. Volcanic textures: A guide to the  
 1109 interpretation of textures in volcanic rocks, Centre for Ore Deposit and  
 1110 Exploration Studies. University of Tasmania, 198.
- 1111 Miall, A.D., 1996. The Geology of Fluvial Deposits: Sedimentary Facies, Basin  
 1112 Analysis, and Petroleum Geology. Springer-Verlag, New York. 582.
- 1113 Minifie, M.J., Kerr, A.C., Ernst, R.E., Hastie, A.R., Ciborowski, T.J.R., Desharnais,  
 1114 G., Millar, I.L., 2013. The northern and southern sections of the western ca. 1880  
 1115 Ma Circum-Superior Large Igneous Province, North America: the Pickle Crow  
 1116 dyke connection? *Lithos* 174, 217-235.
- 1117 Monteiro, L.V.S., Xavier, R.P., de Carvalho, E.R., Hitzman, M.W., Johnson, C.A., de  
 1118 Souza Filho, C.R., Torresi, I., 2008. Spatial and temporal zoning of hydrothermal  
 1119 alteration and mineralization in the Sossego iron oxide-copper-gold deposit,  
 1120 Carajás Mineral Province, Brazil: paragenesis and stable isotope constraints.



- 1121 Miner Deposita 43, 129-159.
- 1122 Mori, L., Gómez-Tuena, A., Cai, Y., Goldstein, S., 2007. Effects of prolonged flat  
1123 subduction on the Miocene magmatic record of the central Trans-Mexican  
1124 Volcanic Belt. Chemical Geology 244, 452-473.
- 1125 Mori, P.E., Reeves, S., Correia, C.T., Haukka, M., 1999. Development of a fused glass  
1126 disc XRF facility and comparison with the pressed powder pellet technique at  
1127 Instituto de Geociências. Rev. Bras. Geociências, 29, 441-446.
- 1128 Mueller, W.U., Concoran, P.L., 1998. Late-orogenic basins in the Archaean Superior  
1129 Province, Canada: characteristics and inferences. Sedimentary Geology 120, 177-  
1130 203.
- 1131 Mueller, W.U., Chown, E.H., Thurston, P.C., 2000a. Processes in physical  
1132 volcanology and volcanoclastic sedimentation: modern and ancient. Precambrian  
1133 Research 101, 81-85.
- 1134 Navarro, M.S., Andrade, S., Ulbrich, H.H.G.J., Gomes, C.B., Girardi, V.A.V., 2008.  
1135 The analysis of rare earth elements with ICP-MS in basaltic and related rocks:  
1136 testing the efficiency of sample decomposition procedures. Geostand. Geoanal.  
1137 Res. 32(2),167-180.
- 1138 Németh, K., Cronin, S.J., Stewart, R.B., Charley, D., 2009. Intra- and extra- caldera  
1139 volcanoclastic facies architecture of a frequently active mafic island-arc volcano,  
1140 Ambryn Island, Vanuatu. Sedimentary Geology 220, 256-270.
- 1141 Oberholzer, J.D., Eriksson, P.G., 2000. Subaerial volcanism in the Palaeoproterozoic  
1142 Heekpoort Formation (Transvaal Supergroup), Kaapvaal craton. Precambrian  
1143 Research 101, 193-210.
- 1144 Pearce, J.A., Harris, N.B.W., and Tindle, A.G., 1984. Trace element discrimination  
1145 diagrams for the tectonic interpretation of granitic rocks. Journal of Petrology 25,  
1146 956-983.
- 1147 Pearce, J.A., 1996. Sources and settings of granitic rocks. Episodes 19 (4), 120-125.
- 1148 Pessoa M.R., Santiago A.F., Andrade A.F., Barreto E.L., Nascimento J.O., Santos  
1149 J.O.S., Oliveira J.R., Lopes R.C., Prazeres W.V. 1977. Projeto Jamanxim.  
1150 CPRM/DNPM, 1-3, 614.
- 1151 Pierosan, R., Lima, E.F., Nardi, L.V.S., Bastos Neto, A.C., Campos, C.P., Jarvis, K.,  
1152 Ferron, J.M.T.M., Prado, M., 2011. Geochemistry of Palaeoproterozoic volcanic  
1153 rocks of the Iricoumé Group, Pitinga Mining District, Amazonian craton, Brazil:  
1154 International Geology Review 53, 946-979.



- 1155 Pinho, S.C.C., Fernandes, C.M.D., Teixeira, N.P., Paiva Jr., A.L., Cruz, V.L.,  
1156 Lamarão, C.N., Moura, C.A.V., 2006. O magmatismo paleoproterozóico da região  
1157 de São Félix do Xingu, Província Estanífera do Sul do Pará: Petrografia e  
1158 geocronologia. *Revista Brasileira de Geociências* 36, 793-802.
- 1159 Pioli, L., Rosi, M., 2005. Rheomorphic structures in a high-grade ignimbrite: the  
1160 Nuraxi tuff, Sulcis volcanic district (SW Sardinia, Italy). *Journal of Volcanology  
1161 and Geothermal Research* 142, 11-28.
- 1162 Polo, L.A., Giordano, D., Janasi, V., Freitas-Guimaraes, L., 2017(a). Effusive silicic  
1163 volcanism in the Paraná Magmatic Province, South Brazil: Physico-chemical  
1164 conditions of storage and eruption and considerations on the rheological behaviour  
1165 during emplacement. *J. Volcanol. Geoth. Res.* 355, 115-135.
- 1166 Polo L.A., Janasi V., Giordano D., Lima E.F., Cañon-Tapia E., Roverato M., 2017(b).  
1167 Effusive silicic volcanism in the Paraná Magmatic Province, South Brazil:  
1168 Evidence for locally-fed lava flows and domes from detailed field work. *J.  
1169 Volcanol. Geoth. Res.* 355, 204-218.
- 1170 Quane, S. L., Russell, J. K., 2005. Welding: Insights from high-temperature analogue  
1171 experiments. *Journal of Volcanology and Geothermal Research* 142 (1-2), 67-87.
- 1172 Reis, N.R., Almeida, M.E., Ferreira, A.L., Riker, S.R., 2006. *Geologia e Recursos  
1173 Minerais do Estado do Amazonas. Sistema de Informações Geográficas  
1174 1:1.000.000. CPRM, Manaus, 144.*
- 1175 Rino, S., Tsuyoshi, K., Windley, B.F., Katayama, I., Motoki, A., Hirata, T., 2004.  
1176 Major episodic increases of continental crustal growth determined from zircon  
1177 ages of river sands; implications for mantle overturns in the Early Precambrian.  
1178 *Physics of the Earth and Planetary Interiors* 146, 369-394.
- 1179 Roverato, M., Capra, L., Sulpizio, R., Norini, G., 2011. Stratigraphic reconstruction of  
1180 two debris avalanche deposits at Colima Volcano (Mexico): insights into pre-  
1181 failure conditions and climate influence. *J. Volc. Geoth. Res.* 207 (1), 33-46.
- 1182 Roverato, M., Cronin, S., Procter, J., Capra, L., 2014. Textural features as indicators of  
1183 debris avalanche transport and emplacement, Taranaki volcano. *Geol. Soc. Am.  
1184 Bull.* B30946-1
- 1185 Roverato, M., 2016. The Montesbelos mass-flow (southern Amazonian craton, Brazil):  
1186 a Paleoproterozoic volcanic debris avalanche deposit? *Bull. Volcanol.* 78, 49.
- 1187 Roverato, M., Giordano, D., Echeverri-Misas, CM., Juliani, C., 2016.  
1188 Paleoproterozoic felsic volcanism of the Tapajós Mineral Province, Southern

- 1189 Amazon Craton, Brazil. *Journal of Volcanology and Geothermal Research* 310,  
1190 98-106.
- 1191 Roverato, M., Juliani, C., Marcelo Dias-Fernandes, C., Capra, L., 2017.
- 1192 Paleoproterozoic andesitic volcanism in the southern Amazonian craton, the  
1193 Sobreiro Formation: new insights from lithofacies analysis of the volcanoclastic  
1194 sequences. *Precambrian Research* 289, 18-30.
- 1195 Russell, J. K., Quane, S. L., 2005. Rheology of welding: Inversion of field constraints.  
1196 *Journal of Volcanology and Geothermal Research* 142 (1-2), 173-191.
- 1197 Santos, J.O.S., Hartmann, L.A., Gaudette, H.E., Groves, D.I., McNaughton, N.J.,  
1198 Fletcher, I.R., 2000. A new understanding of the provinces of the Amazon craton  
1199 based on integration of field mapping and U-Pb and Sm-Nd geochronology.  
1200 *Gondwana Research* 3, 453-488.
- 1201 Santos, J.O.S., Groves D.I., Hartmann L.A., Moura M.A., McNaughton, N.J. 2001.  
1202 Gold deposits of the Tapajós and Alta Floresta Domains, Tapajós-Parima orogenic  
1203 belt, Amazon Craton, Brazil. *Mineralium Deposita* 36, 278-299.
- 1204 Santos, J.O.S., 2003. Geotectônica dos Escudos da Guiana e Brasil Central. In: L.A.  
1205 Bizzi, C. Schobbenhaus, R.M. Vidotti, J.H. Gonçalves (Eds.). *Geologia, tectônica  
1206 e recursos minerais do Brasil. Texto, mapas e SIG. CPRM - Serviço Geológico do  
1207 Brasil, Brasília* 169-226.
- 1208 Santos, J.O.S., Van Breemen, O.B., Groves, D.I., Hartmann, L.A., Almeida, M.E.,  
1209 McNaughton, N.J., Fletcher, I.R., 2004. Timing and evolution of multiple  
1210 Paleoproterozoic magmatic arcs in the Tapajós Domain, Amazon Craton:  
1211 constraints from SHRIMP and TIMS zircon, baddeleyite and titanite U-Pb  
1212 geochronology. *Prec. Res.* 13, 73-109.
- 1213 Silva, F.S., Oliveira, D.C., Antonio, P.Y., D'Agrella-Filho, M., Lamarão, C.N., 2016.  
1214 Bimodal magmatism of the Tucuma area, Carajás Province: U-Pb geochronology,  
1215 classification and processes. *J. S. Am. Earth Sci.* 72, 95-114.
- 1216 Simões, M.S., Lima, E.F., Sommer, C.A., Rossetti, L.M.M., 2017. Structures and  
1217 lithofacies of inferred silicic conduits in the Paraná-Etendeka LIP, southernmost  
1218 Brazil. *Journal of Volcanology and Geothermal Research* 355, 319-336.
- 1219 Sulpizio, R., Mele, D., Dellino, P., La Volpe, L., 2007. Deposits and physical  
1220 properties of pyroclastic density currents during complex Subplinian eruptions: the  
1221 AD 472 (Pollena) eruption of Somma-Vesuvius, Italy. *Sedimentology* 54, 607-  
1222 635.

- 1223 Sumner, J.M., Branney, M.J. 2002. The emplacement history of a remarkable  
1224 heterogeneous, chemically zoned, rheomorphic and locally lava-like ignimbrite:  
1225 ‘TL’ on Gran Canaria. *Journal of Volcanology and Geothermal Research* 115,  
1226 109-138.
- 1227 Tassinari, C.C.G., Macambira, M.J.B., 1999. Geochronological provinces of the  
1228 Amazonian craton. *Episodes* 22, 174-182.
- 1229 Teixeira, M.F.B., Dall’Agnol, R., Santos, J.O.S., Oliveira, D.C., Lamarão, C.N.,  
1230 McNaughton, N.J., 2018. Crystallization ages of Paleoproterozoic A-type granites  
1231 of Carajás province, Amazon craton: Constraints from U-Pb geochronology of  
1232 zircon and titanite. *J. of South American Earth Sciences* 88, 312-331.
- 1233 Teixeira, N.P., Bettencourt, J.S., Moura, C.A.V., Dall’Agnol, R., Macambira, E.M.B.,  
1234 2002. Archean crustal sources for Paleoproterozoic tin-mineralized granites in the  
1235 Carajas Province, SSE Para, Brazil: Pb-Pb geochronology and Nd isotope  
1236 geochemistry. *Precambrian Research* 119, 257-275.
- 1237 Teixeira, W., Tassinari, C.C.G., Cordani, U.G., Kawashita, K., 1989. A review of the  
1238 geochronology of the Amazonian craton: tectonic implications. *Precambrian Res.*  
1239 42, 213-227.
- 1240 Teixeira, W., Nelson, J.R., Bettencourt, J.S., Klein, E.L., Oliveira, D.C., 2019.  
1241 Intraplate Proterozoic magmatism in the Amazonian Craton reviewed:  
1242 geochronology, crustal tectonics and global matches. In book: *Dyke Swarms of the*  
1243 *World: A Modern Perspective*. DOI:10.1007/978-981-13-1666-1\_4
- 1244 Van Kranendonk, M.J., 2006. Volcanic degassing, hydrothermal circulation and the  
1245 flourishing of early life on Earth: a review of the evidence from c. 3490-3240 Ma  
1246 rocks of the Pilbara Supergroup, Pilbara Craton, Western Australia. *Earth Science*  
1247 *Rev.* 74, 197-240.
- 1248 Vasquez, M.L, Klein, E.L, Macambira, M.J.B., Santos, A., Bahia, R.B.C., Ricci, P.,  
1249 dos, S.F., Quadros, M.L.E.S., 2000. Geochronology of granitoids, mafic intrusions  
1250 and mineralizations of the Tapajós Gold Province - Amazonian Craton - Brazil. In:  
1251 *Inter. Geol. Congr.* 31, Abstracts, [CD-ROM].
- 1252 Vasquez, M.L., Sousa, C.S., Carvalho, J.M.A., 2008. Mapa Geológico e de Recursos  
1253 Minerais do Estado do Pará, escala 1:1.000.000. Programa Geologia do Brasil,  
1254 Belém, CPRM.
- 1255 Vasquez, M.L., Dreher, A.M. 2011. Uma avaliação da estratigrafia dos eventos  
1256 magmáticos de 1900-1860 Ma do Cráton Amazônico. In: *SBG, Simp. Geol.*

- 1257 Amaz. 12, Bol. Res. [CD ROM].
- 1258 Walker, G.P.L., 1983. Ignimbrite types and ignimbrite problems. *J. Volcanol.*
- 1259 *Geotherm. Res.* 17, 65-88.
- 1260 Went, D.J., 2016 Alluvial fan, braided river and shallow-marine turbidity current
- 1261 deposits in the Port Lazo and Roche Jagu formations, Northern Brittany:
- 1262 relationships to andesite emplacements and implications for age of the Plourivo-
- 1263 Plouézec Group. *Geol. Mag.* 1-24, Cambridge University Press 2016.
- 1264 White, J.D.L., Houghton, B.F., 2006. Primary volcanoclastic rocks. *Geological Society*
- 1265 *of America Bulletin* 34, 677-680.
- 1266 Willcock, M.A.W., Cas, R.A.F., Giordano, G., Morelli, C., 2013. The eruption,
- 1267 pyroclastic flow behaviour, and caldera in-filling processes of the extremely large
- 1268 volume (N1290 km<sup>3</sup>), intra- to extra-caldera, Permian Ora (Ignimbrite) Formation,
- 1269 Southern Alps, Italy. *J. Volcanol. Geotherm. Res.* 265, 102-126.
- 1270 Williams, I.S., 1998. U-Th-Pb geochronology by ion microprobe. In: McKibben, M.A.,
- 1271 Shanks, W.C.P., Ridley, W.I. (eds) *Applications of Microanalytical Techniques to*
- 1272 *Understanding Mineralizing Processes*, *Rev Econ Geol* vol 7. Soc. Econ. Geol,
- 1273 Littleton, 1-35.
- 1274 Wolff, J.A., Wright, J.V., 1981. Rheomorphism of welded tuffs. *Journal of*
- 1275 *Volcanology and Geothermal Research* 10, 13-34.
- 1276 Zanchetta, G., Sulpizio, R., Di Vito, M.A., 2004. The role of volcanic activity and
- 1277 climate in alluvial fan growth at volcanic areas: an example from southern
- 1278 Campania (Italy). *Sedimentary Geology* 168, 249-280.
- 1279 Zernack, A.V., Cronin, S.J., Neall, V.E., Procter, J.N., 2011. A medial to distal
- 1280 volcanoclastic record of an andesitic stratovolcano: detailed stratigraphy of the
- 1281 ring-plain succession of south-west Taranaki, New Zealand: *International Journal*
- 1282 *of Earth Sciences* 100, 1937-1966.
- 1283 Zhao, G., Cawood, P.A., Wilde, S.A., Sun, M., 2002. Review of global 2.1–1.8 Ga
- 1284 orogens: implications for a pre-Rodinia supercontinent. *Earth-Science Reviews* 59,
- 1285 125-162.
- 1286 Zhao, G., Sun, M., Wilde, S.A., Li, S., 2004. A Paleo-Mesoproterozoic supercontinent:
- 1287 assembly, growth and breakup. *Earth-Science Reviews* 67, 91-123.
- 1288
- 1289
- 1290

Figure Captions

Figure 1: location map of the northern South America and the Amazonian Craton divided into several geochronological provinces and other domains according to Santos et al. (2000); TMP = Tapajós Mineral Province, SFX = São Felix do Xingú Region.

Figure 2: distribution map of the outcrops analyzed during the field campaigns in both regions a) Tapajós Mineral Province (TMP) and b) São Felix do Xingú region (SFX); PW=distribution of the Santa Rosa formation inferred during the present work; F=distribution of the Santa Rosa formation inferred by Fernandes et al. (2011); BIF=Banded Iron Formation; red and white dot refers to primary andesitic deposits analyzed in Roverato et al. (2017). In both figures are reported the outcrops described in the paper.

Figure 3: massive and banded lavas and rheo-ignimbrite (?) deposits. a) Np173 (7°33'52.31" S, 55°10'58.80" W), b) Xu23 (6°41'08.65" S, 52°25'55.67" W), c) Xu101 (6°52'12.82" S, 52°09'16.12" W), d) Xu52 (6°28'19.32" S, 51°50'08.90" W), e), f), g) Np396 (6°32'41.06" S, 55°23'59.37" W); see Fig. 2 for the outcrops location. For the lithofacies description and more details see the text.

Figure 4: massive primary volcanoclastic rocks with different proportion of ash, lapilli and blocks. All the deposits are interpreted to be emplaced from pyroclastic density currents except (f) that is interpreted as a basal-breccia of a lava body. a) Xu104 (6°52'22.96" S, 52°08'15.91" W), b) Np183 (7°32'04.13" S, 55°08'50.02" W), c) Np93 (6°44'16.60" S, 55°27'12.96" W), d) Xu29 (6°41'42.51" S, 52°01'23.06" W), e) Xu07 (6°41'56.36" S, 52°08'42.27" W) f) Xu192 (6°31'31.92" S, 53°02'36.60" W); see Fig. 2 for the outcrops location. For the lithofacies description see the text and Table 1.

Figure 5: microphotographs of different massive ash and lapilli ignimbrite deposits in thin section: a) broken crystals suggesting the fragmental character of the rock; b) detail of a devitrified juvenile fragment displaying axiolitic fabric; c) banded sub-millimetric to millimetric lithic fragments immersed in a devitrified groundmass.

Figure 6: reconstructed schematic stratigraphic column and associated photographs

representing the evolution of ignimbrite deposits cropping out in the TMP (Np183; 7°32'04.13" S, 55°08'50.02" W); note the increase of welding from the base to the top.

Figure 7: schematic stratigraphic column and relative photographs of a >150 m thick felsic banded lava(s) cropping out in SFX (Xu192; 6°31'31.92" S, 53°02'36.60" W) overlying a basal breccia (Lf mLB) and an ignimbrite deposit characterized by a low grade of welding (Lf *l-gwLA*).

Figure 8: stratified primary volcanoclastic rocks, a) related to sedimentation by highly dilute ash-cloud (Np130; 6°54'16.09" S, 55°10'59.38" W) and, b) attribute to pyroclastic surge-type depositional condition from dilute currents (XU162; 6°32'28.39" S, 52°25'26.07" W); see Fig. 2 for the outcrops location. Relative thin section microphotographs (c/d) showing micrometric shards. For the lithofacies description see the text and Table 1.

Figure 9: massive sedimentary rocks. a) The alternation of lithofacies *csG* and *mS* indicates changes in energy conditions of sedimentation belonging to a subaqueous-subaerial fan-delta interface (Np146; 6°42'58.24" S, 55°28'53.49" W); b) detail of centimeters ripples of Lf *mS* (Np89; 6°54'39.36" S, 55°26'12.28 W); c) Lf *csG* is also associated to Lf *xsSG* (see stratified rocks in section 6.2) (Np27; 8°08'18.43" S, 54°54'37.33" W). d) Np27, e) Xu209 (6°13'55.26" S, 52°42'29.25" W), f) Np158 (7°03'33.79" S, 55°24'11.84" W); the rounded and clast supported character of these lithofacies is linked with fluvial/alluvial deposition by debris-flow dominated processes; see Fig. 2 for the outcrops location. For a more detailed lithofacies description see the text and Table 1.

Figure 10: stratified sedimentary rocks. a) The quartzitic sandy cross-bedded lithofacies is interpreted as formed in fluvial channel or around margins of immature marine basins (?) (Xu 201; 6°16'12.95" S, 52°52'18.84" W); b) the cross-stratified water reworked lithofacies is linked with stream-dominated fluvial/alluvial settings (Np82; 8°03'40.79" S, 54°50'43.52" W); c) the silty sedimentation likely belong to a lacustrine environment characterized by small turbidities (Np158; 7°03'33.79" S, 55°24'11.84" W); d) the top of the photographs shows the Lf *bChs* interpreted as inorganic precipitation of silica (chert) in a closed lake basin; white arrows show

fragments of the chert deposit eroded by low-energy sandy stream flows or local lacustrine turbidites (Np90; 6°49'50.20" S, 55°28'15.47" W); see Fig. 2 for the outcrops location. For a more detailed lithofacies description see the text and Table 1.

Figure 11: sketch of a wide (300 x 80 m) outcrop in the TMP (Np407; 6°40'35.21" S, 55°21'14.63" W). The stratigraphic sequence is tilted showing sub-vertical contacts of the different deposits. The sequence is interpreted displaying at the base banded (or rheo-ignimbrite) and massive lava flows passing to fragmental deposits to the top. a) ignimbrite medium-grade welded; b) the diffuse-stratified lithofacies indicates tractive processes usually attribute to pyroclastic surge-type depositional condition from dilute currents; c) sedimentary clast-supported deposit ; d) non-welded lapilli to ash ignimbrite; e) banded lava o highly reomorphc ignimbrite (lava-like). For a more detailed lithofacies description see the text and Table 1.

Figure 12: classification diagrams for the Tapajos volcanics (TMP-V) and lava flow (TMP-LF). TAS diagram with limits of alkaline series from Kuno (1968), dashed line, and Irvine and Baragar (1971), solid line. AFM diagram with alkaline field from Irvine and Baragard (1971). SiO<sub>2</sub> vs K<sub>2</sub>O classification diagram (Ewart, 1982). Literature values are from: VR (a) Vila Rozinho and MA (a) Moraes Almeida volcanic sequences from Lamarão et al. (2002); SF (b) Sobreiro Formation and SRF (b) Santa Rosa Formation from Fernandes et al. (2011).

Figure 13: REE and spider-diagrams of volcanics and lava flow rocks from the Tapajos region (TMP-V and TMP-LF). REE data are normalized to Chondrite I (CI; values from Ander and Ebihara, 1982) and trace elements are normalized to Mid Ocean Ridge Basalt (MORB; values from Hoffman, 1988). Literature values are from: VR (a) Vila Rozinho and MA (a) Moraes Almeida volcanic sequences are average values from Lamarão et al. (2002); SRF (b) Santa Rosa Formation from Fernandes et al. (2011) divided in -V volcanoclastics and -LF lava flow. Due to the lack of literature data, comparison of VR (a) and MA (a) is reported only for REE diagram.

Figure 14: tectonic affinity discriminant diagrams for the Tapajos volcanics (TMP-V) and lava flow (TMP-LF). Zr+Nb+Ce+Y (ppm) vs FeO<sub>tot</sub>/MgO (wt.%) diagram. Yb vs

Ta diagram. La/Yb vs Nb/La diagram. Th-Ta-Hf/3 diagram. Literature values are from:  
 VR (a) Vila Rozinho and MA (a) Moraes Almeida volcanic sequences from Lamarão  
 et al. (2002); SF (b) Sobreiro Formation and SRF (b) Santa Rosa Formation from  
 Fernandes et al. (2011).

Figure 15: geochronological U-Pb data from Tapajos zircons. Average  $^{206}\text{Pb}/^{207}\text{Pb}$  age  
 (errors are calculated as  $2\sigma$ ) of the three samples. Probability density plot of  $^{206}\text{Pb}/^{207}\text{Pb}$   
 ages. Calculated concordia age for sample NP396 (lava flow) and NP183 (ignimbrite).

Figure 16: geochronological U-Pb data from Xingu zircons. Calculated concordia age  
 for ignimbrite sample XU-08. Probability density plot of  $^{206}\text{Pb}/^{207}\text{Pb}$  ages.

Figure 17: peoleogeographic reconstruction of the fissural and calderic volcanic activity  
 during the Late-Paleoproterozoic in the southern part of the Amazonian craton. In the  
 foreground is shown a section of a caldera and a post-caldera ignimbrite uplift that  
 could facilitate the production of new sediments to be reworked and transported. The  
 rising magma could form sporadic intra-caldera domes and volcanic centers as also  
 shown in the background calderas. Reworked sediments can accumulate into volcano-  
 tectonic depressions, which often collects intra-caldera lakes. In the background a  
 fissure-fed volcanism is the responsible of the emission of lava flows and/or high-  
 grade to rheomorphic ignimbrites. Fluvial deposits that occur throughout all  
 successions represent periods of stream and river reworking. The area is punctuated by  
 little scoria cones and maars that contribute to the amount of the fragmental products  
 well represented in the study regions.

## Tables

Table 1: Summary of the main characteristics of volcaniclastic lithofacies of the  
 primary and secondary products analyzed and their interpretation.



1426 Table 2: Major and trace element bulk rock composition of Tapajos samples. Class  
 1427 identify the lithological features of the rocks: VC: volcanoclastic; I: ignimbrite; R:  
 1428 rhyolite; Type identify the geochemical affinity according to the granite classification  
 1429 (Zr+Nb+Ce+Y (ppm) vs  $\text{FeO}_{\text{tot}}/\text{MgO}$  (wt.%) diagram, Fig. 14): I is for I-type granites  
 1430 and A is for A-type granites; b.d.l. is below detection limits; Mg# is calculated as  $\text{Mg}^{2+}$   
 1431 / ( $\text{Fe}^{2+}_{\text{t}} + \text{Mg}^{2+}$ ); (\*) major elements analyses already published in Roverato et. (2016).  
 1432  
 1433  
 1434  
 1435  
 1436  
 1437

Figure 1  
[Click here to download high resolution image](#)

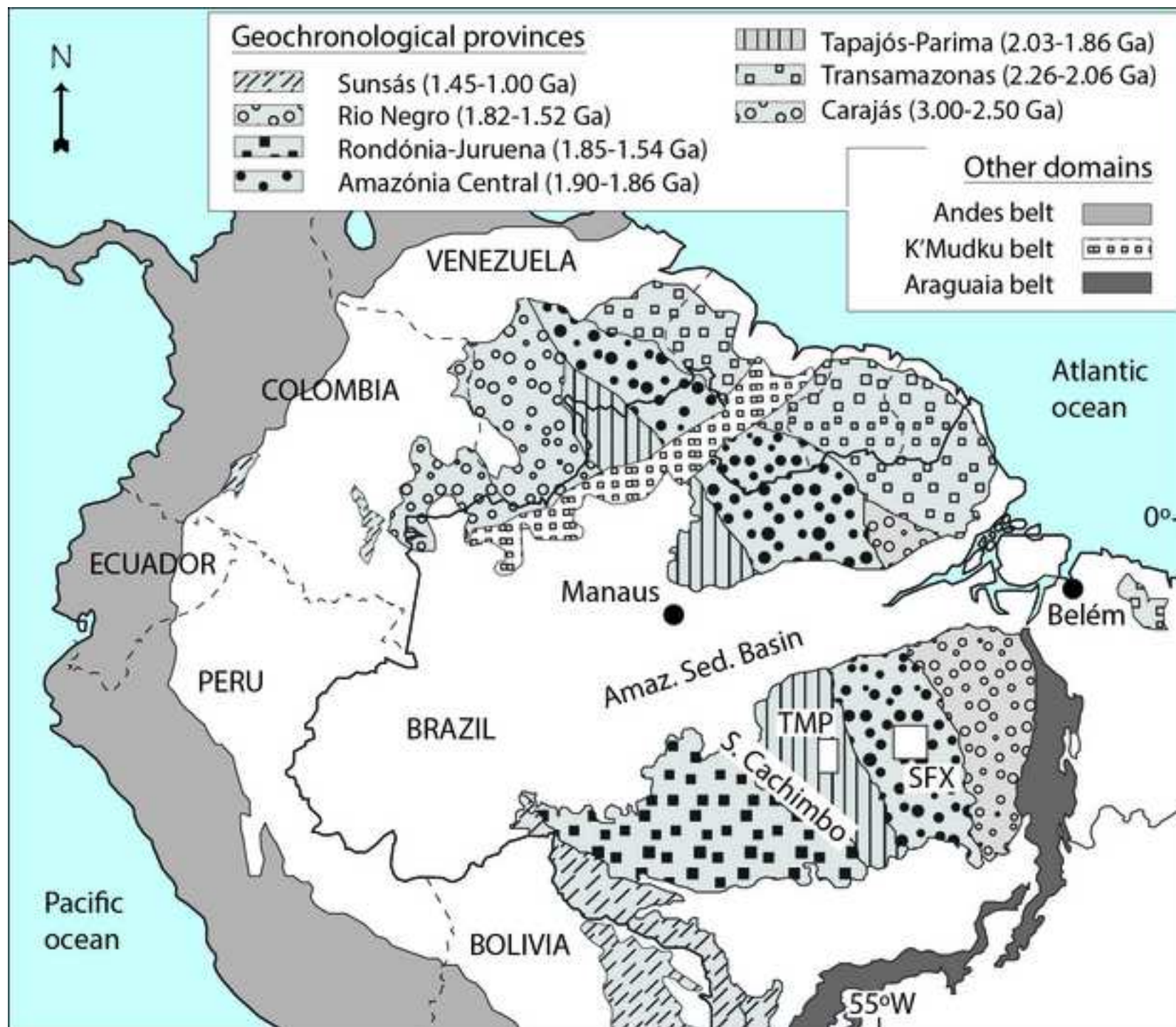
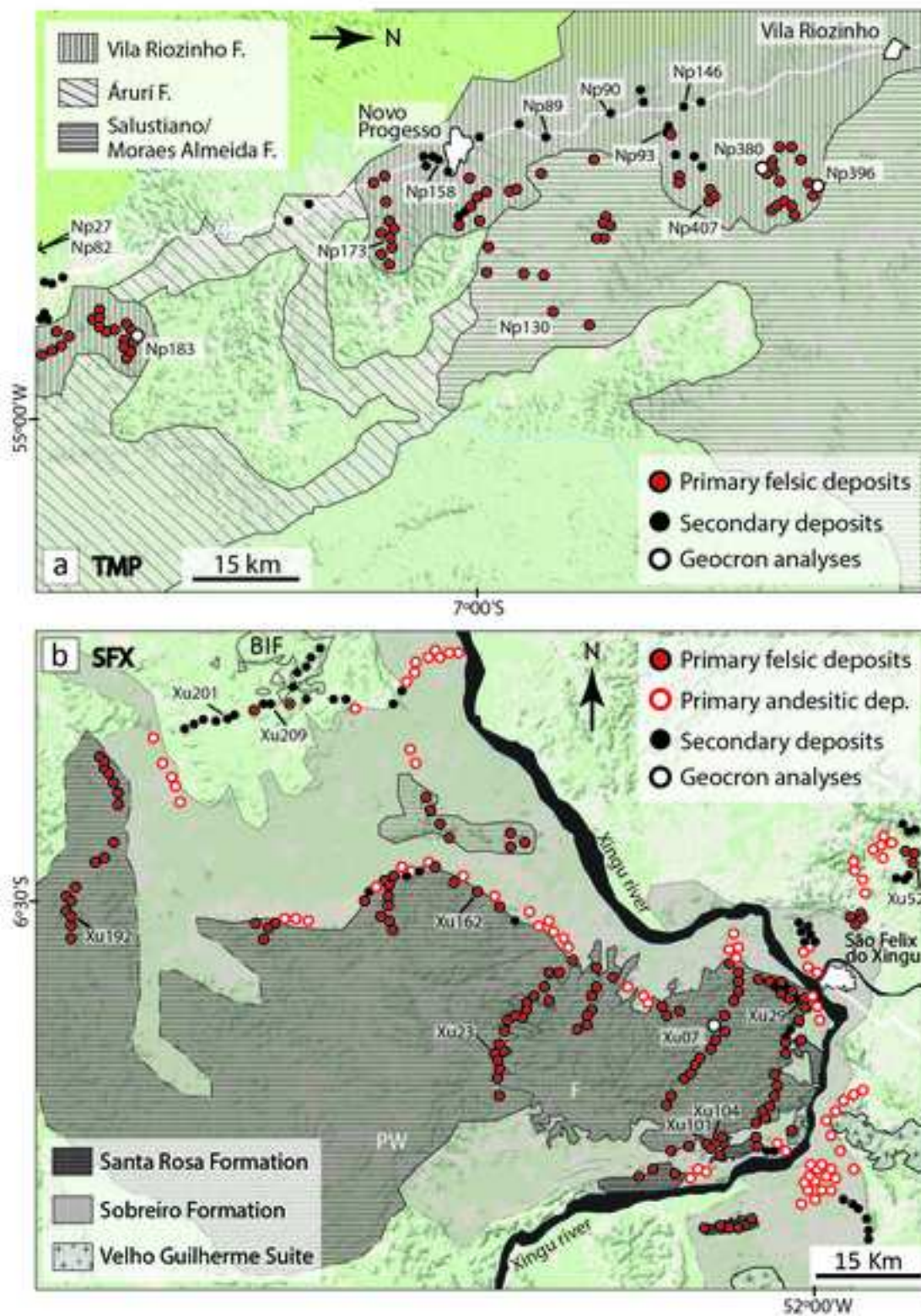


Figure 2  
[Click here to download high resolution image](#)





**Figure 3**  
[Click here to download high resolution image](#)



Figure 4  
[Click here to download high resolution image](#)

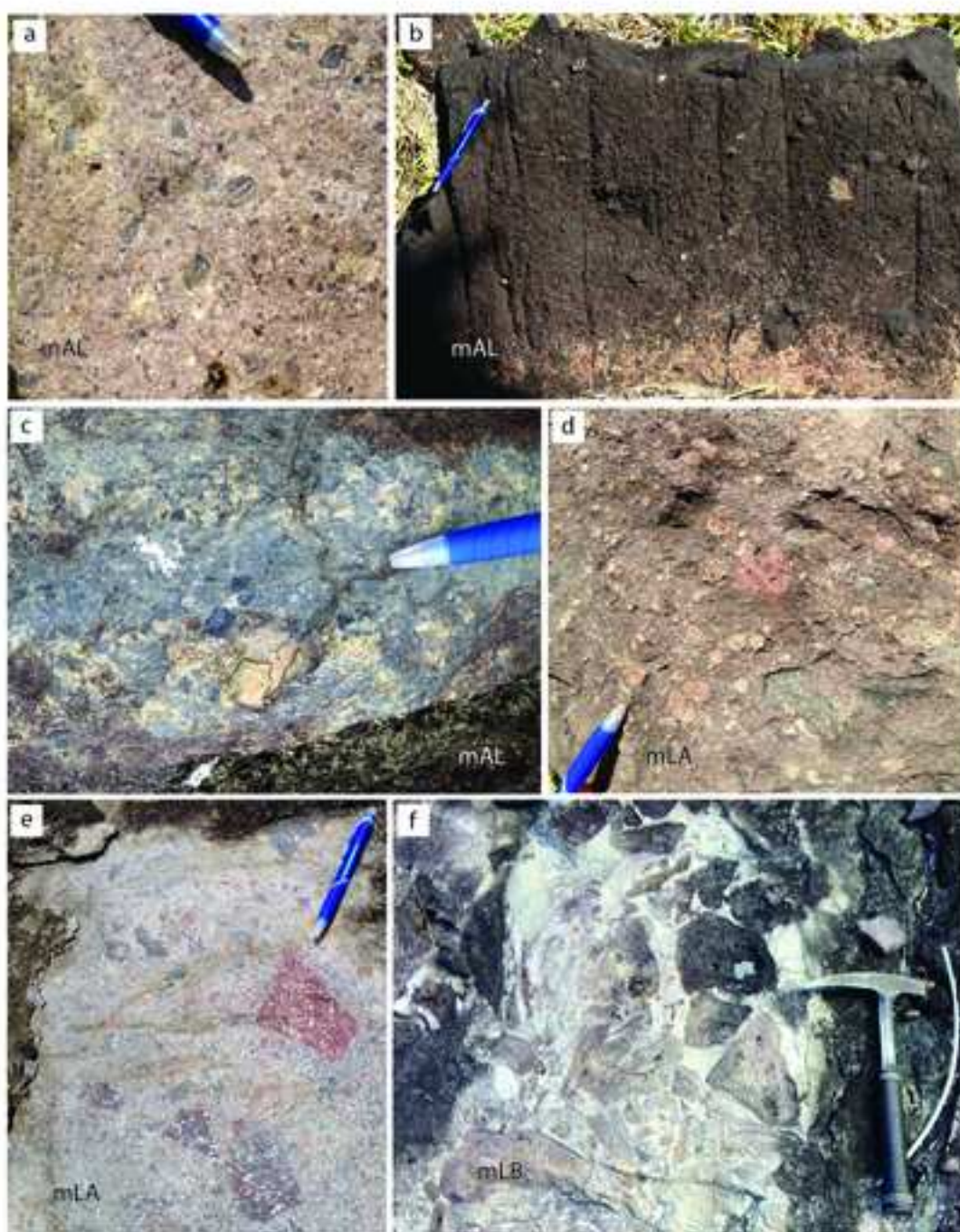




Figure 5  
[Click here to download high resolution image](#)

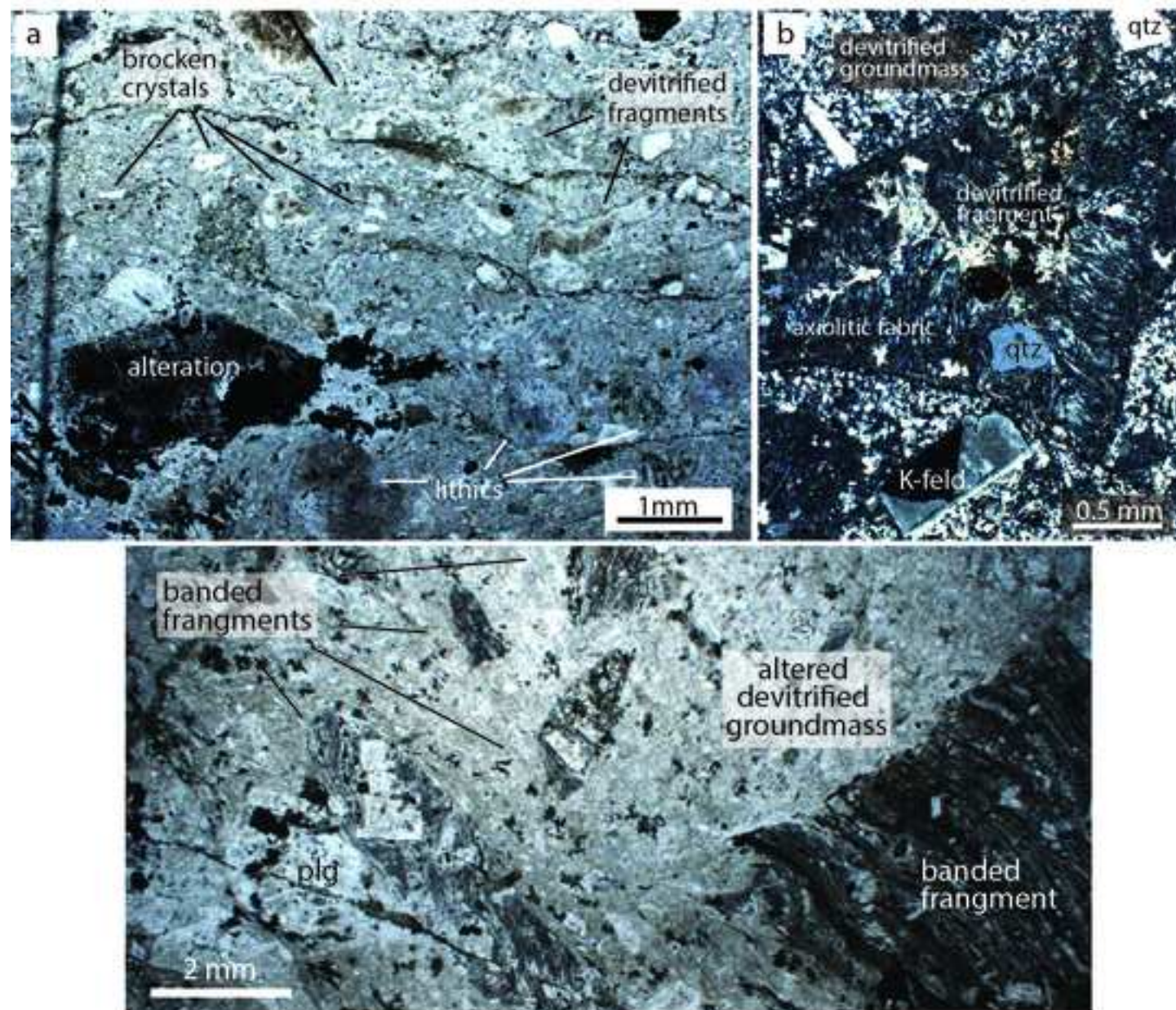


Figure 6  
[Click here to download high resolution image](#)

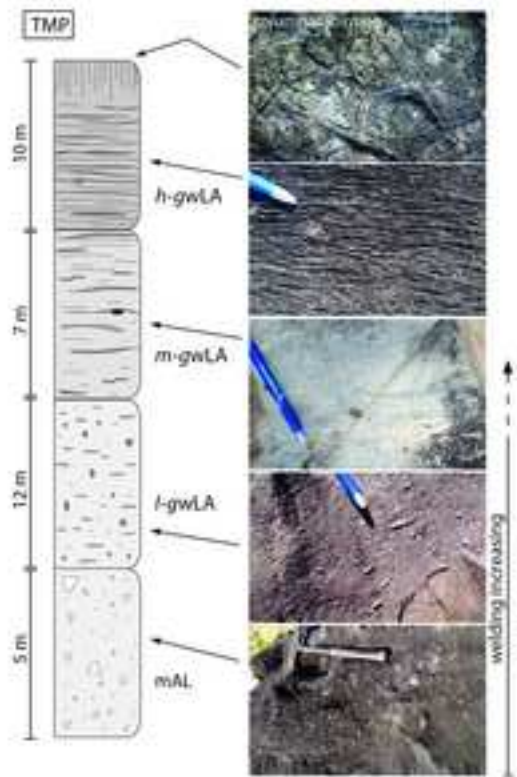
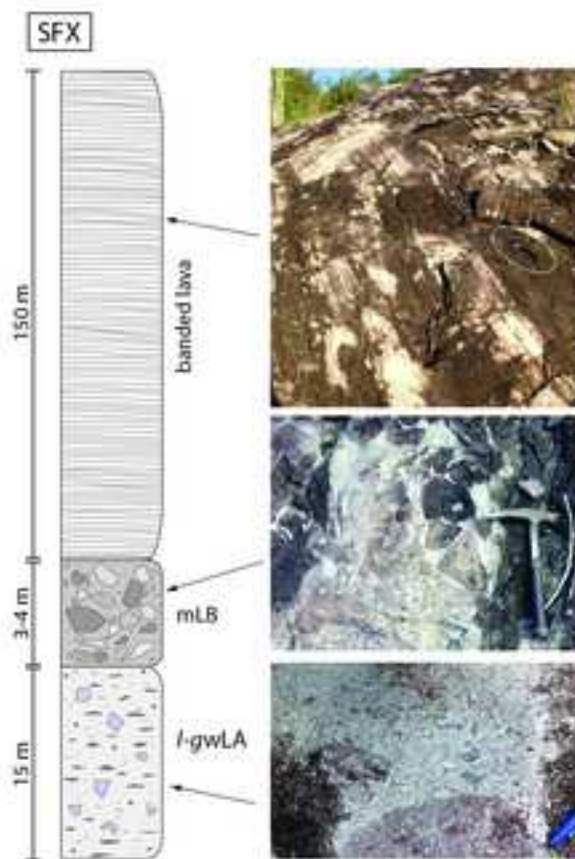


Figure 7  
[Click here to download high resolution image](#)





**Figure 8**  
[Click here to download high resolution image](#)

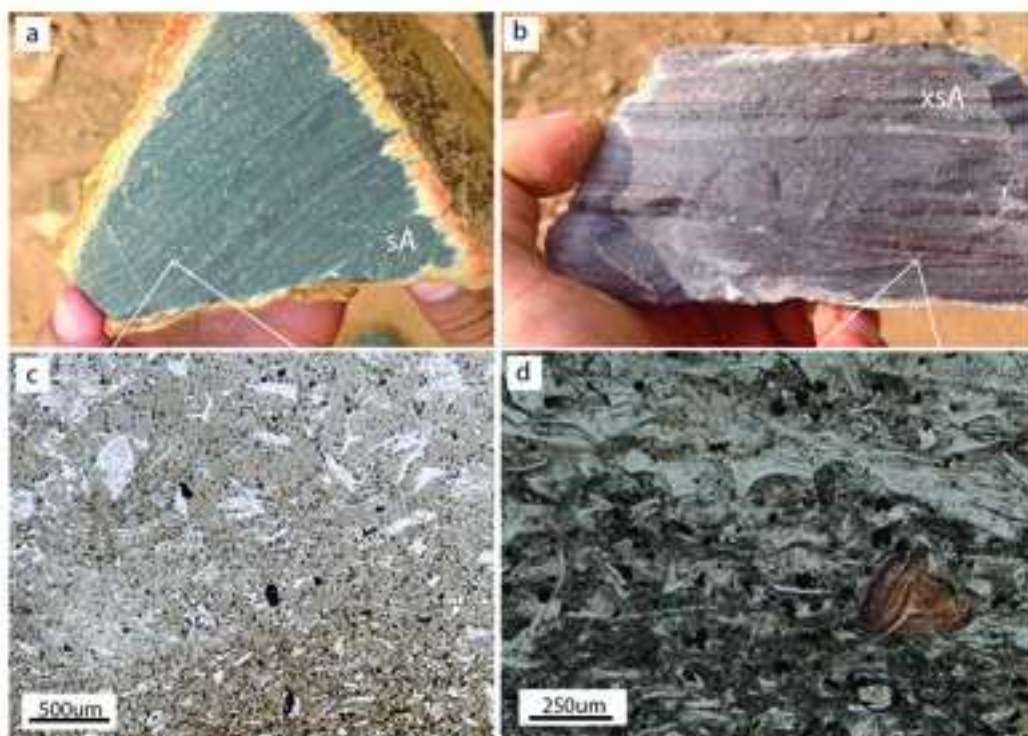


Figure 9  
[Click here to download high resolution image](#)

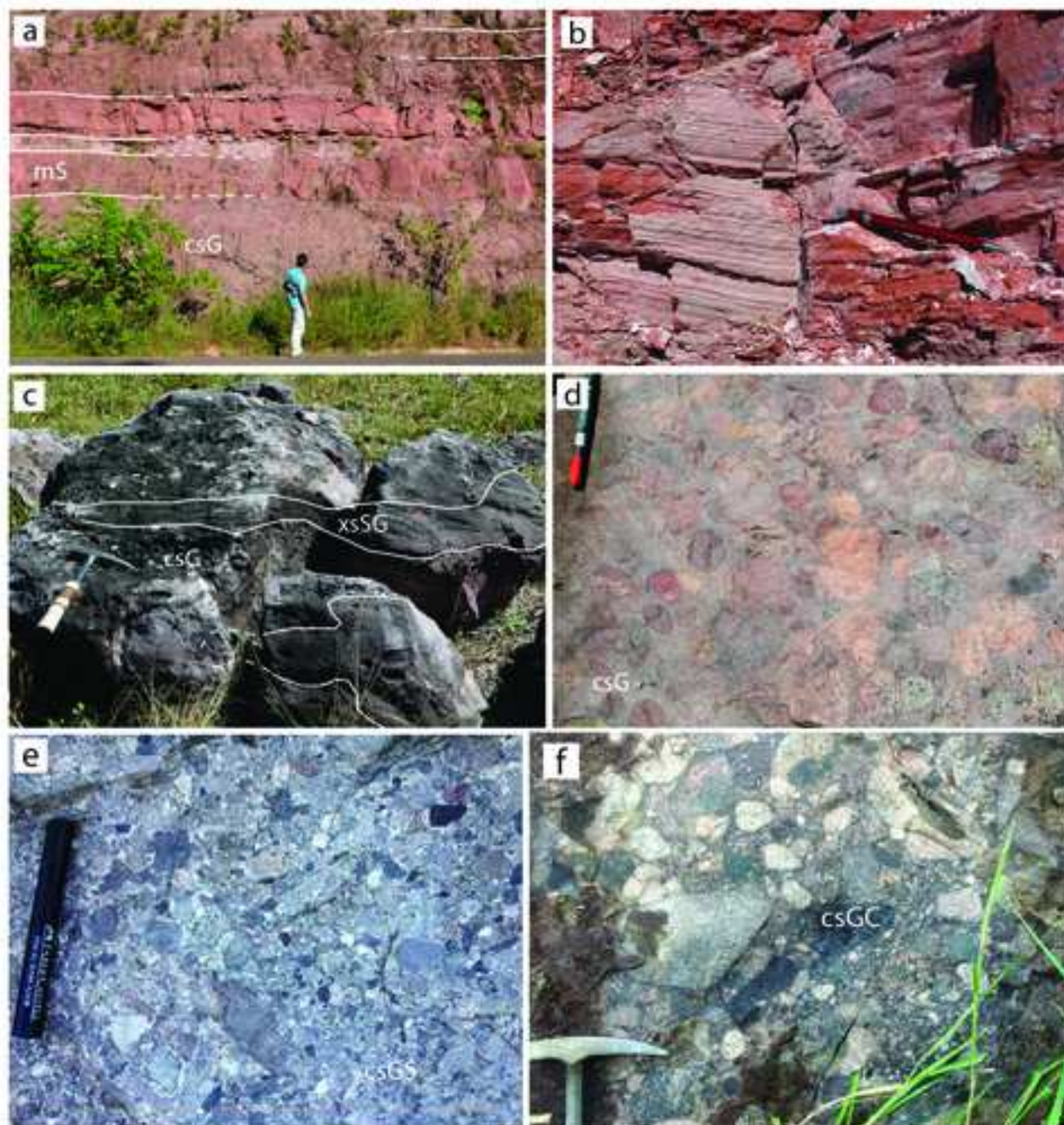




Figure 10  
[Click here to download high resolution image](#)

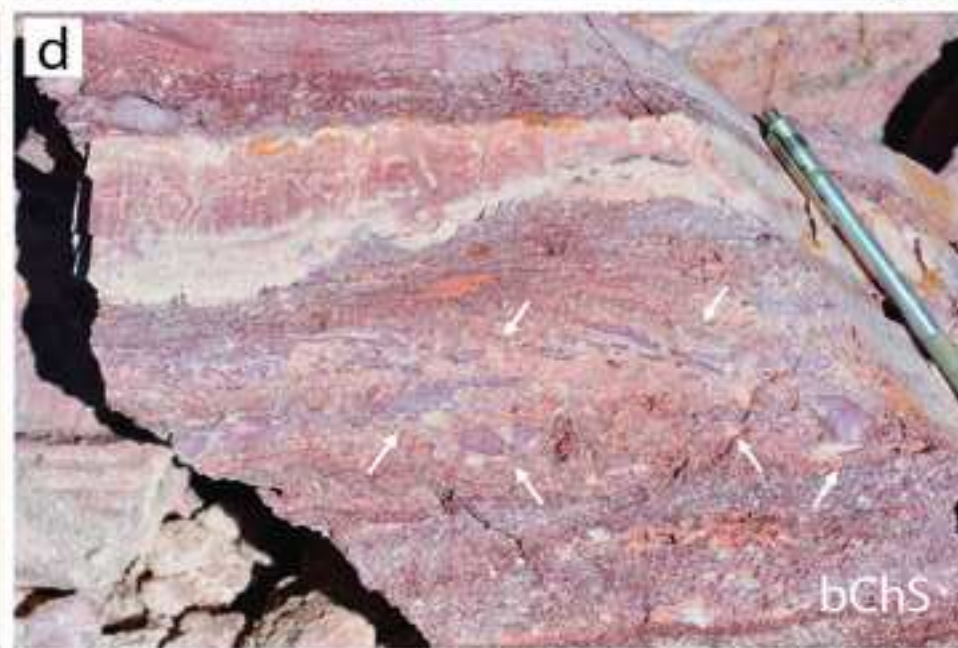
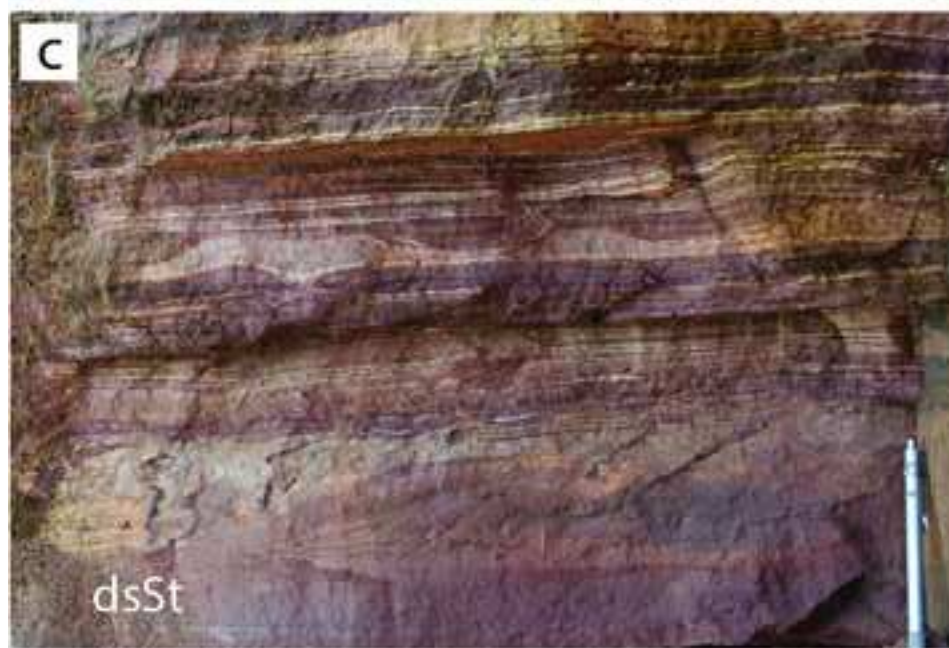




Figure 11  
[Click here to download high resolution image](#)

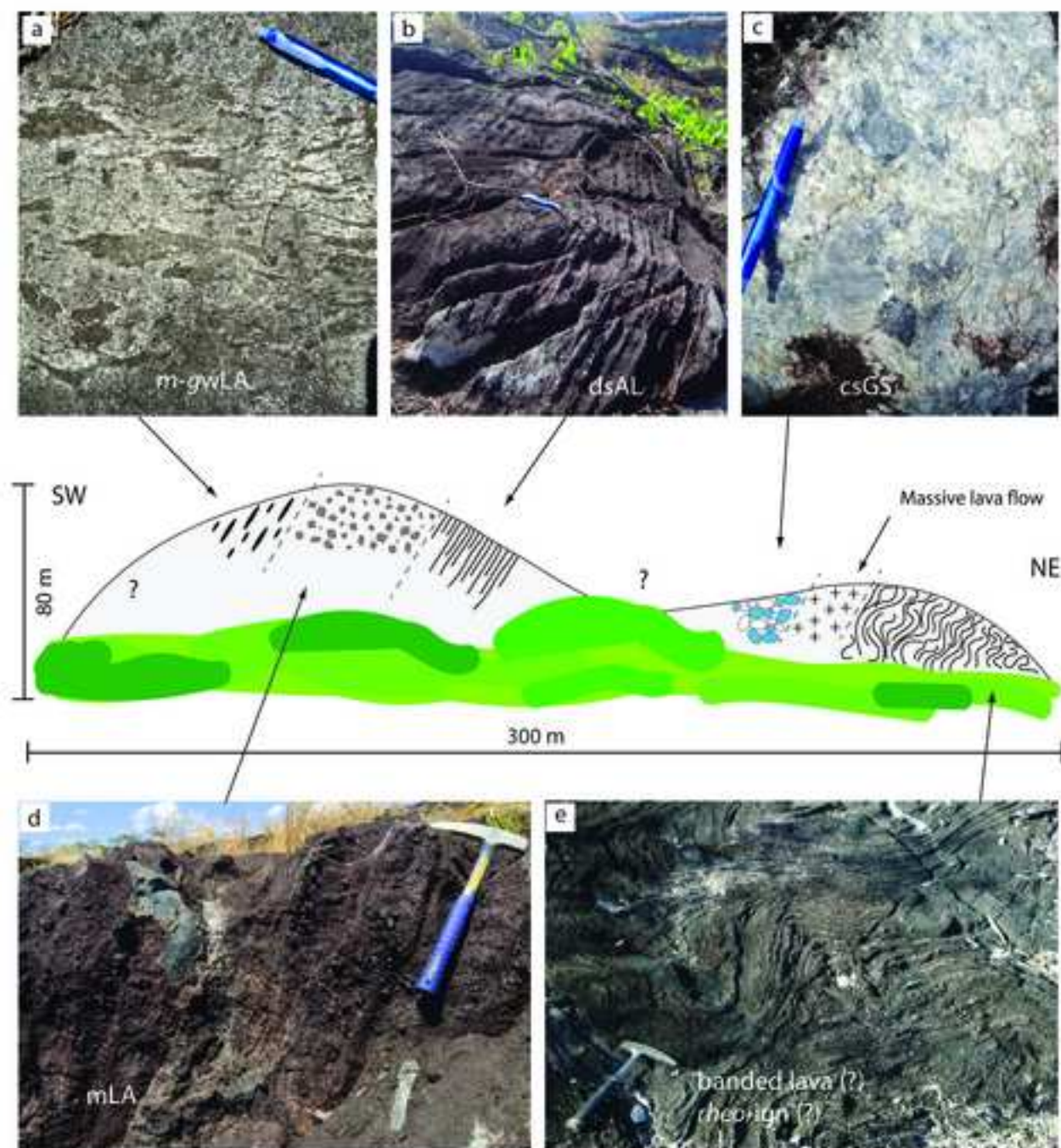
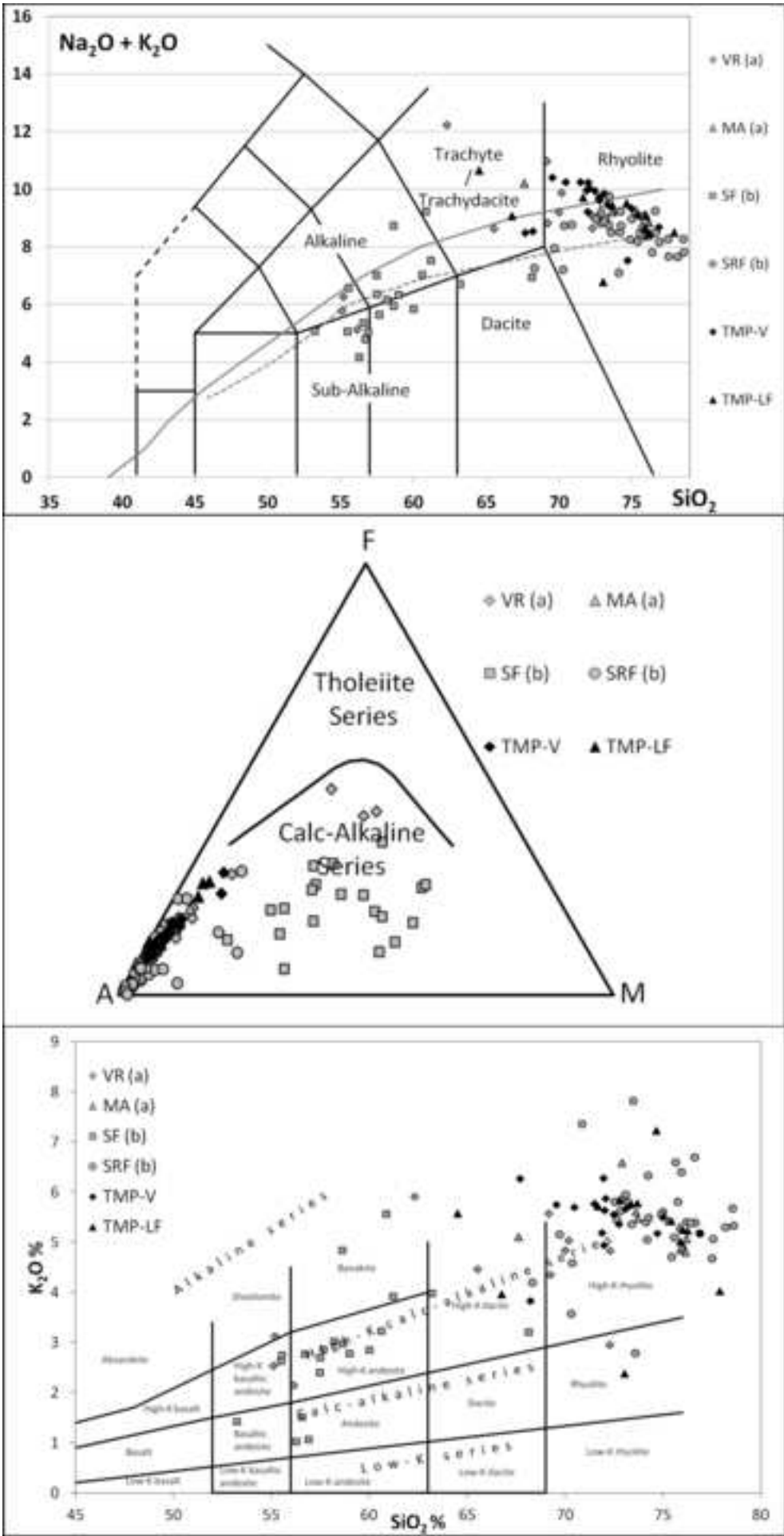


Figure 12  
[Click here to download high resolution image](#)



**Figure 13**  
[Click here to download high resolution image](#)

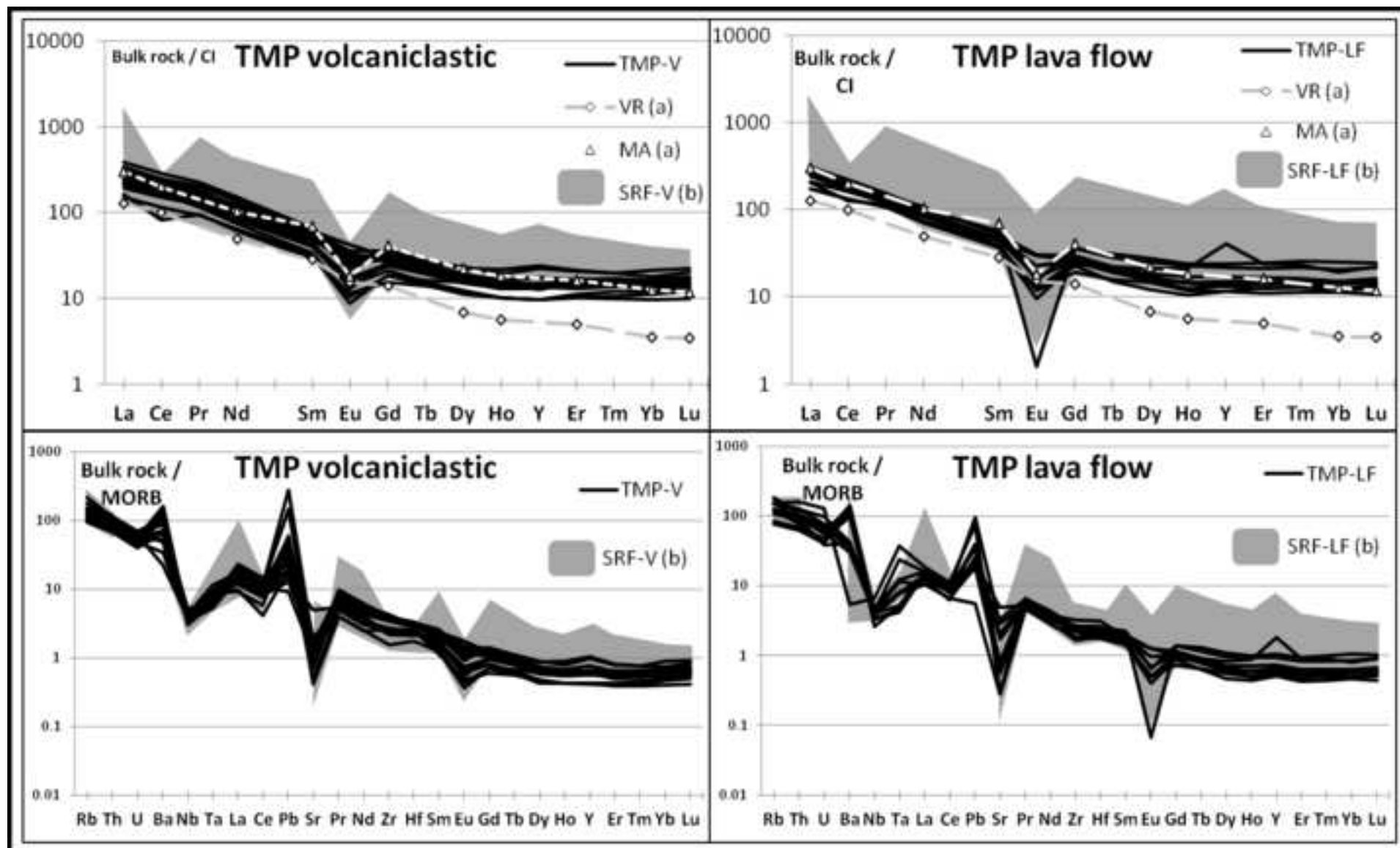




Figure 14  
[Click here to download high resolution image](#)

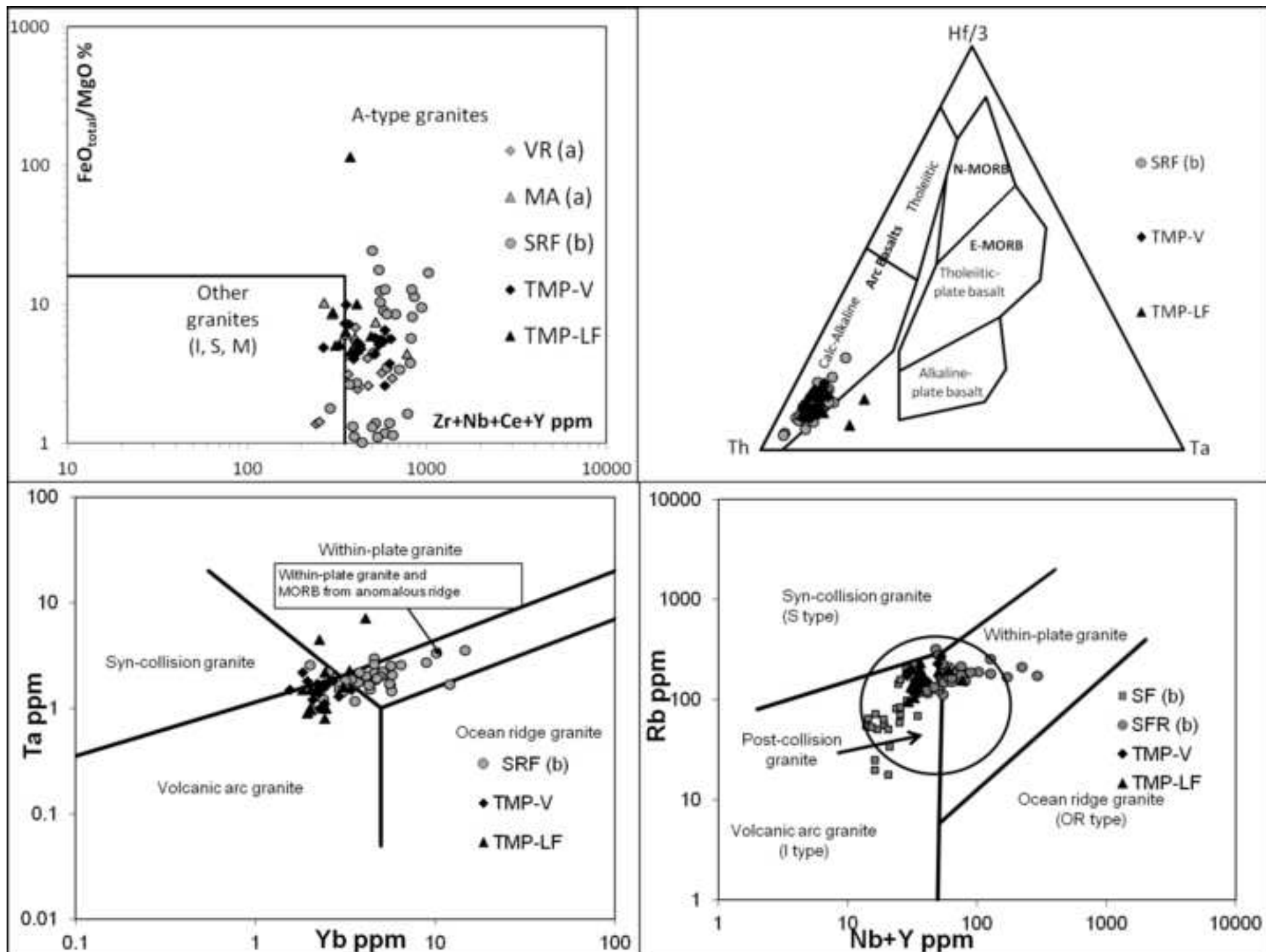


Figure 15  
[Click here to download high resolution image](#)

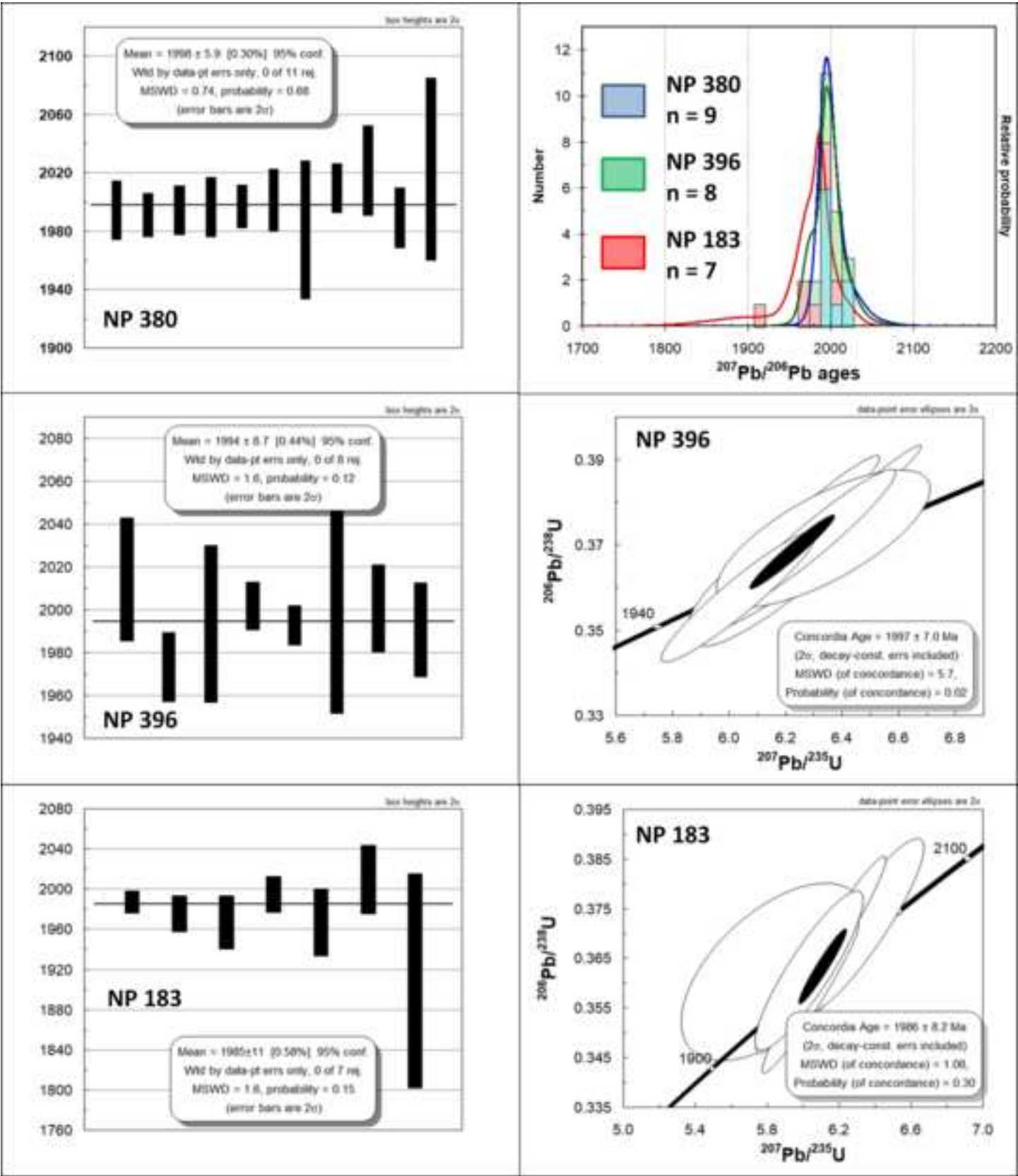




Figure 16  
[Click here to download high resolution image](#)

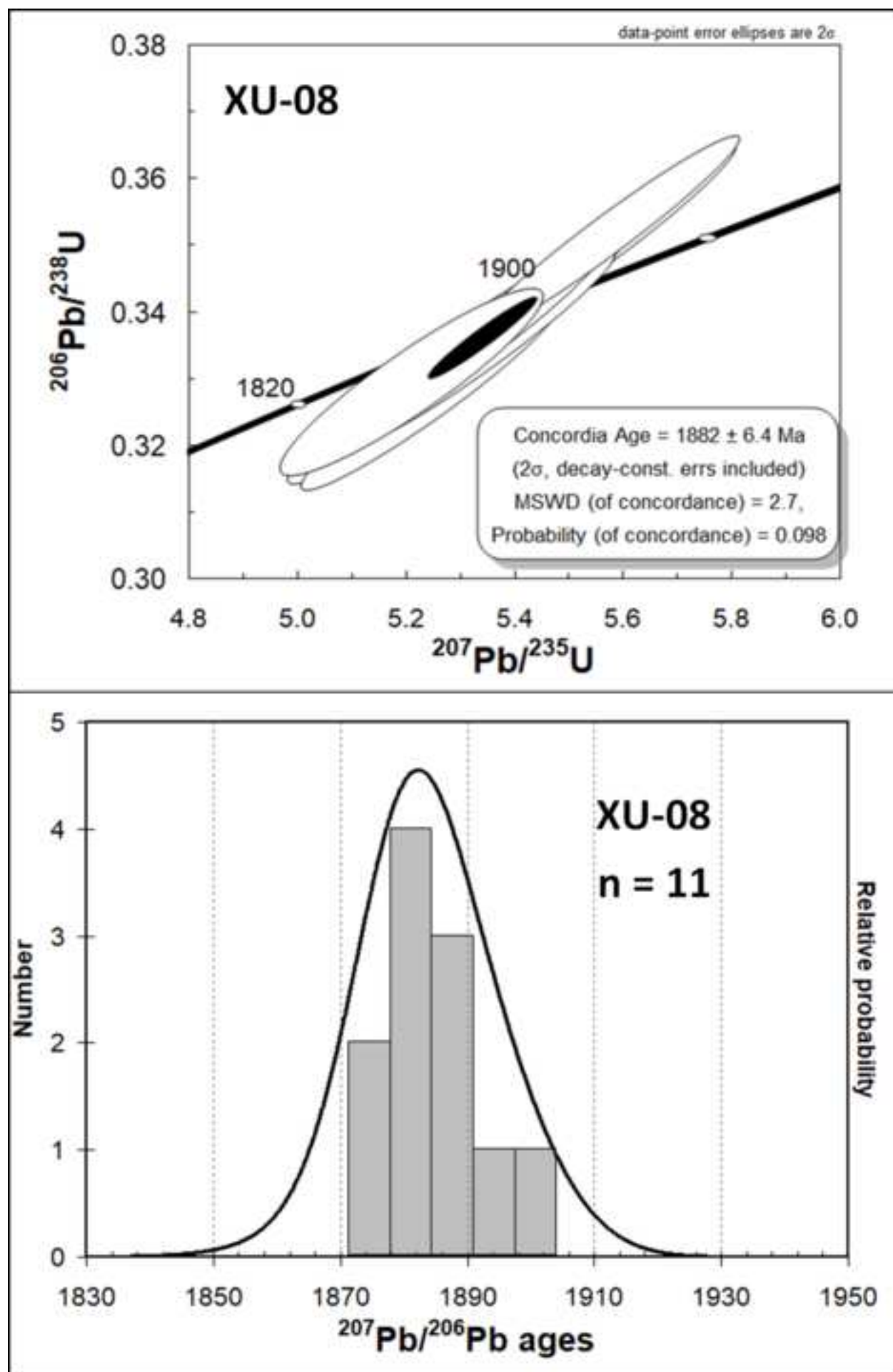


Figure 17  
[Click here to download high resolution image](#)

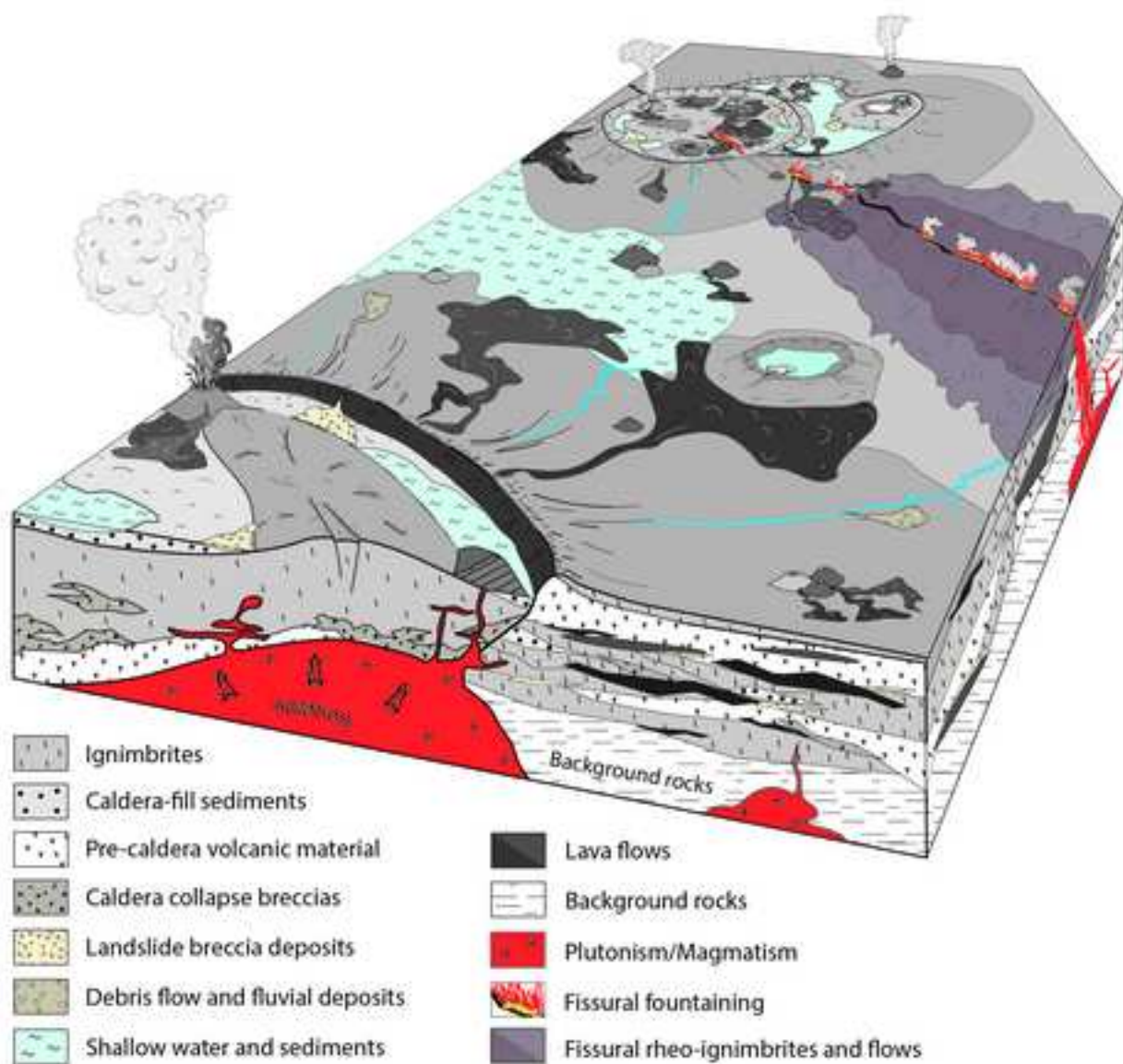


Table 1

		Lithofacies		Description	Interpretation
Primary volcaniclastic rocks	Massive	<b>mAL</b> Massive Ash to Lapilli		Massive fine and coarse ash and variable fine to coarse lithic lapilli content. Devitrified fragments immersed. Brocken crystal (plg/prx) content. Moderate to bed sorting.	The massive fine aspect suggests deposition from a dilute pyroclastic density current (PDC). Brocken crystals confirm the fragmental character. Granular flow regime.
		<b>mLA</b> Massive Lapilli and Ash		Massive, fine, fine to coarse and coarse devitrified lapilli immerse in ash matrix, less blocks immersed, maximum size 20-25 cm. Moderate sorting.	The massive aspect suggests deposition from a dilute PDC. The coarser character could be also related to proximal co-ignimbritic breccias as result of deposition by denser pyroclastic granular flows.
		<b>mLB,</b> Massive Lapilli and Block		Massive, monolithologic, angular coarse lapilli and blocks (50-60 cm) immersed in lapilli matrix. Moderate sorting.	Basal auto-brecciation of lava flows and/or rheo-ignimbrite flows
	Banded	Welded ignimbrites	<b><i>l-gwLA,</i></b> <b><i>m-gwLA,</i></b> <b><i>h-gwLA</i></b> low-, medium-, high-grade welded Lapilli and Ash	Massive, fine to coarse, moderately to strongly flattened devitrified lapilli ( <i>fiamme</i> ) varying from millimetric to 3–4 cm in size and lithic lapilli and ash. Crystal content. Clasts are immersed in a homogeneous ashy matrix. Low- to high-grade welded deposits. Eutaxitic texture. Moderate sorting.	The massive aspect suggests deposition from a pyroclastic density current. Welding is the result of post-depositional loading and are favored by low-viscosity pyroclasts that are promoted by high emplacement temperature, porosity and dissolved water.
			<b>rheo-ign</b> Rheoignimbrite (lava -like)	Layering of thin, dark and light bands and boudinaged fiamme. Parataxitic fabric displays subhorizontal bands and intricate small-scale intrafolial folds are present. The bands are deformed and flattened around lithic fragments and crystals.	The vitric fragments immersed in the welded ignimbrite distort and stretch up to the volcaniclastic flow becomes banded and starts to flow viscously.
	Stratified	<b>sA</b> Stratified Ash		Stratification of millimetric fine, devitrified, angular, sharply ash fragments.	The stratification is due to the bedding of shards fragments from a fall-out activity or from a dilute ignimbrite cloud.
		<b>dsAL</b> Diffusely stratified Ash to Lapilli		Diffusely stratified lithic and devitrified coarse ash and lapilli. Thickness of individual bedding surfaces ranges between few to several centimeters. Moderate sorting.	The diffuse stratification could indicates a flow boundary which is influenced by traction processes such as for pyroclastic density currents. Fall-out deposit (?).

Secondary volcaniclastic/epiclastic rocks		<b>xsA</b> Cross-stratified Ash	Cross-stratified fine ash formed by angular and sharply devitrified fragments (shards). Cross stratification is discontinuous over decimeters in macro-scale and as well as over millimeters in microscopic scale. Well to moderate sorted.	The internal cross-stratification indicates a grain by grain deposition process from a turbulent current with a flow boundary zone dominated by traction mechanism. Pyroclastic density currents (surge).
	Massive	<b>mS</b> Massive Sand	Massive quartzitic sand, good sorting. No internal structures. centimeter ripples at the top of the strata.	Continental supply in a shallow, low energy, water sedimentary setting. Subaerial to sub-aqueous transition.
		<b>csG</b> Clast supported Gravel	Clast supported polymictic gravel with rounded clasts, good sphericity and sorting. Clasts are mainly characterized by massive and banded felsic lava fragments.	Clast-supported with minor matrix content is indicative of water flow. Shallow water to subaerial. Laminar debris-flow regime in a medial reaches of stream-dominated fluvial/alluvial fans.
		<b>csGS</b> Clast supported Gravel to Sand	Clast supported polymictic, gravel to coarse sand with sub-rounded/sub-angular fragments, low-medium shericity.	Clast-supported with minor matrix content is indicative of water flow. Deposition within a debris-flow dominated fluvial/alluvial environment.
		<b>csGC</b> Clast supported Gravel and Cobble	Clast supported polymictic, gravel and cobble with sub-rounded fragments (<20 cm), low-medium shericity, low-sorted.	Water removed the finer particles during transport and deposition. Deposition within a debris-flow dominated alluvial environment.
	Stratified	<b>xsS</b> Cross-stratified Sand	Low angle cross-stratified quartzitic sand, good sorting. Layers ranges between millimeters to centimeters.	Wave-induce structure in a coastal sub-aqueous marine-basin environment or fluvial channels environment in low energy regime.
		<b>xsSG</b> Cross-stratified Sand and Gravel	Fine to coarse sand and fine crystal-lithic gravel, poor sorting, layers ranges between millimeters to centimeters.	Low to medium energy processes. Hyperconcentrated flood in stream reworking setting.
		<b>dsSt</b> Diffusely layered Silt	Diffusely millimetric layered silt. Presence of ripples and low energy wave structures, good sorting.	Shallow water basin, sedimentation in lacustrine basin and/or ponds. Some turbidite sedimentation.
		<b>bChS</b> Bedded Chert (and Sand)	Bedded chert with local sand contribution. Thinly multicolor laminated deposit with < 1 mm microcrystalline quartz-dominate layers.	Precipitation of silica particles in closed lake basins in association with volcanic rocks and sandstone.

Table 1

Table 2

Region	Tapajos										
Sample	NP – 079*	NP269a	Np380b	Np411c	NP- CO67*	NP - 080C	NP – 084A*	NP – 101*	NP - 123	NP - 156B*	NP - 159B
Class	VC	I	I	I	I	I	I	I	I	I	I
Type	A	A	A	A	A	A	A	A	A	A	A
XRF(%)											
SiO <sub>2</sub>	71.80	68.78	72.20	66.36	70.81	70.80	68.15	72.22	72.80	71.59	65.48
TiO <sub>2</sub>	0.34	0.32	0.35	0.72	0.40	0.40	0.48	0.32	0.31	0.36	0.58
Al <sub>2</sub> O <sub>3</sub>	14.16	15.37	14.24	15.57	14.76	14.52	15.43	14.28	13.59	14.27	18.22
Cr <sub>2</sub> O <sub>3</sub>	b.d.l.	b.d.l.	b.d.l.	b.d.l.	b.d.l.	b.d.l.	b.d.l.	b.d.l.	b.d.l.	b.d.l.	b.d.l.
FeOt	1.41	1.81	1.48	3.64	1.53	1.59	2.02	1.34	1.64	1.39	2.86
MnO	0.04	0.02	0.05	0.07	0.09	0.07	0.09	0.04	0.06	0.04	0.04
MgO	0.32	0.25	0.29	0.90	0.35	0.31	0.54	0.25	0.37	0.19	1.10
CaO	1.04	0.15	0.94	1.49	0.91	0.63	0.98	0.59	1.29	0.50	0.14
Na <sub>2</sub> O	3.75	2.80	4.31	4.57	4.42	4.07	4.56	4.12	2.28	3.63	2.14
K <sub>2</sub> O	5.73	6.00	5.32	3.73	5.71	5.77	5.63	5.60	5.04	5.60	6.06
P <sub>2</sub> O <sub>5</sub>	0.04	0.06	0.05	0.22	0.07	0.06	0.09	0.04	0.06	0.04	0.10
LOI	0.99	3.51	0.32	1.30	1.03	1.48	1.34	0.82	2.59	1.28	3.42
Tot	99.62	99.07	99.55	98.57	100.08	99.70	99.31	99.62	100.03	98.89	100.14
Mg#	0.29	0.20	0.26	0.31	0.29	0.26	0.32	0.25	0.29	0.20	0.41
ppm											
V	20	11	11	34	14	17	29	13	28	10	38
Co	34	38	2	15	17	31	29	43	25	32	12
Ni	1.20	2.50	0.50	0.50	0.40	0.70	0.90	0.80	0.60	0.60	2.80
Zn	28	33	45	71	55	50	55	36	33	27	55
Rb	185	194	179	121	155	144	122	191	230	174	273
Sr	221	188	209	557	141	124	187	174	172	148	127
Y	15	15	22	23	21	22	21	22	37	15	35
Zr	267	241	277	245	361	371	440	276	224	272	401
Nb	13	15	14	12	12	13	11	14	13	14	18
Cs	2.10	1.20	2.30	3.0	2.70	2.10	2.80	2.60	15	2.10	7.1
Ba	673	945	1425	1536	2185	1813	2245	1365	898	1362	1202
La	53	67	56	57	64	72	79	51	70	38	72
Ce	100	98	111	110	117	136	149	99	126	50	129
Pr	10	12	11	11	13	16	18	11	13	8.4	16
Nd	34	40	39	42	47	53	63	37	45	28	54
Sm	4.9	5.8	6.4	6.9	7.3	7.9	9.0	6.0	8.0	4.3	8.2
Eu	0.58	0.80	0.98	1.52	1.83	1.58	2.36	0.90	1.23	0.64	1.67
Gd	3.6	4.1	5.0	5.4	5.4	5.4	6.1	4.8	7.2	3.0	6.7
Tb	0.52	0.56	0.73	0.76	0.73	0.78	0.76	0.69	0.99	0.50	0.97
Dy	2.69	3.0	3.9	4.1	3.8	4.0	3.9	3.6	5.4	2.92	5.6
Ho	0.57	0.57	0.74	0.76	0.78	0.75	0.77	0.73	1.21	0.57	1.06
Er	1.61	1.65	2.19	2.17	2.08	2.33	2.19	2.21	3.3	1.77	3.3
Tm	0.24	0.26	0.35	0.36	0.33	0.34	0.34	0.36	0.48	0.29	0.48
Yb	1.56	1.83	2.38	2.22	2.30	2.12	2.08	2.41	3.43	1.95	2.90
Lu	0.24	0.29	0.38	0.35	0.36	0.36	0.34	0.36	0.54	0.33	0.49
Hf	7.7	7.0	7.3	6.4	8.4	8.5	8.9	7.2	6.3	7.6	9.8
Ta	1.50	2.20	1.00	1.50	1.00	1.40	1.20	1.70	1.50	1.80	1.30
Pb	23	6.3	13	7.3	24	73	20	10	26	9.2	4.5
Th	21	21	19	13	15	17	14	20	22	20	21
U	4.9	3.4	5.0	2.90	3.3	3.6	2.90	4.0	2.90	4.6	4.8

Table 2: continued

Region	Tapajos										
Sample	NP - 175A	NP - 176*	NP - 178B*	NP - 179*	NP - 180*	NP - 183A*	NP - 184*	NP - 093	NP - 094	Np272a	Np393A
Class	I	I	I	I	I	I	I	VC	VC	R	R
Type	A	I	A	A	A	A	A	A	A	A	A
XRF (%)											
SiO <sub>2</sub>	73.86	75.93	70.86	72.53	69.73	71.25	70.99	60.36	62.46	71.13	76.57
TiO <sub>2</sub>	0.24	0.20	0.39	0.37	0.44	0.41	0.37	0.81	0.89	0.49	0.09
Al <sub>2</sub> O <sub>3</sub>	13.40	12.71	14.62	14.44	15.20	14.65	14.54	15.42	16.36	14.44	11.93
Cr <sub>2</sub> O <sub>3</sub>	b.d.l.	b.d.l.	b.d.l.	b.d.l.	0.01	b.d.l.	b.d.l.	0.01	b.d.l.	b.d.l.	b.d.l.
FeOt	1.10	0.78	1.57	1.67	2.03	1.57	1.75	5.70	4.97	2.52	1.16
MnO	0.07	0.06	0.07	0.09	0.09	0.09	0.08	0.11	0.09	0.06	0.03
MgO	0.11	0.16	0.29	0.30	0.36	0.24	0.30	3.24	1.68	0.51	0.01
CaO	0.50	0.34	0.88	0.65	0.88	0.56	0.68	4.59	3.03	1.57	0.14
Na <sub>2</sub> O	3.78	3.46	4.70	4.38	4.49	4.54	4.97	2.79	3.11	4.27	4.39
K <sub>2</sub> O	5.41	5.11	5.11	5.56	5.64	5.57	4.87	4.67	5.86	2.32	3.95
P <sub>2</sub> O <sub>5</sub>	0.02	0.01	0.06	0.06	0.07	0.05	0.06	0.35	0.39	0.06	b.d.l.
LOI	1.15	0.88	1.28	0.85	1.00	0.81	1.07	1.37	0.64	1.38	0.58
Tot	99.64	99.64	99.83	100.90	99.94	99.74	99.68	99.43	99.48	98.75	98.85
Mg#	0.15	0.27	0.25	0.24	0.24	0.21	0.23	0.50	0.38	0.27	0.02
ppm											
V	b.d.l.	b.d.l.	14	b.d.l.	17	b.d.l.	10	112	59	11	b.d.l.
Co	36	34	32	40	28	37	38	27	24	2.60	63
Ni	0.50	0.50	0.80	2.30	3.4	1.50	0.60	19	0.50	0.60	1.10
Zn	20	32	45	51	46	52	60	55	73	55	33
Rb	156	158	136	153	136	133	127	116	169	105	196
Sr	54	46	179	120	115	78	103	614	620	321	33
Y	27	20	23	27	22	23	20	16	23	21	37
Zr	223	162	397	370	423	402	360	174	257	279	181
Nb	13	13	13	14	11	12	12	7.3	11	12	23
Cs	3.2	3.9	2.10	3.10	2.60	1.80	0.70	4.2	6.2	1.70	1.60
Ba	477	310	2021	998	880	746	2243	1362	2063	1363	75
La	45	36	75	76	91	80	64	35	53	59	72
Ce	92	70	140	138	174	151	122	70	106	108	133
Pr	11	8.3	15	15	20	18	14	8.5	13	11	14
Nd	39	29	57	52	69	64	52	31	48	38	45
Sm	6.7	4.7	8.9	8.1	10	9.4	7.9	5.2	7.6	6.5	8.1
Eu	0.72	0.49	1.98	1.36	1.63	1.51	1.84	1.35	1.71	1.27	0.09
Gd	5.3	3.7	6.9	6.9	6.6	6.6	5.7	4.3	5.5	4.9	7.0
Tb	0.81	0.59	0.76	0.87	0.92	0.91	0.78	0.57	0.81	0.70	1.14
Dy	4.7	3.7	4.5	4.3	4.4	4.6	4.0	3.0	4.3	3.7	6.8
Ho	0.90	0.72	0.86	0.91	0.80	0.83	0.82	0.56	0.82	0.69	1.31
Er	2.63	2.25	2.73	2.57	2.23	2.31	2.51	1.52	2.32	1.99	3.9
Tm	0.41	0.35	0.39	0.36	0.36	0.37	0.36	0.23	0.32	0.31	0.62
Yb	2.61	2.21	2.44	2.71	2.25	2.43	2.32	1.43	2.08	1.95	4.1
Lu	0.39	0.33	0.42	0.43	0.36	0.40	0.37	0.24	0.33	0.30	0.60
Hf	6.6	5.2	8.7	8.5	9.6	9.3	8.4	4.3	6.2	7.1	7.4
Ta	1.80	1.70	1.10	1.80	1.40	1.60	1.60	0.60	1.00	0.90	7.1
Pb	16	29	137	10	17	11	28	4.0	6.9	46	36
Th	17	18	17	16	16	17	17	6.1	11	13	30
U	3.4	4.4	3.5	3.9	3.5	3.7	4.0	1.30	2.10	3.4	9.1

Table 2: continued

Region	Tapajos										
Sample	Np405	Np406	NP - 039B	NP - 073	NP - 114	NP - 121	NP - 173*	NP - 175B	NP - 182C		
Class	R	R	R	R	R	R	R	R	R		
Type	A	A	A	A	A	A	I	I	I		
XRF (%)											
SiO <sub>2</sub>	73.67	69.79	65.32	72.82	63.80	75.09	75.58	75.03	74.44		
TiO <sub>2</sub>	0.33	0.45	0.86	0.31	0.74	0.27	0.20	0.22	0.22		
Al <sub>2</sub> O <sub>3</sub>	13.09	14.72	16.61	13.84	17.99	13.16	12.96	13.46	13.50		
Cr <sub>2</sub> O <sub>3</sub>	b.d.l.	b.d.l.	b.d.l.	b.d.l.	b.d.l.	b.d.l.	b.d.l.	b.d.l.	b.d.l.		
FeOt	1.33	1.78	3.27	1.29	3.30	1.01	0.99	0.96	1.23		
MnO	0.05	0.05	0.09	0.04	0.05	0.03	0.07	0.09	0.02		
MgO	0.26	0.30	0.51	0.28	0.70	0.10	0.19	0.19	0.14		
CaO	0.53	0.76	2.07	0.89	1.54	0.15	0.72	0.42	0.04		
Na <sub>2</sub> O	2.25	3.87	4.99	3.61	5.02	3.78	3.21	3.69	3.56		
K <sub>2</sub> O	7.13	5.57	3.88	5.71	5.51	5.19	5.18	5.39	4.92		
P <sub>2</sub> O <sub>5</sub>	0.03	0.07	0.22	0.04	0.22	0.03	0.02	0.02	0.02		
LOI	0.55	1.26	1.50	0.75	1.45	0.95	1.49	0.83	2.09		
Tot	99.22	98.62	99.32	99.58	100.32	99.76	100.61	100.30	100.18		
Mg#	0.26	0.23	0.22	0.28	0.27	0.15	0.25	0.26	0.17		
ppm											
V	8	<8	55	14	83	18	<8	<8	<8		
Co	1.00	36	19	19	14	52	25	45	100		
Ni	0.40	2.40	2.20	3.60	1.90	0.60	0.70	0.70	1.30		
Zn	30	38	49	21	48	18	16	28	8		
Rb	232	194	96	200	153	190	156	158	133		
Sr	204	229	552	193	377	91	79	63	32		
Y	23	22	20	18	26	34	64	24	18		
Zr	272	336	228	246	265	245	173	191	189		
Nb	14	15	9.2	14	12	17	13	14	13		
Cs	2.20	2.50	2.10	2.30	1.30	3.1	4.1	3.5	1.10		
Ba	1634	1965	1615	534	1918	583	485	413	569		
La	63	62	50	57	58	62	48	41	41		
Ce	120	117	96	101	107	112	76	80	80		
Pr	12	12	11	11	13	13	10	10	10		
Nd	43	42	38	38	49	45	34	32	32		
Sm	6.6	6.9	6.4	5.6	7.5	8.4	5.4	5.8	5.4		
Eu	0.93	1.27	1.68	0.68	1.70	0.87	0.69	0.53	0.66		
Gd	5.2	5.3	5.1	4.5	5.8	7.0	5.0	4.6	3.8		
Tb	0.73	0.74	0.69	0.55	0.80	1.02	0.80	0.76	0.58		
Dy	3.9	4.0	3.8	3.0	4.4	6.1	5.2	4.2	3.6		
Ho	0.82	0.79	0.79	0.58	0.94	1.25	1.17	0.80	0.66		
Er	2.21	2.31	2.31	1.76	2.64	3.4	3.8	2.42	2.02		
Tm	0.35	0.34	0.34	0.27	0.39	0.52	0.56	0.36	0.31		
Yb	2.47	2.28	2.01	1.83	2.43	3.3	3.1	2.43	2.03		
Lu	0.39	0.37	0.30	0.26	0.35	0.53	0.54	0.36	0.33		
Hf	8	9.3	5.9	7.3	6.3	7.6	5.5	6.0	5.3		
Ta	1.00	4.5	1.00	1.50	0.80	2.30	1.60	2.20	1.50		
Pb	10	11	10	19	8.6	16	13	9.2	2.70		
Th	20	17	12	24	14	23	19	17	17		
U	4.5	3.9	2.90	5.4	3.2	6.9	5.0	4.2	2.70		

